JANUARY 2017

Ph.D in Physics Engineering

DÜNDAR EVİS

UNIVERSITY OF GAZİANTEP

GRADUATE SCHOOL OF

NATURAL & APPLIED SCIENCES

SYNTHESIS AND THERMOLUMINESCENCE CHARACTERISTICS OF RARE EARTH DOPED NANOPHOSPHORS

Ph.D THESIS

IN

PHYSICS ENGINEERING

BY

DÜNDAR EVİS

JANUARY 2017

Synthesis and Thermoluminescence Characteristics of Rare Earth Doped Nanophosphors

Ph.D.

In

Physics Engineering

University of Gaziantep

Supervisor

Assist. Prof. Dr. R. Güler YILDIRIM

Co-Supervisor

Assoc. Prof. Dr. Vural Emir KAFADAR

By

Dündar EVİS

January 2017

REPUBLIC OF TURKEY
UNIVERSITY OF GAZİANTEP
GRADUATE SCHOOL OF NATURAL & APPLIED SCIENCES
PHYSICS ENGINEERING DEPARTMENT

Name of the thesis: Synthesis and Thermoluminescence Characteristics of Rare Earth Doped Nanophosphors

Name of the student: Dündar EVİS

Exam date: 18.01.2017

Approval of the Graduate School of Natural and Applied Sciences

Prof. Dr. A. Necmeddin YAZICI

Director

I certify that this thesis satisfies all the requirements as a thesis for the degree of Doctor of Philosophy.

Prof. Dr. Ramazan KOÇ

Head of Department

This is to certify that we have read this thesis and that in our consensus opinion it is fully adequate, in scope and quality, as a thesis for the degree of Doctor of Philosophy.

Assist. Prof. Dr. Rabia Güler YILDIRIM — Supervisor

Assoc. Prof. Dr. Vural Emir KAFADAR — Co-Supervisor

Examining Committee Members:	Signature
Prof. Dr. Zihni ÖZTÜRK	.....
Prof. Dr. A. Necmeddin YAZICI	.....
Prof. Dr. Ayşen YILMAZ	.....
Prof. Dr. Mustafa TOPAKSU	.....
Assist. Prof. Dr. R. Güler YILDIRIM	.....

I hereby declare that all information in this document has been obtained and presented in accordance with academic rules and ethical conduct. I also declare that, as required by these rules and conduct, I have fully cited and referenced all material and results that are not original to this work.

Dündar EVİS

ABSTRACT

SYNTHESIS AND THERMOLUMINESCENCE CHARACTERISTICS OF RARE EARTH DOPED NANOPHOSPHORS

EVİS, Dündar
Ph.D. in Physics Engineering
Supervisor:
Supervisor: Assist. Prof. Dr. R. Güler YILDIRIM
Co-Supervisor: Assoc. Prof. Dr. Vural Emir KAFADAR
January 2017, 87 pages

In this study we have investigated the thermoluminescence (TL) properties of Sr-doped magnesium tetraborate (MBO) and KCl doped zinc borate (ZnB_2O_4) nano phosphors, which were synthesized by using the high temperature solid-state and solution combustion method. The glow curves of the samples were evaluated by using ^{90}Sr-^{90}Y (≈ 0.04 Gy/s) beta source for different dose levels between 0.2 Gy and 288 Gy and the kinetic parameters such as activation energy (E_a), and order of kinetics (b) were calculated by using different methods. The experimental results for Sr-doped MBO nano phosphor indicated that it has main glow peak with highest intensity at approximately 200 °C with good linearity of the dose–response up to 570 Gy. On the other hand the experimental results for KCl doped ZnB_2O_4 nano phosphor has shown that it has a broad glow curve structure, which consists of nine glow peaks. The fading characteristics of the samples were also studied over a period time. The samples were irradiated and stored in a darkroom at room temperature. At the end of the planned storage times the normalized TL area, of Sr-doped MBO reduced typically 50% and KCl doped ZnB_2O_4 reduced 70% of its original value.

Keywords: Thermoluminescence, dosimeter, kinetic parameter, MgB_4O_7:Sr, ZnB_2O_4:KCl, solid-state reaction method, solution combustion method, nanoparticle

ÖZET

NADİR TOPRAK ELEMENTİ KATKILI NANOFOSFOR SENTEZİ VE TERMOLÜMİNESANS ÖZELLİKLERİ

EVİS, Dündar
Doktora Tezi, Fizik Mühendisliği Bölümü
Tez Yöneticileri:
Yrd. Doç. Dr. Rabia Güler YILDIRIM
Doç. Dr. Vural Emir KAFADAR
Ocak 2017, 87 sayfa

Bu çalışmada, yüksek sıcaklık katı hal ve çözelti yanma yöntemiyle sentezlenen Sr-katkılı magnezyum tetraborat (MBO) ve KCl katkılı çinko borat (ZnB_2O_4) nano fosforların termoluminesans (TL) özellikleri araştırılmıştır. ^{90}Sr-^{90}Y (≈ 0.04 Gy/s) beta kaynağı ile 0.2 Gy ile 288 Gy arasında değişen dozlarda ışıma eğrileri elde edilmiş ve kinetik derece, aktivasyon enerjisi gibi tuzak parametreleri, çeşitli metodları kullanılarak elde edilmiştir. Sr katkılı MBO nano fosforunun deney sonuçları, yaklaşık 200 °C'de en yüksek yoğunlukla ana ışıma tepesine sahip olduğunu ve doz cevabının 570 Gy' ye kadar iyi doğrusallığa sahip olduğunu göstermiştir. Öte yandan, KCl katkılı ZnB_2O_4 nano fosforun deney sonuçları, dokuz ışıma tepesinden oluşan geniş bir ışıma eğrisi yapısına sahip olduğunu göstermiştir. Örneklerin sabit bir doz oranında radyasyona maruz bırakılarak karanlık ortamda ve oda sıcaklığında bekletilerek farklı zaman süreleri için termal sönüm karakteristiği de çalışılmıştır. Planlanan saklama zamanlarının sonunda, Sr katkılı MBO'nun normalleştirilmiş TL alanı tipik olarak %50 ve KCl katkılı ZnB_2O_4 orijinal değerinin %70 oranında azalma görülmüştür.

Anahtar Kelimeler: Termoluminesans, dozimetre, kinetik parametre, MgB_4O_7:Sr, ZnB_2O_4:KCl, katı hal reaksiyon yöntemi, çözelti yanma yöntemi, nanoparçacık

To My Parents

ACKNOWLEDGEMENTS

During the writing of this thesis, the author received many helps from people to whom he would like to thank.

First of all, I would like to thank my supervisor Assoc. Assist. Prof. Dr. R.Güler YILDIRIM for her help and invaluable advice during this thesis. I am truly grateful for the encouragement and consideration of her. It is now my privilege to thank her.

Secondly, I wish to thank to my co-supervisor Assoc. Prof. Dr. Vural Emir KAFADAR. I have benefited from assistance and directions throughout the course of my research, the writing and preparation of this thesis.

I am deeply grateful to my wife Ülger EVİS for her constant and loving support to my work.

I would like to thank my gratitude to my family for their support at every stage of my life.

I want to thank Assoc. Prof. Dr. Tolga DEPCİ from Inonu University, for the synthesis of materials. Also Ayşegül Yücel from Inonu University, for her kind help and friendship.

This work was supported by the University of Gaziantep Scientific Research Projects Coordination Unit under the project number MF. DT.16.04.

TABLE OF CONTENTS

LİST OF TABLES

Page

LIST OF FIGURE

CHAPTER 1

INTRODUCTION

1.1 Introduction

Human beings and other living creatures have been living under the influence of radiation along with the existence of the world. The cause for the existence of this radiation is radioactive materials and cosmic rays in the world. The materials, such as uranium and thorium that naturally emit light are called radioactive. These materials contain rays such as alpha, beta, and gamma, which are harmful to living things. Because of this, our environment is exposed to continuous radiation. Measurement of this radiation has become important for scientific studies, primarily for those on living creatures' health. A dosimeter is a device that measures exposure to ionizing radiation dose. Dose unit is Gray (Gy) or Sievert (Sv) in the International System of Units (SI) and Rad in the centimeter, gram and second system of units (CGS). Gray can be defined as the absorption of one joule of radiation energy per one kilogram of material. At the present time, there are several dosimeters classified according to the area of usage. One of them is thermoluminescence dosimeter (TLD). For nearly 40 years, with technological improvements, serious developments have been observed in new generation TLD. Nowadays, personal, medical, and environmental TLDs are used commonly.

1.2 Luminescence

Some materials like insulators and semiconductors absorb some of radiation energy, and energy accumulates when exposed to radiation (This energy can be radiation, alpha particles, electrons flow, etc., in the electromagnetic spectrum). This is an important feature in dosimeters, because it may cause the stimulation of free electrons and holes and then cause them to be trapped within crystal lattice defects in material. As a result, the material becomes unstable. Due to the nature of the material, to become stable again, the material may emit its own energy as electromagnetic waves. If the electromagnetic wave emitted is the long-wavelength light (Stoke's Law), this process is called Luminescence. The emitted light depicts characteristics of the material. In this process, electromagnetic

waves like ultraviolet (UV) and infrared (IR) may emit from the material. Light emission creates a characteristic time (τ_c) after absorption of the radiation, and this parameter (τ_c) has two main parts according to the time as illustrated in Figure 1.1.

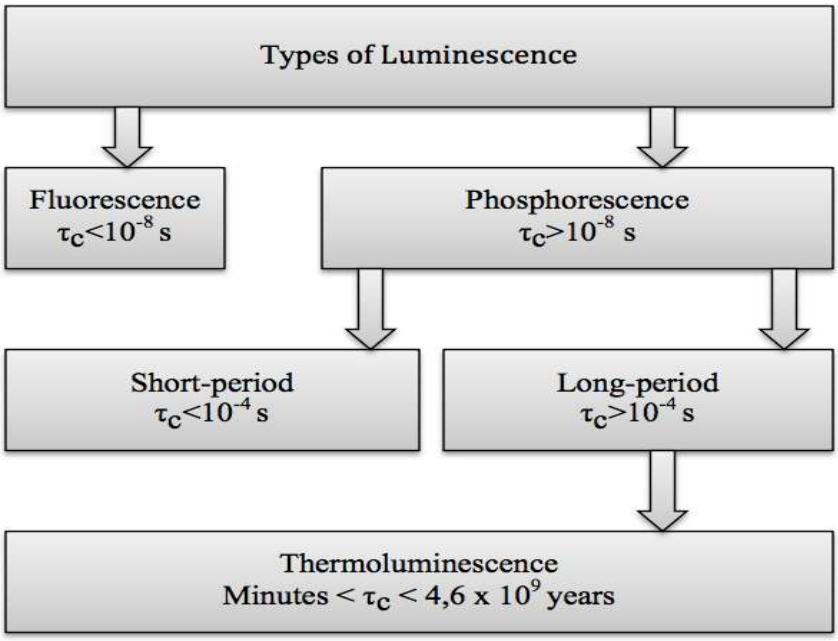

Figure: 1.1 Fluorescence and phosphorescence time table [1]

If the $\tau_c<10^{-8}$ second, it is called fluorescence; if the $\tau_c>10^{-8}$ second, it is called phosphorescence. Fluorescence is a process that it is formed at the same time as the absorption of radiation and stops just by cutting. However, phosphorescence takes places within the delay between absorption of the radiation and the elapsed time to reach the maximum intensity (t_{max}). Moreover, after removal of the stimulation process, phosphorescence continues for a while.

Phosphorescence can be divided into two parts: short- period ($\tau_c<10^{-4}$ s) and long period ($\tau_c>10^{-4}$s). Fluorescence is independent from temperature; but phosphorescence is dependent on temperature, which is a significant difference between each other. In addition, the delay in phosphorescence is related to the time the electron spends in the trap. The main time spent in the trap given, as T is ambient temperature

$$\tau = s^{-1} \exp (E/kT) \qquad (1.1)$$

where s is constant, E is the energy difference between the trap and the band (called the trap depth), and k is the Boltzmann's constant. According to the band theory of solids, the conduction band and valance band are found in in crystal lattice. These two bands are

separated by a forbidden energy gap, which lacks electrons. A valence band is the lowest energy state. The state in which an electron is the highest allowed energy is expressed as E_v in this band. That's why electrons firstly want to fill the valence band. As a result, the valance band is completely filled with electrons in an atom.

Although the conduction band is the allowed highest energy state, the state in which electron is the lowest allowed energy is expressed as E_c in this band. Electrons are free in a conduction band. The Band gap which is required energy to break the bond in a crystal is expressed as $E_g = E_c - E_v$. The phenomenon here is that an electron in the valance band takes energy and passes it to the conduction band.

In the emission of luminescence, it can be shown that a ground state energy level is g and an excited state level is e, as illustrated in Figure 1.2.a. The solid gets energy from radiation, so exciting the electrons form *g* to *e* (i). Luminescence emission (photon release) takes place when an electron returns to level g (ii). As it is well known, the elapsed time between (i) and (ii) is the fluorescence process, which is independent of temperature. The energy level changes with the presence of a metastable level of m in the forbidden band gab, as illustrated in Figure 1.2.b. As an electron excited from the ground state (g) to an excited state (e), it may be trapped in (m) and delay in it till it is given sufficient energy (E) to turn to the excited state (e), and then luminescence emission (photon release) takes place when an electron returns to level g. This delay is known as phosphorescence.

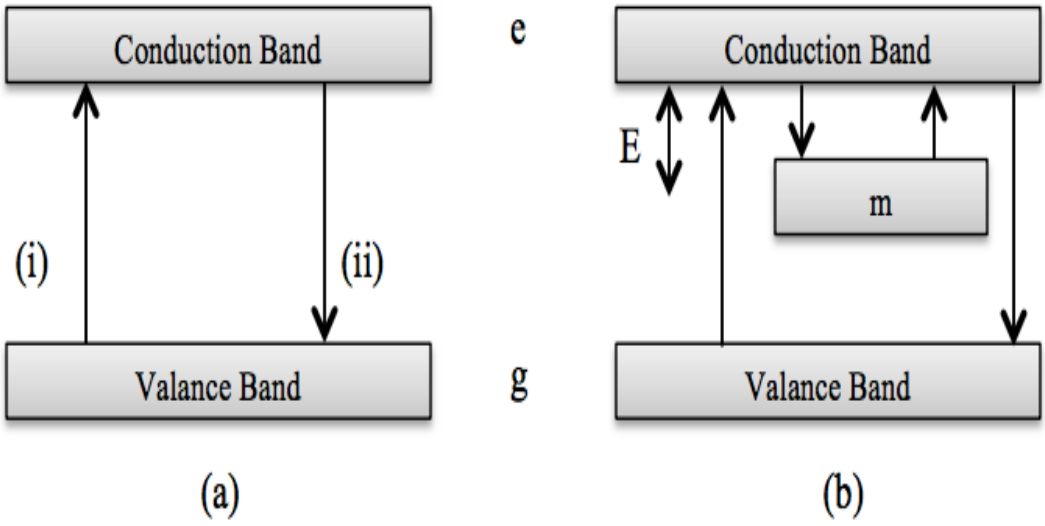

Figure 1.2 The energy transitions for fluorescence (a) and phosphorescence (b) [1].

The various types of luminescence phenomena are categorized according to the excitation method. Some of them are given below.

Table 1.1 The various types of luminescence and the excitation methods.

TYPES OF LUMINESCENCE	METHODS OF STIMULATION
Bioluminescence	Biochemical reactions energy
Cathodoluminescence	Electron beam
Chemiluminescence	Chemical reactions energy
Photoluminescence	Ultraviolet, visible, and infrared light
Electroluminescence	Electric field
Piezoluminescence	Pressure (10 tons/m^2)
Radioluminescence	Ionizing radiation
Sonoluminescence	Sound waves
Triboluminescence	Mechanical/frictional forces
Fluorescence, Phosphorescence and Thermoluminescence	Ionizing radiation, ultraviolet, visible light

1.3 Thermoluminescence

Thermoluminescence (TL) is the emission of light of insulator or semiconductor material (formerly excited by suitable radiation, thus holes arise in valance band because the electrons are released from the conduction band to the valance band) when the material is heated to favorable temperature. This energy is taken place as visible light.

According to TL theory, excited material is heated uniformly at a certain heating rate. Trapped electrons escape from trap during the heating process in the material. The freed electrons combine with holes at the suitable recombination center in the forbidden band gap and the emission of TL light. The emitted light can be detected by a photomultiplier as a function of temperature. The graph obtained is called a glow curve in TL theory. The temperature of maximum intensity expresses the trap depth in this graph.

The parameters such as the activation energy of the trap (E), frequency factor (s), and kinetic degree (b) can be found from the measurement and the analysis of obtained glow. Additionally, the trap and capture cross-sections of recombination center and the concentration of the trap center can be obtained.

The first theoretical study about glow curve in TL theory was carried out by a group of researchers [2] from the University of Birmingham. The thermoluminescence theory was formulated by the researchers in accordance with the band theory of solids.

1.3.1 Electronic Transitions within the Band Gap

TL phenomenon is described according to the band theory of solids, as previously mentioned. The band gap is between the valence band and the conduction band in a material. The valence band has an electron in bound form. The conduction band contains free electrons in crystal lattice.

The metastable energy states are formed by crystal structure imperfection or doping (addition of foreign atoms) in the band gap. The metastable energy states are expressed as a trap for electrons and holes. When the material is exposed to radiation, free electrons and holes form in the material.

Some of these traps are existed in crystalline lattice. Electrons in the trap take the thermal energy needed to escape the trap. The time of electrons and holes within traps depend on trap depth and environmental conditions. The number of trapped electrons is proportional to the absorbed ionization radiation dose in the material. Each trap has a certain temperature value in the material. If the material is heated smoothly, electrons discharge from shallow traps to deep traps.

Both electrons and holes may be re-trapped within lattice imperfections in crystalline solids. Apart from this, the escaping electrons combine with holes in a recombination center and emit light. This phenomenon is called thermoluminescence [3,4]. The stored energy is released in light form in this way. The light is proportional to the stored energy. The intensity of emitted light is proportional to the total dose of radiation. Each material has its own glow curve, so glow curve is characteristic for a material.

In brief, the electron transitions barely take place between valance band and conduction energy band. Electrons in the valence band are given radiation energy to overcome an energy gap to be excited to the conduction energy band (a). The hole in the valence band is created by the electron passed to the conduction band. Then, the free electron-hole pairs are formed, and they act freely.

The movement is continued until trapped as (b). The stimulated (by heat) electrons begin to move around freely within the crystal as (c) and indirectly combined electrons and holes as (d). The (a) is direct combinations. This light is emitted in both transitions and is called luminescence.

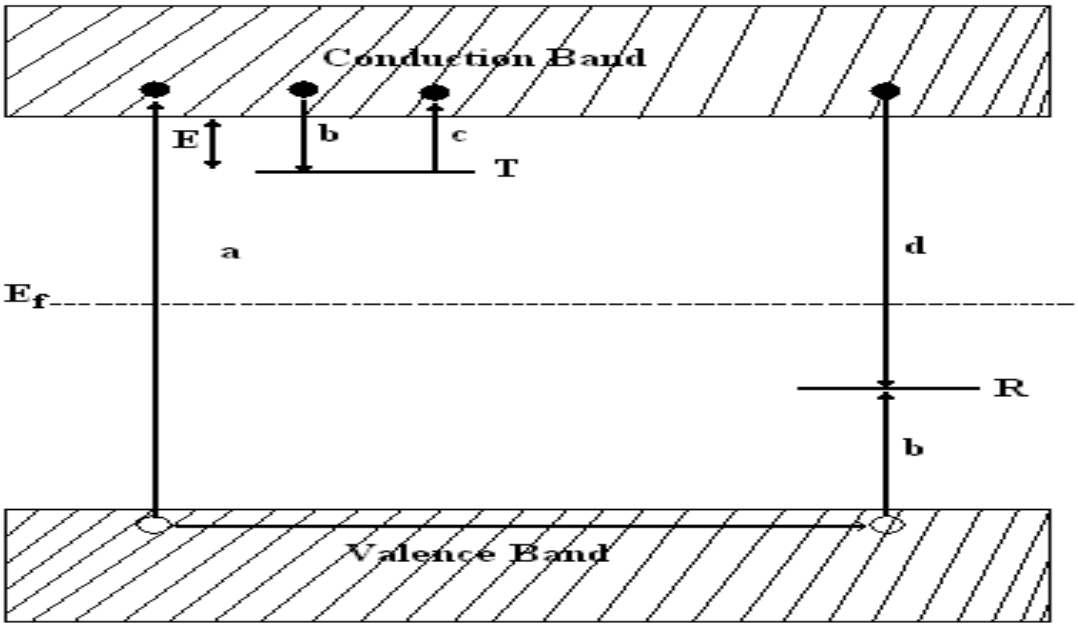

Figure 1.3 The model of the energy band for electronic transitions is given in a TL material according to the two-level model a simple (a) The occurrence of holes and electrons; (b) hole trapping and electron; (c) is the discharge of electrons because of thermal stimulation; (d) is recombination. (●) electrons, (o) holes, electron trapping level is T, center of recombination is a level R and E_f is the Fermi level [5].

1.3.2 Dosimeter and Application Fields

A dosimeter is an apparatus that measures and detects the dose of absorbed ionization radiation. A thermoluminescent dosimeter (TLD) may be explained as the measure of emitted light from a material when the crystal is heated after irradiation. In order to a thermoluminescent material to be a dosimeter, it is tested in dose, energy, and time. Kinetic parameters of the graph obtained by these tests are calculated as theoretical and experimental.

According to the purpose of usage, thermoluminescent dosimeters can be divided into several categories such as personal, environmental, medical, retrospective, and high doses [5]. TLD materials that are close to the tissue equivalent in the medical are widely used. Some of them are LiF, LiF: Mg, Ti (TLD 100), LiF: Mg, Cu, P $Li_2B_4O_7$: Mn. In addition, TLD materials that have high sensitivity, such as $CaSO_4$: Dy, Al_2O_3 and CaF_2: Mn are used.

The usage goals of dosimeters are nuclear medicine production, audit, quality control, calibration procedures, etc. Furthermore, nuclear accidents, nuclear weapons testing or resulting from the use are used for radiation measurement. As mentioned above,

dosimeters application fields are extensive and important, because of this many studies have been done and are being done to improve the properties. The material for a good dosimeter should;

* be inexpensive

* be durable for environmental factors

* be suitable reproducibility property

* have sufficient storage feature

* have simple trap structure

* have simple glow curve

* be low fading

* have high sensitivity

* be close to live tissue and

*be nontoxic

The features above are important for improving the sensitivity and reliability of the dosimeter. There are several types such as dust, chips, and rods [6].

1.3.3 Thermoluminescence properties of MgB_4O_7

Radiation measurements in recent years, synthesize of thermoluminescent (TL) material has been more sensitively in the investigation of thermoluminescent dosimeters (TLD) and TL properties of the obtained material to examine continue in detail in the world of science. In the TL dosimeters studies, various specific of materials, such as phosphate, sulfate, fluoride, borate, and oxide have been investigated for innovation an appropriate thermoluminescence material [7]. At present, various types of commercial thermoluminescence materials are used for dosimeters, but some of them can be used satisfactorily in technique.

To determine the appropriate commercial dosimeter, the researchers has been comprehensively studied the materials for the ultimate TL dosimeter. Today, many commercial thermoluminescence dosimeters are found, and mainly as thermoluminescent dosimeters, LiF:Mg, Ti (TLD-100), $Li_2B_4O_7$:Cu,Ag (TLD-800) and CaF_2:Mn (TLD-400)

are used. In this study, Sr doped MgB_4O_7 was synthesized initially. Then, the TL properties of the material were analyzed.

The principal dosimetric characteristics, which are explicitly the TL dose response, TL sensitivity, fading, minimum detectable dose, reproducibility, accuracy of dose measurement, and annealing process, will be examined for the phosphors having best glow curves to identify the usability of them in dosimetric applications. Considering magnesium tetra borate produced for dosimetric application, other magnesium borate as an impurity phase in the structure can be seen.

In these days, different borate compounds have a significant place in technology because of their being luminescent, optical communication components, super-conductive materials, high temperature resistance and high corrosion resistance, fluorescent, ceramics industry, friction-reducing additives, and catalysts [8-18]. Therefore, the researcher progress about the synthesis of borate compounds. The magnesium tetraborate dosimeters utilized in experimental studies have attracted the attention of many scientists recent years.

As the effective atomic number of magnesium tetraborate (Z_{eff} = 8.55) is close to the effective atomic number of human tissue (Z_{eff} = 7.42), studies on the usability of it as thermoluminescence dosimeters have been conducted by many groups [19- 23].

Borate compounds have attracted considerable attention in thermoluminescence studies due to their low synthesis temperature, height of optical quality, low cost, thermal stability, high sensitivity and mechanical properties, easy preparation, and tissue equivalence of the superior characteristics. Many studies have been done regarding the use of magnesium borate. In one of these earliest studies, the first poly-crystalline magnesium borates doped with Dy were reported in 1974.

In order to resolve the problems, such as sensitivity and thermal decay, different synthesis methods have been developed and detailed studies are continuing today. Borates have an extensive usage area due to their wide band width gap and tissue equivalent of the proximate as medical staff and dosimeter [11,12,24]. However, the dosimetric properties such as thermal stability and TL sensitivity of the compounds depend on the method of construction of the material. The literature review shows that borate-based TLD dosimeters are usually prepared to micro-crystalline structure and have a wide range of usage such as solidification, solution, melting, sintering, solid diffusion, and the single crystallization method in preparing TLDs. Synthesis method affects some properties of the obtained

material, and also causes some changes in its form [25,26]. Therefore, determination of the most appropriate synthesis method is extremely important for the production of materials.

Lithium triborate samples can be synthesized with different methods such as microwave solid-state reaction, microwave-assisted high temperature solid-state reaction and precipitation assisted high temperature solid-state reaction methods, and better TL characteristic are observed [27]. Depending on the synthesis method, different grain sizes were observed. Due to the particle size, TL glow curves show that they have a different intensity of dosimeters. The peak of glow curve has been determined with decreasing particle size. Before the effects of particles, several researchers have studied the size of the TL. According to some literature, it was observed that properties of the thermoluminescence were reduced with the decrease of the particle size in the form of microcrystalline powder [28,29].

On the other hand, as different from the above mentioned points, it was observed that the characteristics of a material change in a different way in a nano-sized dosimetric material. Specifically, during the preparation of nano-materials, the structure of a nano-sized dosimetric material undergoes a change, and accordingly TL glow curves of different intensity are obtained [30-32].

Due to the obtained nano-sized dosimetric material, a considerable increase in the intensity of the TL glow curve was determined. The reason of the observed change in nano-dosimeter is that nano-sized materials have the property of more accessibility carrier and ions depending on increase very quickly over the base material in the doping process. It is explained by the increase of trapped charged particles [29,33,34]. In this thesis magnesium tetra borate (MgB_4O_7) doped Sr was synthesized with various synthetic methods in microcrystalline and nano-sized structure. To improve the TL properties of the synthesized main structure, the doping process is performed [27].

In literature, methods of synthesis of the nanoparticles are expressed such as sol-gel, solution combustion synthesis, hydrothermal synthesis, and thermal decomposition of organometallic compounds, electrochemical reduction, radiological reduction, photochemical reduction, chemical reduction of metal salts in the literature. Furthermore, in their works in different years, Procik and co-researchers stated that magnesium borate is a complicated crystal structure [12,35]. They were produced MgB_4O_7 doped dysprosium, thallium, terbium, sodium and calcium, the dosimetric properties were examined and they have found an excellent dosimeter. MgB_4O_7: Dy, Na were synthesized in nano-sized with the combustion method and the nanoscale were decided by using X-ray powder diffraction

pattern in 2013.

In this study, it is emphasized that the particle size was approximately 100 nm [36]. Commonly, MgB_4O_7 was produced in microcrystalline form in some study [9,15,37]. The particle size of material is reduced with surface/volume ratio for the nano level, and activator ions are uniformly distributed in the phosphor crystals. As a result, the quantum yield of the phosphor and the luminescence efficiency is increased.

1.3.4 Thermoluminescence properties of ZnB_2O_4

As mentioned above, various specific of materials, such as phosphate, sulfate, fluoride, borate, and oxide have been investigated for innovation an appropriate thermoluminescence material in the TL dosimeters studies. Nowadays, to determine the appropriate commercial dosimeter, widely studies are being done by researcher for the ultimate TL dosimeter.

In another study, KCl doped ZnB_2O_4 was synthesized initially. Then, the TL properties of the material were analyzed. The principal dosimetric characteristics, which are explicitly the TL dose response, TL sensitivity, fading, minimum detectable dose, reproducibility, accuracy of dose measurement, and annealing process, will be examined for the phosphors having best glow curves to identify the usability of them in dosimetric applications.

As mentioned before, different borate compounds have a important place in technology because of their being luminescent, optical communication components, super-conductive materials, high temperature resistance and high corrosion resistance, fluorescent, ceramics industry, friction-reducing additives, and catalysts [8-18]. Therefore, the researcher progress about the synthesis of borate compounds. The zinc borate utilized in experimental studies have attracted the attention of many scientists recent years.

Borates and compounds have an extensive usage area due to their wide band width gap and tissue equivalent of the proximate as medical staff and dosimeter. However, the dosimetric properties such as thermal stability and TL sensitivity of the compounds depend on the method of construction of the material. The literature review shows that borate-based TLD dosimeters are usually prepared to microcrystalline structure and have a wide range of usage such as solidification, solution, melting, sintering, solid diffusion, and the single crystallization method in preparing TLDs. In this thesis zinc borate (ZnB_2O_4) doped KCl was synthesized with various synthetic methods in microcrystalline and nano-sized

structure. To improve the TL properties of the synthesized main structure, the doping process is performed [27].

In literature, methods of synthesis of the nanoparticles are expressed such as sol-gel, hydrothermal synthesis, and thermal decomposition of organometallic compounds, electrochemical reduction, radiological reduction, photochemical reduction, chemical reduction of metal salts in the literature. Furthermore, in their works in different years, Prokic and co-researchers stated that magnesium borate is a complicated crystal structure [12,35]. The same team produced MgB_4O_7 doped dysprosium, thallium, terbium, sodium and calcium, the dosimetric properties were examined and they have found an excellent dosimeter. MgB_4O_7: Dy, Na were synthesized in nano-sized with the combustion method and the nanoscale were decided by using X-ray powder diffraction pattern in 2013. In this study, it is emphasized that the particle size was approximately below 100 nm [36]. The particle size of material is reduced with surface/volume ratio for the nano level, and activator ions are uniformly distributed in the phosphor crystals. As a result, the quantum yield of the phosphor and the luminescence efficiency is increased.

In several studies, Zinc borate (ZnB_2O_4) is a boron-based material widely used for TL dosimeter investigations. In several studies, to increase and improve TL properties of ZnB_2O_4 several dopants (activators), like lanthanum, thulium, bismuth, dysprosium etc. have been applied on photoluminescence and thermoluminescence [38-40].

According to literature, there is no paper on this subject, which is potassium chloride (KCl) on as a dopant for ZnB_2O_4. Because of this Zinc borate was doped with KCl at several different concentrations in the study. The aim to examine the effect of KCl and KCl concentrations on thermoluminescance (TL) properties of compound, ZnB_2O_4.

CHAPTER 2

MODELS AND ANALYSIS OF THERMOLUMINESCENCE

2.1 Principles of Models for Thermoluminescence

As pointed out in chapter 1, according to the energy-band theory of solids, the obtained TL intensity explains properties of materials in the thermally stimulated process. The radiation incident on a TL material produces mobile electrons and holes then these are trapped in their states inside the band gap of the available material. The number of the filled traps is directly proportional to the incident amount of radiation dose. Nonetheless, TL intensity is evenly proportional to the filled traps' density. One of the purposes of dosimeters is to obtain knowledge about to absorbed dose and the radiation field from the measured TL emission [41].

The examination of thermoluminescence intensity is based on principles that describe the number of electrons and holes present in the traps and centers depend on time and temperature [42].

2.1.1 Randall - Wilkins model (First Order Kinetics)

The main mathematical process of TL was first extensively used by Randall and Wilkins in 1945. The process was performed obtained peak in the glow curve by them [2]. The mathematical process was investigated with the energy band model and formulated the well-known first order expression. In order to explain the event of model, Randall and Wilkins supposed that disregard trapping during the thermal phase.

To determine the TL theory, the energy-band theory of solids should be taking place only one type of electron trap (T) and just one type of recombination center (R) in the forbidden gap as shown in chapter 1, Fig. 2.1. It is considered that number of electrons present in the valence band in a (made in semiconductor or insulator) material.

According to this figure, the theoretical expression is applied with mathematical equations in TL theory [43]. In this theory, the electrons in the valance band release throughout the band gap when received radiation energy is greater than band gap energy ($h\gamma > E_g$). Due to the event, electron-hole pairs that have energy occur, after the thermal

process, generate free electrons and holes in the conduction band and the valence band respectively.

As is known the electron and the hole may combine in recombination center or catch in the trap. Furthermore, these processes are explained in detail in the previous chapter. According to the Arhenius equation, which is given below, there is a probability of releasing an electron from the trap.

$$p = s\exp\left\{-\frac{E}{kT}\right\} \tag{2.1}$$

At this point, p is the possibility per unit time, s is the factor of frequency, k the Boltzmann's constant, E is called the activation energy (eV) or depth of trap, here the activation energy required for transfer an electron from the trap to reach the conduction band of material, T the absolute temperature (K). The TL intensity $I(t)$ at specific time t during the thermal process is dependent upon the ratio of recombination of electrons and holes at any recombination centre R. Assume that m (m^{-3}) is equal the concentration of trapped holes at any R, then the intensity of TL can be given by

$$I(t) = -\frac{dm}{dt} \tag{2.2}$$

from here we consider that each one recombination process produces a photon and each created photons are revealed and recorded by the photomultiplier tube of the TLD reader. The amount of recombination must be related to the concentration of free electrons inside the conduction band n_c and the holes concentration m,

$$I(t) = -\frac{dm}{dt} = n_c mA \tag{2.3a}$$

where A is constant which is the recombination probability and considered that it is not dependent on temperature. The amount variation of the trapped electrons concentration n is equal to the amount of thermal release minus the amount of retrapping.

$$\frac{dn_c}{dt} = np - n_c(N-n)A_r - n_c mA \tag{2.3b}$$

If a trapped electron escapes from a single electron trap and recombination in an individual center, this electron/hole movement will be explained with Eqs.(2.3a)-(2.3b). As a result of the escape of the holes, rate equations are written as Eqs. (2.3a)-(2.3b) for TL.

These mathematical expressions are important and basic for analysis of TL development. Typical analytical solution cannot be found, so some simplifying assumptions must be made to develop critical expression. One of the significant assumptions is expressed by Chen and McKeever [43].

$$\left|\frac{dn_c}{dt}\right| << \left|\frac{dn}{dt}\right|, \qquad \left|\frac{dn_c}{dt}\right| << \left|\frac{dm}{dt}\right| \tag{2.4}$$

Above this assumption is named the quasi-equilibrium assumption in the theory. According to this assumption, the concentration of free electron must be quasi-stationary in the conduction band. The electron-hole pairs occur during the irradiation. Hence;

$$n_c + n = m \tag{2.5}$$

in case of $n_c \approx 0$, free charge can't accumulate in the conduction band throughout the thermal process, also in the case of $n \approx m$,

$$I(t) = -\frac{dm}{dt} \approx -\frac{dn}{dt} \tag{2.6}$$

Since $dn_c/dt \approx 0$ one obtains from (2.3a) and (2.3b):

$$I(t) = \frac{mAns \exp\left\{-\frac{E}{kT}\right\}}{(N-n)A_r + mA} \tag{2.7}$$

Here (2.7) can be solved analytically with added simplifying assumptions. Randall and Wilkins [2] assumed insignificant retrapping during the thermal process, i.e. they assumed $mA >> (N\text{-}n)A_r$. Thus, this asupposition Eq.(2.7) may be expressed

$$I(t) = -\frac{dn}{dt} = sn \exp\left\{-\frac{E}{kT}\right\} \tag{2.8}$$

The charge transport in the lattice is explained with this differential equation which is first-order (b=1) condition and the glow peaks are obtained from this equation, which is named first-order glow peaks. After by solving the distinctive equation (2.8) derivable,

$$I(t) = -\frac{dn}{dt} = n_o s \exp\left\{-\frac{E}{kT}\right\} \exp\left\{-s\int_0^t \exp\left\{-\frac{E}{kT(t')}\right\} dt'\right\} \tag{2.9}$$

in this equation n_0 is the whole of trapped electrons at time t=0. Commonly the temperature is changed to depend on the linear function of time

$$T(t) = T_o + \beta t \tag{2.10}$$

here T_0 is the temperature of material at time t=0 and β is the heating rate. This gives for the intensity as function of temperature

$$I(T) = -\frac{1}{\beta}\frac{dn}{dt} = n_o \frac{s}{\beta}\exp\left\{-\frac{E}{kT}\right\}\exp\left\{-\frac{s}{\beta}\int_{T_o}^{T}\exp\left\{-\frac{E}{kT'}\right\}dT'\right\} \tag{2.11}$$

In theory, this equation is the famous Randall–Wilkins first-order expression for a single glow peak. The peak shape of any form is characteristic of material. The theory is expressed that the low temperature part is wider than the high temperature part.

In the low temperature section, i.e. in time of the initial rise of the graph (the glow peak), the intensity is controlled by the first exponential equation (exp (-E/kT)). So, if the graph is drawn function of 1/T versus I, a linear line is expected in the initial rise temperature section. The activation energy E is smoothly found from slope of -E/k.

There are some properties of the Randall–Wilkins equation in Fig. 2.2. In Fig. 2.2 (a) it is demonstrated I(T) varies when n_0 varies from n_0 = 0.25 m^{-3} till n_0 = 2 m^{-3} while E=1 eV, s=1.0×10^{12} s^{-1} and β=1 K/s are saved constant.

In glow curve, the temperature at the peak is represented as maximum(T_m) and remains stabled. This characteristic case is observed for all first-order TL curves. The situation for the maximum value may be evaluated by setting dI/dt=0 (or, easier from dlnI(T)/dt=0). From this situation one obtains

$$\frac{\beta E}{kT_m^2} = s\exp\left\{-\frac{E}{kT_m}\right\} \tag{2.12}$$

Because of T_m independent on n_0, in this above equation n_0 do not exist. From Fig .2.2 (a) it may be additional understood that not only each point of the curve is proportional to n_0, but also the peak height at the maximum. In this equation n_0 is the important parameter for dosimetry application. Because, the absorbed dose is proportional to the parameter n_0. The area under the glow peak is equal to n_0, which can be obtained in the following equations.

$$\int_0^{\infty} I(t)dt = -\int_0^{\infty}\frac{dn}{dt}dt = -\int_{n_0}^{n_\infty} dn = n_0 - n_\infty \tag{2.13}$$

In equation n_∞ is must be zero for $t \to \infty$. In Fig. 2.2 (b) in this case, the activation energy of material has been transformed from 0.8 to 1.2 eV. While the activation energy increases the peak moves to higher temperatures with a decrease in the height and an increase in the breadth protection zone (i.e. n_0) constant.

Identical variations may be observed as s is altered. (see Fig.2.2(c)) however, the new status exactly contrary: the peak moves to lower temperatures when s increases at the same time the peak of height increase and the peak of breadth decreases. In Fig. 2.2 (d) the heating rate has been altered.

The peak moves to higher temperatures when β increases at the same time the peak of height decreases but in the case of decreasing s peak of breadth decreases. As a result of this can be obtained from s and β, then may be written a ratio s/β in Eq. (2.11).

It is significant to note that of the four factors, the activation energy E and the frequency factor s, are the essential physical factors. There are four important agents, which are the activation energy, the frequency factor, specific heating rate and specific dose in the theory.

The trapping parameters, which are activation energy, the frequency factor obtained for the characteristic of the trapping center. The specific heating rate and the specific dose are may be selected by the researcher. In new TL material research, practice of the absorbed dose and the heating rate to be continue as a kind of work.

The consideration of Eqn. (2.11) is hindered because of the integral on the right adjacent is not basic in the event of linear heating [44]. The integral can be solved by asymptotic series in the equation. It is appropriate to define terms of parameters for exact solution in the glow peak.

The parameters are easy to derive from the glow curve experimentally. Both the intensity of peak and the temperature for their maximum value is represented with I_m and T_m, respectively.

The expression of integral in Eqn. (2.11) cannot be resulted with an analytical solution, but if some successive integration is applied, it is obtained within second-order integral approximation, then it changes,

$$\int_{T_0}^{T} \exp(-\frac{E}{kT'})dT' = \frac{kT^2}{E}(1-\frac{2kT}{E})\exp(-\frac{E}{kT}) \tag{2.14}$$

Hence, Eqn. (2.14) becomes

$$I(T) = sn_0 \exp\left(-\frac{E}{kT}\exp\left[-\frac{skT^2}{\beta E}(1-\frac{2kT}{E})\exp(-\frac{E}{kT})\right]\right) \tag{2.15}$$

Since here the condition at the top is written as in Eqn. (2.12) or

$$s = \frac{\beta E}{kT_m^2}\exp\left\{-\frac{E}{kT_m}\right\} \tag{2.16}$$

Inserting Eqn.(2.16) into Eqn.(2.15) one gets

$$I_m = \frac{n_0 \beta E}{kT_m^2}\exp\left[-\left(1-\frac{2kT_m}{E}\right)\right] \tag{2.17a}$$

or better

$$I_m = \frac{n_0 \beta E}{kT_m^2}\exp\left[-(1-\Delta_m)\right] \tag{2.17b}$$

Equation (2.17b) can be noted down as

$$\frac{n_0 \beta E}{kT_m^2} = I_m \exp\left[-(1-\Delta_m)\right] \tag{2.18}$$

Putting into Eqn. (2.12) into Eqn.(2.11), Kitis et al[45] have expressed that Eqn. (2.11) can be very accurately perceived as

$$I(T) = I_m \exp\left[1+\frac{E}{kT}\frac{T-T_m}{T_m}-\frac{T^2}{T_m^2}\exp\left\{\frac{E}{kT}\frac{T-T_m}{T_m}\right\}(1-\Delta)-\Delta_m\right] \tag{2.19}$$

with

$\Delta=2kT/E$ and $\Delta_m=2kT_m/E$.

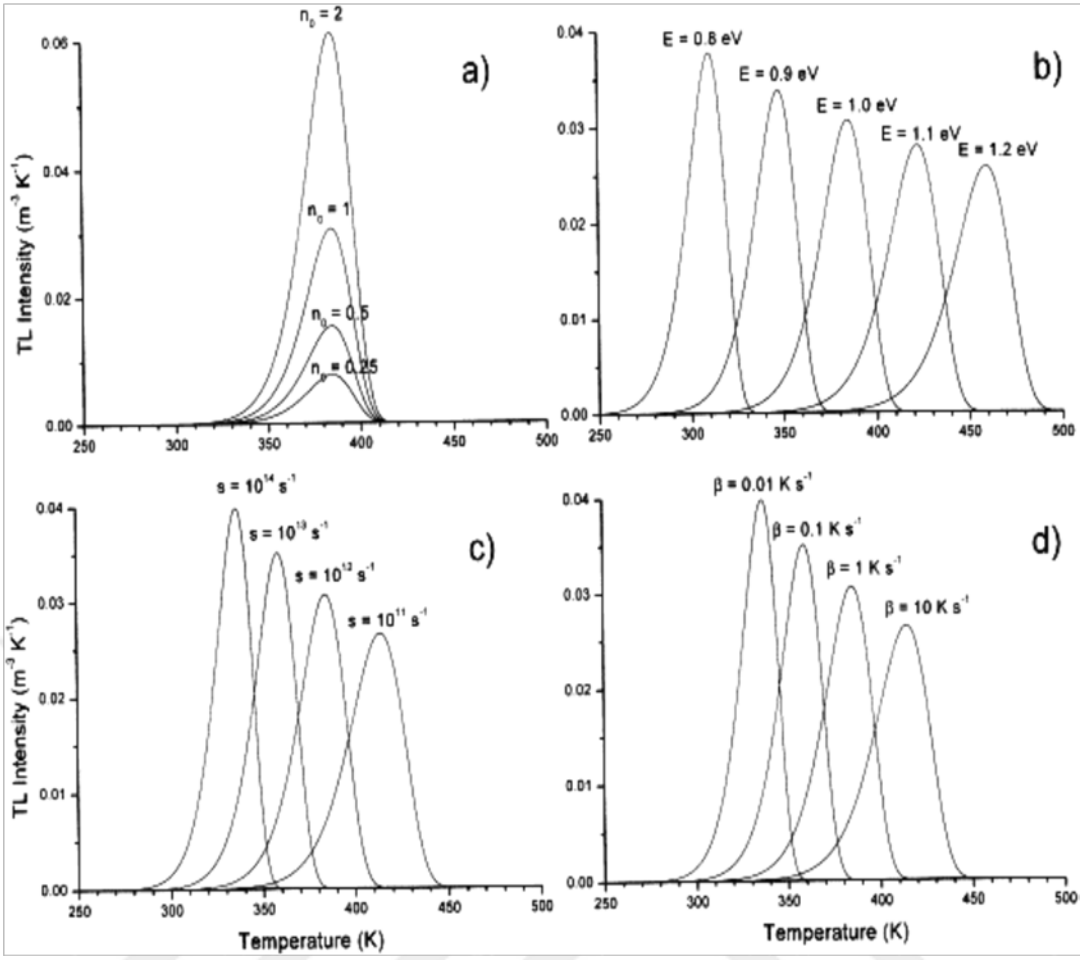

Figure 2.1 Statuses of the R–W first-order TL equation are demonstrated, (a) variation with n_0, the concentration of trapped charge carriers after irradiation; (b) the variation with E, the activation energy; (c) the variation with s, the escape frequency factor; (d) the variation with β, the heating rate. Parameter values: n_0=1 m^{-3}; E=1 eV; s=1×10^{12} s^{-1}, β=1 K/s of which one parameter is altered while the others are kept constant [43].

2.1.2 Garlick- Gibson model (Second Order Kinetics)

Garlick and Gibson [46] asserted different options that retrapping or recombining in their studies on phosphorescence. In this theory, free electron and hole can be either re-trapped within a trap or recombining inside of a recombination center. In equation of the second order kinetics, $mA << (N\text{-}n)A_r$ situation used to describe retrapping event.

They considered that the free electrons (they trapped before) have equal possibility of being retrapped or recombining with a hole in a recombination center. Additional they considered that the trap is far from being saturation condition, i.e. $N>>n$ and $n=m$. By using these assumptions, Eqn. (2.7) becomes

$$I(t) = -\frac{dn}{dt} = s\frac{A}{NA_r}n^2 \exp\left\{-\frac{E}{kT}\right\} \tag{2.20}$$

The rate of dn/dt is proportional to n^2 for second-order equation. If the equal probabilities of recombination and retrapping is supposed in this circumstance, A=A_r may take for integration of Eqn. (2.20) and gives

$$I(T) = \frac{n_0^2}{N}\frac{s}{\beta}\exp\left\{-\frac{E}{kT}\right\}\left[1+\frac{n_0 s}{N\beta}\int_{T_0}^{T}\exp\left\{-\frac{E}{kT'}\right\}dT'\right]^{-2} \tag{2.21}$$

This equation is well known as the Garlick–Gibson TL equation for second-order kinetics. If the glow curve is examined carefully, it is appear nearly symmetric. But there is a small difference that the high temperature half of the camber partially wider than the low temperature half. We deduce that considerable concentrations of free electrons are re-trapped before they recombine in a second-order reaction. Thus, bringing about a delay in the luminescence emission and emit light over a widespread temperature range. Where, in the first-order situation, the initial concentration n_0 is obtained a constant value, thus the shape of the curve can be changed variation at different dose levels. This is demonstrated in Fig.2.1 (a). It is realized that T_m decreases as n_0 increases. It may be resulting [5] that the temperature shift may be approached by

$$T_1 - T_2 \approx T_1 T_2 \frac{k}{E}\ln f \tag{2.22}$$

There are two temperatures in this equation, at a specific dose T_1 is the temperature (at maximum intensity) at f times higher dose T_2 (at maximum intensity). By using parameter values of Fig.2.1 (a) the move is 25 K. While conditions are suitable as E=1 eV, T_1 = 400 K and the absorbed doses are increased thanks to a factor of 1000, which is achieved with experiment, in this case the temperature movement of 77 K can be estimated. By means of Eqn. (2.22) in the shallower trap it follows the path for a given increase of the dose, i.e., the minor E, the major peak shift. Fig. 2.1 (b) demonstrates the shift of graphs in size and status of a second-order peak by using function of E, in Fig.2.1 (c) s represent function of s/N, and in Fig.2.1 (d) demonstrates as a function of the heating rate. The region under the glow curve is proportional to the initial concentration n_0 in first-order kinetics status in figure. Following this the peak height is proportional to the region under the peak, though the variation is minor.

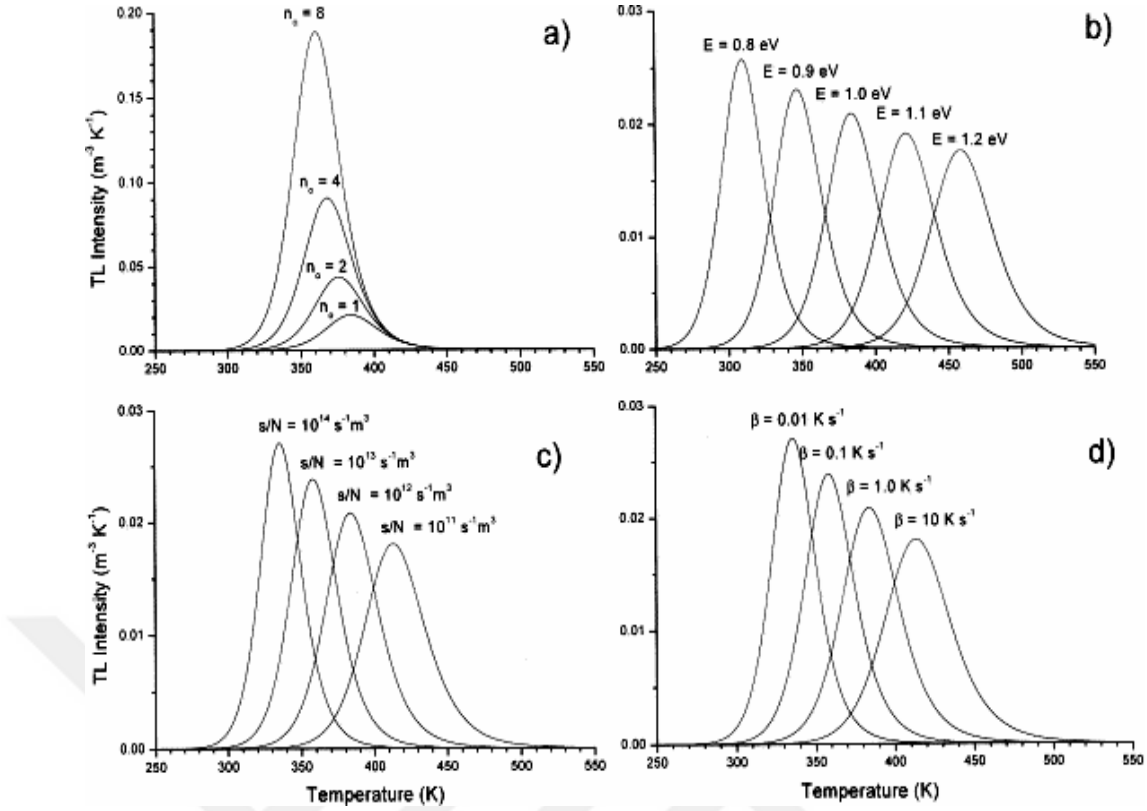

Figure 2.2 Statuses of the Garlick–Gibson second-order TL equation, exhibition: (a) the concentration of trapped electron/hole after irradiation, change with n_0; (b) the activation energy,change with E; (c) the change with s/N; (d) the change with β(heating rate). Parameter values: n_0=1 m^{-3}; E=1 eV; s/N=1×10^{12} s^{-1} m^3, β=1 K/s of which one of the parameters is variables while the others are remain constant [43].

This theory, in addition to the first-order status, in the initial rise the dominant temperature proportional to exp(-E/kT). Because of this the Initial Rise Method can be applied for the assignment of the trap depth.

Adding the integral approximation given by Eqn.(2.14) in Eqn.(2.18), one gets

$$I(T) = sn_0 \exp\left\{-\frac{E}{kT}\right\}\left[\frac{skT^2}{\beta E}(1-\Delta)\exp(-\frac{E}{kT})+1\right]^{-2} \tag{2.23}$$

from which the state is written below at the maximum

$$s = \frac{\beta E}{kT_m^2}\frac{1}{1+\Delta_m}\exp\left(\frac{E}{kT_m}\right) \tag{2.24}$$

or in alternative shape

$$s\exp\left(-\frac{E}{kT_m}\right)=\frac{\beta E}{kT_m^2}\frac{1}{1+\Delta_m} \tag{2.25}$$

Additionally, Eqn.(2.23) may be modified for the peak at the maximum:

$$I_m = sn_0\exp\left\{-\frac{E}{kT}\right\}\left[\frac{skT_m^2}{\beta E}(1-\Delta_m)\exp(-\frac{E}{kT})+1\right]^{-2} \tag{2.26}$$

The addition of Eqn.(2.24) into Eqn.(2.23) gives the next statement for *I(T)*

$$I(T)=\frac{n_0\beta E}{kT_m^2}\frac{1}{1+\Delta_m}\exp\left[\frac{E}{kT}\left(\frac{T-T_m}{T_m}\right)\right]\ x\left(\frac{T^2}{T_m^2}\frac{1-\Delta}{1+\Delta_m}\exp\left[\frac{E}{kT}\left(\frac{T-T_m}{T_m}\right)\right]+1\right)^{-2} \tag{2.27}$$

Adding Eqn.(2.25) into Eqn.(2.26) becomes a more simplified statement for I_m:

$$I_m=\frac{n_0\beta E}{kT_m^2}\frac{1}{1+\Delta_m}(\frac{2}{1+\Delta_m})^2 \tag{2.28}$$

which may be modified as

$$\frac{n_0\beta E}{kT_m^2}\frac{1}{1+\Delta_m}=I_m(\frac{2}{1+\Delta_m})^2 \tag{2.29}$$

Eqn.(2.28) is now added into Eqn.(2.27) the final statement will be reached the TL intensity:

$$I(T)=4I_m\exp(\frac{E}{kT}\frac{T-T_m}{T_m})\times\left[\frac{T^2}{T_m^2}(1-\Delta)\exp\left\{\frac{E}{kT}\frac{T-T_m}{T_m}\right\}+1+\Delta_m\right]^{-2} \tag{2.30}$$

with Δ and Δ_m the same meaning as in Eqn. (2.19).

2.1.3 May – Partridge model (General Order Kinetics)

If the obtained curve is unsuitable for first or second order kinetics status, the general order kinetics status can be applied in case of intermediate equations. The general order kinetics, was formulized by May and Partridge [47]. In the intermediate kinetic process, an empirical expression was written due to experimental situations. According to these

researchers, the energy level of traps must be single in the model. The general-order kinetics can be written by

$$I(t) = -\frac{dn}{dt} = n^b s' \exp\left\{-\frac{E}{kT}\right\} \tag{2.31}$$

where s' has the dimension of $m^{3(b-1)}$ s^{-1} and b are expressed as the general-order parameter. Integration of Eqn.(2.31) for $b \neq 1$ yields

$$I(T) = sn_0 \exp\left\{-\frac{E}{kT}\right\}\left[1 + \frac{s(b-1)}{\beta}\int_{T_0}^{T} \exp\left\{-\frac{E}{kT'}\right\} dT'\right]^{-\frac{b}{b-1}} \tag{2.32}$$

here $s'' = s' n_0^{b-1}$ with unit s^{-1}. Eqn. (2.32) involves the second-order status (b=2) and decreases to Eqn.(2.11) when $b \rightarrow 1$.

Expression must be written that according to Eqn. (2.31) the dimension of s' must be $m^{3(b-1)}$ s^{-1} the dimension alters with the order b and hard to evaluate physically.

It converts in the subsequent equation using the approximation in Eqn. (2.14):

$$I(T) = sn_0 \exp\left\{-\frac{E}{kT}\right\}\left[\frac{(b-1)skT^2}{\beta E}(1-\Delta)\exp\left(-\frac{E}{kT}\right)+1\right]^{b/(b-1)} \tag{2.33}$$

Here, at the peak maximum, the intensity is formulated by

$$I_m = sn_0 \exp\left\{-\frac{E}{kT}\right\}\left[\frac{(b-1)skT^2}{\beta E}(1-\Delta_m)\exp\left(-\frac{E}{kT_m}\right)+1\right]^{b/(b-1)} \tag{2.34}$$

The maximum condition, obtained from Eqn.(2.33), is

$$\frac{\beta E}{kT_m^2} = Z_m s \exp\left(-\frac{E}{kT_m}\right) \tag{2.35}$$

with

$$Z_m = 1 + (b-1)\Delta_m \tag{2.36}$$

Eqn.(2.35) may be interpreted two alternative style:

$$s = \frac{\beta E}{kT_m^2}\frac{1}{Z_m}\exp(-\frac{E}{kT_m}) \tag{2.37}$$

or

$$s\exp\left(-\frac{E}{kT_m}\right) = \frac{\beta E}{kT_m^2 Z_m} \tag{2.38}$$

Adding Eqn.(2.37) into Eqn.(2.33) we get the subsequent expression for the intensity:

$$I(T) = \frac{n_0 \beta E}{kT_m^2 Z_m}\exp\left\{-\frac{E}{kT}\frac{T-T_m}{T_m}\right\} x\left[\frac{(b-1)}{Z_m}\frac{T^2}{T_m^2}(1-\Delta_m)\exp\left(-\frac{E}{kT}\frac{T-T_m}{T_m}\right)+1\right]^{b/(b-1)} \tag{2.39}$$

Inserting Eqn.(2.39) into Eqn.(2.33), the expression is obtained at the maximum for the intensity, after editing

$$I_m = \frac{n_0 \beta E}{kT_m^2 Z_m}(\frac{b}{Z_m})^{-\frac{b}{b-1}} \tag{2.40}$$

from which

$$\frac{n_0 \beta E}{kT_m^2 Z_m} = I_m(\frac{b}{Z_m})^{-\frac{b}{b-1}} \tag{2.41}$$

Insertion of Eqn.(2.41) into Eqn.(2.39) the final equation is obtained for the TL intensity:

$$I(T) = I_m(b)^{\frac{b}{b-1}}\exp\left\{\frac{E}{kT}\frac{T-T_m}{T_m}\right\} x\left[(b-1)(1-\Delta)\frac{T^2}{T_m^2}\exp\left(\frac{E}{kT}\frac{T-T_m}{T_m}\right)+Z_m\right]^{-\frac{b}{b-1}} \tag{2.42}$$

The general-order situation is convenient for intermediate situation. Furthermore, it may be applied for first- and second-orders when $b \to 1$ and $b \to 2$, respectively.

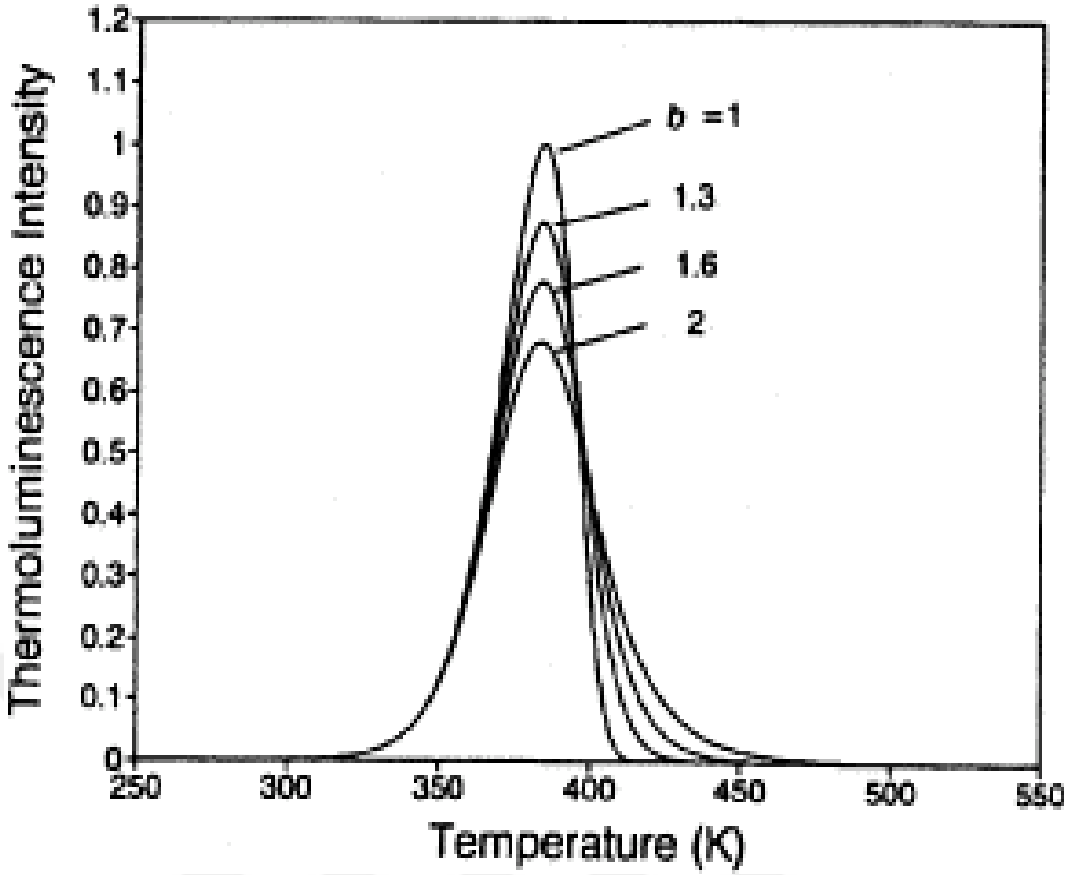

Figure 2.3 Comparing of first-order (b=1), second-order (b=2) and intermediate-order (b=1.3 and 1.6) TL peaks, with E=1 eV, s=1×10^{12} s^{-1}, n_0=N=1 m^{-3} and β=1 K/s [41].

2.1.4 Advanced models

In this model, if the material is heated, some of the traps will be active in the specific temperature. The traps can be filled with electrons during irradiation when the thermally disconnected traps. However, if the material is heated, the trap depth will be much greater than the active trap, and so electrons trapped in the active trap (AT) and the shallow trap (ST) (see Fig.2.4 (a)).

The electrons, which are trapped in deeper traps, are uninfluenced and this deep trap of electron is considered to be thermally disconnected. (shown in Fig.2.4 (a) with DET) According to its existence, there is an impact on the trapping filling and finally on the glow curve peak [48].

As mentioned in section 2.1.1 it was supposed that the trapped holes are stabled in the recombination center while the trapped electrons are released during heating process. Contrary to the above, the electrons are fixed while holes are released during heating

process is statistically similar. But, if holes and electrons are released from their traps at the same temperature and time phase, the condition will alter.

In this situation, the holes and electrons are thermally released from the same centers and move the recombination places (see Fig.2.4 (b)). In this state Eqn. (2.2) is no more valid.

According to the chosen values of the parameters, this complex kinetic model emerges a TL glow curve, which appears the Randall–Wilkins equation. (Eqn.(2.11)) or Garlick–Gibson (Eqn.(2.21)) shape. Nonetheless, the E and s values used in Eqn. (2.11) and Eqn.(2.21) to get a suitable complex kinetic model and we need more explication.

Furthermore, in the conduction bands a recombination event may take place without a transition of the electron (Fig.2.4(c)). By using the heat process, the electron is stimulated into an excited state, and so the transition event occurs in the recombination center.

The electron/hole transition probability can be vigorously related to the distance, which is between the two centers. The TL intensity can be derived from Eqn. (2.11) with the same format, but with *s* replaced by a quantity linked to the probability of recombination. It is known as the first order kinetics due to these localized transitions.

Another possibility, there could be a trapped electron in the defect which is not stable but is participating with another defect interaction (Fig.2.4 (d)). The trap depth can be changing at low temperature when the trapped electron concentration is stable.

On the other hand, there are two processes, which are related to electrons at higher temperatures: the getaway to the conduction band and the reaction of imperfection. Piters and Bos [49] said that imperfection reactions placed into the rate equations and glow curves. It seems that the glow curves may be very well settled by Eqn. (2.11).

As mentioned already, there are many parameters in a TL peak, such as, the frequency factor (*s*), the trap depth (*E*), the concentrations of the numerous recombination centers and traps, the capture cross-sections, etc.

The thermoluminescence experiments are carried out to get data from an experimental cluster of glow-curves. Then, the data is used to calculate the some parameters values related to the electron/hole transmission in the material.

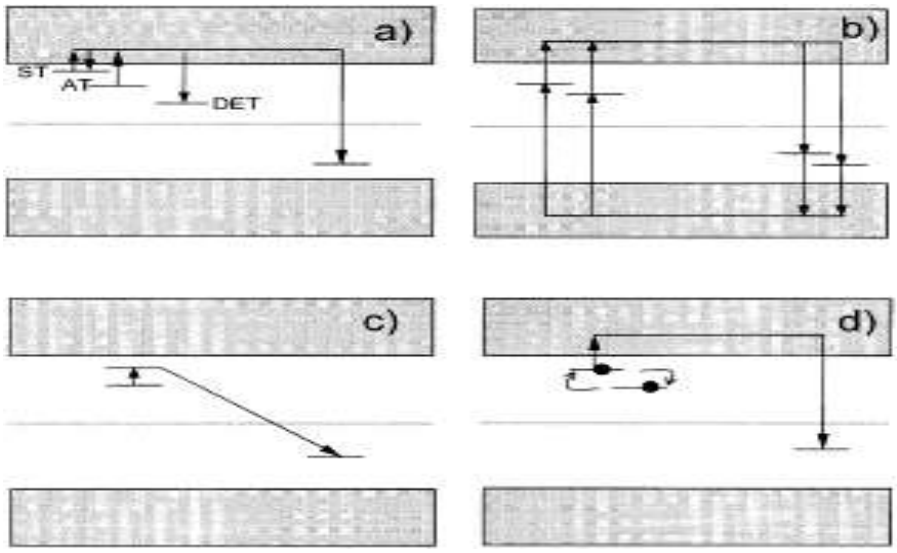

Figure 2.4 In advanced models, the trapped charged carriers stimulated thermally: (a) a shallow trap (ST), a deep electron trap (DET), and a active trap (AT); (b) two recombination centers and two active traps; (c) localized transitions; (d) defect interaction (trapping center interacts with another defect) [44].

2.2 Thermoluminescence Analysis

In general terms, thermoluminescence analysis starts by selecting the rate equations suitable a particular model and continuous by introducing simplifying assumptions into these equations in order to reach an analytical expression. The change is explained in thermoluminescence intensity with temperature, in terms of the desired parameters by the critical expression.

From these mentioned equations even simpler expressions are obtained, which concern the parameters directly to the data. In order to describe the thermoluminescence production, firstly the operation requires an assumption, and secondly by introducing further assumptions play bounds the generalization, and probably the validity, of the results obtained.

The very often-preferred model is the basic two-level model for analysis, sometimes with the addition of a third level (i.e., thermally disconnected traps). Nevertheless, no tests are carried out to (a) check the validity of the simple model, and (b) verify that the approximations place violent restrictions on the kinetics of the thermoluminescence emission [47].

2.3 Methods of Analysis

As is known by using the glow-curve the trapping parameters can be get with some analysis methods. The successful contributions of Randall & Wilkins and Garlick & Gibson obviously cannot be ignored. After their work, many researchers worked on their studies with methods of analysis. On the subject of the dosimeter, the identification of parameters from the glow curves has been obtained for the last fifty years. Today, researchers have numerous methods of analysis for determining the trapping parameters from the values of glow curves [2,48-53]. If one glow peak is used with isolated from the others; in general, the experimental methods are applied such as isothermal decay, peak shape, variable-heating rates and initial raise methods. These methods are convenient to obtain the kinetic parameters of materials. These methods will be described in detail below.

2.3.1 Heating Rate Method

To compute the trap depth (activation energy), various heating rate methods are used for TL analysis. In this method, both the heating function and the heating rate are constant but the heating function is linear, and the shape of the TL peak changes at the maximum temperature Tm. According to this, if a material is given heat at two different linear heating rates β_1 and β_2 result of the peak should be different values. Then, the equation (2.43) may be formulated for each heating rate and dividing the equation for β_1 (and T_{m1}) by the equation for β_2 (and T_{m2}) and reorganizing, as a result we can obtain an accurate equation for the compute of E

$$E = k \frac{T_{m1} T_{m2}}{T_{m1} - T_{m2}} \ln[(\frac{\beta_1}{\beta_2})(\frac{T_{m2}}{T_{m1}})^2] \qquad (2.43)$$

In the event of obtaining a big peak wrapped by smaller hill, may be evaluated by data. This data is may be found at a peak maximum (T_m, I_m) from the glow curve, and the data is enough for analyzing in the heating rate method. In this method, computation of E is independent of thermal quenching, but there was the problem in the initial rise method.

On the other hand, this method is not sufficient for the activation energies of the smaller peaks, which is to be desired. To determine the T_m, thermal cleaning may separate the smaller peaks. This situation is valid just for first order curves. Identical situations

apply when two (or more) peaks are nearly overlapping, they appear as one mixed peak [50].

In this method, the important point that has to be taken into consideration to avoid large errors which is lag (TLA) the temperature lag (TLA) in the kinetic parameters. The temperature lag (TLA) occurs between the thermoluminescent sample and the heating factor during the TL readout in contact heating. Kitties and Tuyn proposed a simple method prevent from this problem [54]. The following equation is used for exact peak by them after different heating rates:

$$T_m^j = T_m^i - C\ln\left(\frac{\beta_i}{\beta j}\right) \tag{2.44}$$

where T_m^j and T_m^i are the maximum temperatures of a glow peak with heating rates β_j and β_i, respectively, and *C* is a constant, which is initially assessed by using two very low heating rates where TLA may be regard as trivial. In order to compute the constant C, It is recommended that the low heating rates should be chosen below $1^oC\ s^{-1}$.

The various heating rates for the first-order kinetics are used, the equation below can be described as:

$$\ln(\frac{T_m^{\ 2}}{\beta}) = (\frac{E}{k})(\frac{1}{Tm}) + cons\tan t \tag{2.45}$$

Taking these considerations into account, A plot of $\ln(T_m^2/\beta)$ versus $(1/T_m)$ must yield a straight line with a slope *E/k*, where *E* is found. Moreover, extrapolating to $1/T_m = 0$, a value for $\ln(sk/E)$ is gotten from which *s* can be calculated by inserting the value of *E/k* found from the slope. The various heating rates method is feasible for general-order kinetics. In the general order case the graph can be plotted in $\left[I_m^{\ b-1}(T_m^{\ 2}/\beta)^b\right]$ versus $1/T_m$, whose slope is equal to *E/k.*

2.3.2 Peak Shape Method

The calculations of trap parameters are dependent on the shape of the glow curve peak. In this method two or three points are selected from the glow curve. The shape of peak, T_m is the maximum peak temperature, T_1 is the low temperature half height and T_2 is the high-temperature half height. They are determined from the glow curve. There are some definitions in this method for calculation of *E* from the shape of the peaks. These

definitions which are $\omega = T_2-T_1$, $\delta = T_2-T_m$, $\tau = T_m-T_1$, and $\mu_g=\delta/\omega$ are called the shape parameter and are shown in Figure 2.5.

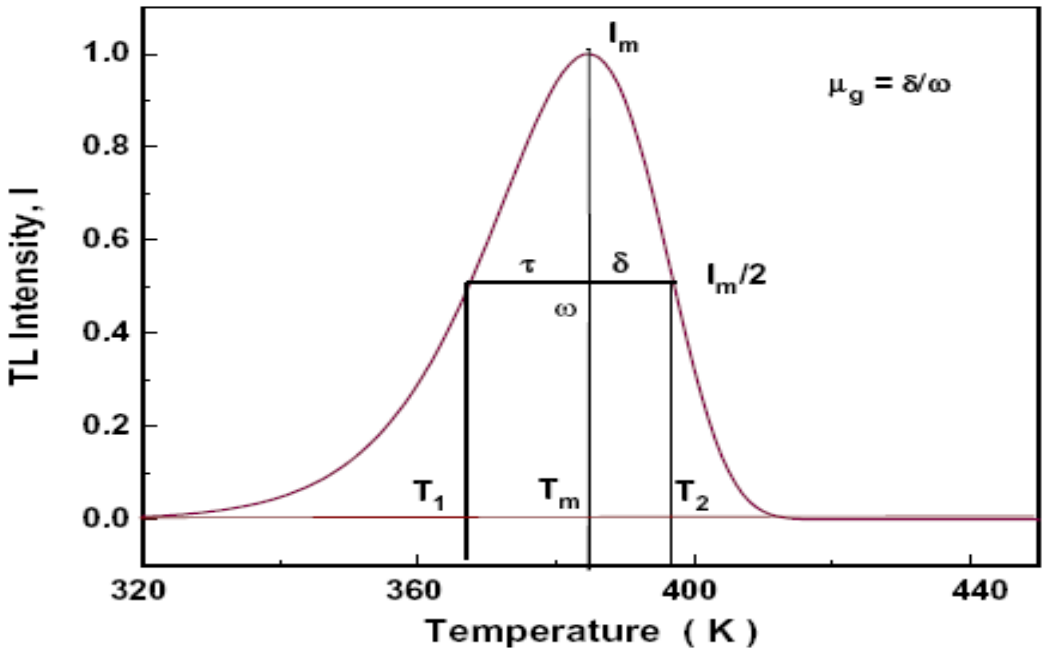

Figure 2.5 The peak-shape parameters on a TL glow curve [55].

The detection of kinetics b can be determined via the shape parameters in this method [52] revealed that μ_g is not a sufficient calculating alteration for E and s, but it can alter with the kinetics order (b) in this method. It can be expressed with domains of μ_g changes from 0.42 for b=1 to 0.52 for b=2 for linear heating in this system (Figure 2.6).

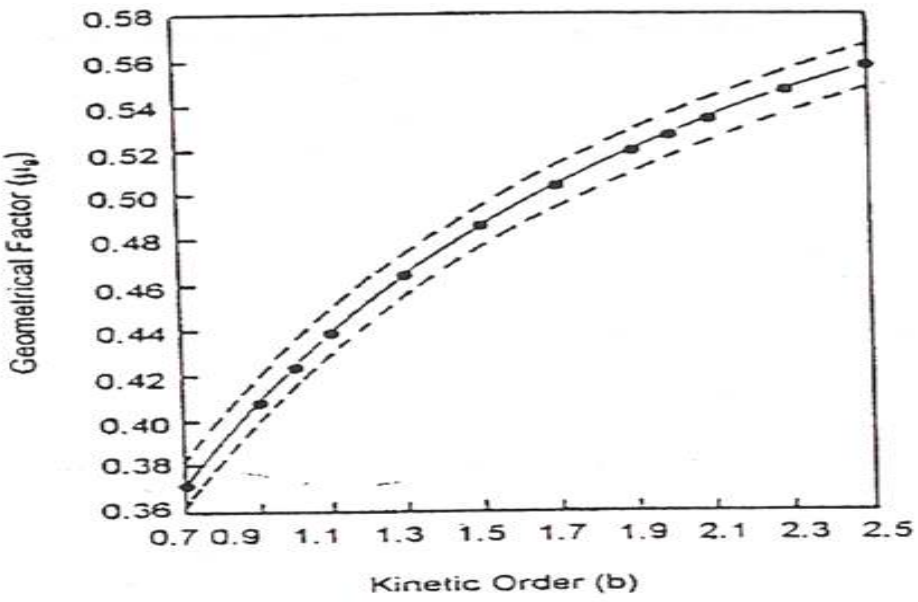

Figure 2.6 Geometrical factors(μ_g), as a function of the given order[56].

Grossweiner [55] improved the first peak shape method, and then Chen [49] reformulated Halperin and Braner's equations [57] for computing E values;

$$E_\tau = \left[1.51 + 3(\mu_g - 0.42)\right]\frac{kT_m^2}{\tau} - \left[1.58 + 4.2(\mu_g - 0.42)\right]2kT_m$$
$$E_\delta = \left[0.976 + 7.3(\mu_g - 0.42)\right]\frac{kT_m^2}{\delta} \qquad (2.46)$$
$$E_\omega = \left[2.52 + 10.2(\mu_g - 0.42)\right]\frac{kT_m^2}{\omega} - 2kT_m$$

From the above equation, kinetic order and the activation energy are obtained, and then the frequency factor *s* is produced from the following expressions, the equation's result can be referred to the as pre-exponential factor in the general order kinetic.

$$s = \frac{\beta E}{kT_m^2}\ \exp\left[\frac{E}{kT_m}\right]$$
$$s = \frac{\beta E}{kT_m^2}\left[\exp(-\frac{E}{kT_m})(1 + (b-1)\frac{2kT_m}{E})\right]^{\frac{b}{b-1}} \qquad (2.47)$$

In addition, the kinetic parameters of peak are obtained from Gartia, Singh & Mazumdar [58] the peak shape method. In this method, activation energy is calculated by using any three points of a peak. This energy is expressed as follows

$$E_a = \frac{CkT_m^2}{\left|T_x - T_y\right|} + DkT_m \qquad (2.48)$$

where $\left|T_x - T_y\right| = \tau, \delta, \omega$. In the equation above, *C* and *D* are coefficients which are obtained from least squares method for different kinetics order in the domain from 0.7 to 2.5 and for *x* = 1/2, 2/3, 4/3. For a particular value of *x* the measurements' results are dependent on *b* and can be expressed as a quadratic function of *b* itself. So that, the previous equation can be rewritten as

$$E_a = \frac{(C_0 + C_1 + C_2 b^2)kT_m^2}{\left|T_x - T_y\right|} + (D_0 + D_1 b + D_2 b^2)kT_m \qquad (2.49)$$

2.3.3 CGCD Method

In this method, instead of heating and adding addition doses to obtain values for the parameters E, s and b, by using this method many overlapping glow peaks can be separated. The methods of computerized curve fitting have been applied for overlapping glow peaks on several occasions with apparent success.

The process is to determine the closed positions of the most evident peaks in the glow curve. By using the general-order equation for b ≠ 1, or the first-order equation for b=1 a theoretical curve is calculated. The calculated curve, which is obtained from this method, is correlated with the exact result of the experimental curve. Root Mean Square (RMS) deviation method is applied between the two results.

Due to the reasons, which are mentioned above, the method has proved to be more successful than experimental methods [50]. This program was developed at the Reactor Institute at Delft, The Netherlands [59]. This program which is gifted of simultaneous deconvolution as many times as possible peaks (obtained from glowcurve). In this computer program two different patterns were used. In the first pattern, by using the following statetment the glow curve is approached from first order kinetics.

$$I(T) = n_0 s \ \exp(-\frac{E}{kT})\exp\left[(-\frac{s}{\beta}\frac{kT^2}{E}\exp(-\frac{E}{kT}) * (0.9920 - 1.620\frac{kT}{E_a})\right] \tag{2.50}$$

By using the following statement, the glow curve is approached from general order kinetics,

$$I(T) = n_0 s \ \exp(-\frac{E}{kT})\left[1 + (-\frac{(b-1)s}{\beta}\frac{kT^2}{E}\exp(-\frac{E}{kT}) * (0.9920 - 1.620\frac{kT}{E_a})\right]^{\frac{b}{b-1}} \tag{2.51}$$

As is known, statement n_0 (m^{-3}) is represented as the concentration of trapped electrons at t=0, s (s^{-1}) is represented as the frequency factor both first-order and the general-order (the pre-exponential factor), E (eV) is represented as the activation energy, T (K) is represented as the absolute temperature, k (eVK^{-1}) Boltzmann's constant, β($^0Cs^{-1}$) is represented as heating rate and b is represented as the kinetic order.

The summary of total peaks and background contribution can lead to composite glow curve formula as written below

$$I(T) = \sum_{i=1}^{n} I_i(T) + a + b\exp(T) \tag{2.52}$$

here, *I(T)* is the settled value for total glow curve, *a*is the factor which accepts electronic noise value for the planchet and dosimeters infrared value for the background.

By using the above equation (2.52), the minimum square minimization process and FOM (Figure of Merit) was applied to critic the agreed on results.

$$FOM = \sum_{i=1}^{n} \frac{\left|N_i(T) - I(T)\right|}{A} = \sum_{i=1}^{n} \frac{\left|\Delta N_i\right|}{A} \tag{2.53}$$

in this expression, $N_i(T)$ is the i-th experimental points (as approximately n=200 data points), *I(T)* is the i-th fitted points, and *A* is the totalfield of the settled glow curve.

There are three obtained states in studies for FOM values [42,60]. These are from 0.0% to 2.5% the fitting is good, 2.5 % and 3.5% the fitting is fair and value > 3.5% fitting is bad. In order to obtain an agreement between fitted glow curves and experimental results, a graphic representation is plotted via the computer program with the following function,

$$X(T) = \frac{N_i(T) - I_i(T)}{\sqrt{I_i(T)}} \tag{2.54}$$

in expression as a usual variant value 0 and σ=1 where $\sigma^2(T)=I_i(T)$ is expected.

CHAPTER 3

NANOPARTICLES

Nanoscience is basically to be able to control materials in molecular and atomic scale. The Nanoscience concept, measuring the quantity of existing objects in the universe, with the identification and characterization, the property of those objects is foreseen examining with a deeper perspective [63].

The word nano is one billionth of any physical size. It takes place from 10-100 atoms as evaluated with magnitude. The basic work field of nanoscience is a structure, which contains a range from 10 nm to 100 nm.

Nanoscience, by treating the matter in nano level, produces detectable new material in molecular/atomic scale such as systems, material, structures. Generally, there have been several differences between nanoparticle and macroparticle in the same matter. The goal is to obtain operational devices and systems, by using the matter, which has gained by various physical, chemical and biological properties in this size [64].

The material structure gets stronger and harder for metal; it becomes more easily processed for ceramics, on a descending scale from bulk to nano-sized [65]. The insulating materials can transmit heat or electricity and was observed to use the return to form as a protective coating in nanoscale.

The properties of the material are not continuous, they are no longer discrete such as; energy, momentum, and mass in the nanoscale. The properties of nanostructures, which act as a quantum well, are explained by quantum physics and optical, electronic, magnetic and chemical behavior is defined as quantum not classical.

These changes are due to two reasons; the first is surface effects caused by the increased ratio of surface atoms in the structure, the second quantum effects (Quantum limitations arising from the impact is discontinuous behavior) [66,67]. This affects the mechanical, optical, electrical and magnetic properties of material influences as well as affecting the chemical reactivity. The ratio of the total atom number of atoms at the crystal surface has a large effect on the overall properties of crystalline [68]. As material volume

decreases, the ratio of surface atoms increases.

Size effects can be explained using only quantum mechanics; quantum affects the smaller regions where electrons can produce the greater effect. According to quantum mechanics, an electron can be represented as a wave and the movement of an electron wave and interaction with its surface bonds are taken away from the quantization of energy, passed and reflected waves of interference and the potential barrier of tunneling in a nano-sized structure.

Research, in recent years, on low-dimensional structures, has focused on obtaining structures and examining their properties such as quantum wells, quantum dots, and nanowires. In addition, general differences were observed in the magnetic properties. According to observed variations, scientific and technological application possibilities are to be found in the nanoscience field. Some of them are magnetic nanostructures, electronics, optoelectronics, ferro fluid, flexible disk copy, biomedical materials and catalysts etc [69].

The potential applications of nanotechnology and nano structure are; material manufacturing, electronics, medicine, health, environment, energy, chemistry, biotechnology, agriculture, computer and information technology.

According to the technological applying field, researchers developed different methods from each other, for nanostructure. There are many synthesis methods such as, mechanical grinding, sol-gel, hydrothermal, gas atomization, laser beam melting, chemical vapor deposition, physical vapor deposition, aerosol application, in nanoscale where structure is synthesized. There are advantages and disadvantages for each of the methods in its field of use.

There are some advantages, which are exceptional lightness, hardness, long continuity, strength, durability and high chemical activity in nanoscience; which are of benefit to us all. In addition, parts made of materials in nano-size, may have many useful properties still to be investigated.

In particular, infused with rare-earth element metal oxide, nanoparticles due to their unique features which are; a long fluorescence lifetime, high luminescence efficiency, glowing single or different in colors, high photo-chemical stability, recently, some researchers have concentrated their studies on nanomaterial.

Recently, the studies on sensitive screening and early diagnosis of cancer [70,71] have been focused on luminescent material for drug storage and transport. Nano structures are required for designing materials which have both powerful emission properties, and a suitable storage capacity. Due to superior optical and electronic properties, nano structures have been used successfully in imaging studies[72-75]. Some examples are; optical fluorescence microscopy, magnetic resonance imaging (MRI), positron emission tomography (PET), etc [76-78]. Due to high luminescence intensity and low photo-fading, nano structures have been studied for dosimeter in thermoluminescence [79, 80].

CHAPTER 4

EXPERIMENTAL PROCEDURE

In this survey, Sr doped MgB_4O_7 and KCl doped ZnB_2O_4 thermoluminescent materials were examined as a good candidate. Sr doped MgB_4O_7 material was synthesized by high temperature solid-state in the stoichiometric ratio. Furthermore, the same properties of material were obtained with X-ray diffraction (XRD), The photoluminescence (PL), Fourier transforms infrared spectroscopy (FTIR), particle size analyzer and Scanning electron microscope (SEM).

KCl doped ZnB_2O_4 material was synthesized by combustion synthesis method in the stoichiometric ratio. Furthermore, the same properties of material were obtained with X-ray diffraction (XRD), Fourier transforms infrared spectroscopy (FTIR) and Scanning electron microscope (SEM). The materials are exposed to radiation by using beta rays a ^{90}Sr-^{90}Y source (≈ 0.04 Gy/s). The materials and equipment have been used as starting materials and well-known equipment respectively for the synthesis and thermoluminescence (TL) below.

4.1 Materials and Equipment

The materials, which are magnesium (MgO, % 99,9) (Aldrich) and boric acid (H_3BO_3, % 99,9) (Aldrich), with dopant strontium sulfate ($SrSO_4$, % 99,9) (Aldrich) required for the synthesis were organized for Sr doped MgB_4O_7. The materials which are zinc nitrate ($ZnNO_3$, % 99,9) (Aldrich), boric acid (H_3BO_3, % 99,9) (Aldrich) and Urea, with KCl required for the synthesis were organized for KCl doped ZnB_2O_4. Apart from the raw materials, tools and device are used such as agata mortar. Containers for the reaction (porcelain crucibles) should be able to endure high temperatures and furnaces with optimal balanced for high temperature solid-state methods.

In this survey, beta rays ^{90}Sr- ^{90}Y radiation source (Riso TL/OSL System Model DA-20), Thermoluminescence (TL) glow curves were recorded by utulizing a Harshaw TLD System 3500 Manual TL Reader device (Harshaw Chemical Company, Ohio, USA.) in the temperature variety 30–400 °C at a heating rate of 1°C /s. All operations were performed at room temperature.

The other devices are, X-Ray powder diffraction (Rigaku Miniflex 600 with Cu Kα (40 kV, 15 mA, λ=1.54050 Å)) for phase composition and crystallinity of material, FTIR Perkin Elmer Spectrum One to support the XRD results, LeO EVO 40 scanning electron microscope (SEM) for Morphology of material, Malvern Mastersizer 2000 particle size analyzer for particle size and photoluminescence (PL) spectrophotometer with xenon lamb (Photon Technology International, PTI, QuantaMaster^{TM} 30) for excitation, emission spectra and decay curve of the materials were performed for properties of material.

4.2 Production Process of Materials

There are several methods for the production material. In this experiment high temperature solid-state and solution combustion method were applied and its process was described in detail below.

4.2.1 High Temperature Solid-State Method

High temperature solid state method is one of the most widely used methods due to ease and cheapness in the experimental field. According to the method, materials are doped with different elements to produce novel materials. In this method the starting material and admixture material are ground to a fine powder under suitable conditions. The mixture of powdered materials is weighed stoichiometrically in appropriate amounts, and weighed powder materials are mingled until a homogeneous mixture was achieved. The calcination procedure can also be applied for girding and materials to get rid of carbonate during mingling. After homogeneous mixing, the mixed material is heated at a selected high - temperature value for an appropriate time.

4.2.2 Solution Combustion Method

Solution combustion method is one of the most widely used methods for nanoparticle synthesis in experimental field. Undoped zinc borate samples were synthesized by Solution Combustion Synthesis method, which is one of the adopted techniques to obtain nanomaterials. This method relies on an exothermic reaction between an oxidizer (metal nitrates form) and an organic fuel, which is a water-soluble organics containing large quantity of C and H [81].

In this thesis, zinc nitrate and boric acid used as starting materials and urea as an organic fuel was used to synthesize nano zinc borate. The amount of urea was determined by the equivalence ratio "ϕ" that is clarified as $\phi = \phi_s/\phi_m$, where ϕ_m is the mixture ratio

(fuel/oxidizer) and ϕ_s is the stoichiometric ratio [82,83]. The amount of urea was calculated with an elemental stoichiometric coefficient $\phi = 1$. Doped samples were prepared by adding the dopant as sulfate and chloride form. The best TL properties were obtained for K doped zinc borate, so the main TL properties of K doped zinc borate were studied in the present thesis.

4.2.3 Synthesis of Samples

Magnesium tetraborate as a polycrystalline form was synthesized by high temperature solid-state method from stoichiometric quantities of the starting materials, MgO and H_3BO_3 with ball milling assisted. In the literature, main starting materials (MgO or $MgCO_2$ and H_3BO_3) and dopants are mixed and ground together and then heated at 900 °C for 4 and 5 h [84,85].

Contrary to the former procedure, our first investigation indicated that the best TL intensity was obtained, if the host compound was synthesized first and then dopant was added and heated at the same temperature for the same duration of time just like the synthesized condition of the host material.

The well-known starting materials MgO and H_3BO_3, which were weighed with stoichiometric rate then mixed and milled in an agate mortar. Milled materials put into a convenient porcelain crucible carefully. The mixture was heated in an electrical furnace for heating at different temperatures (800, 850, 900 and 950 °C) for different time intervals (1, 2, 3, 4 and 5 hours). The possible and expected chemical reaction is given below:

$$MgO + 4H_3BO_3 \rightarrow MgB_4O_7 + 6H_2O$$

After some heating process at different temperature, the experiment was applied at 900 °C for 2 h in air atmosphere. After heating first step, the obtained MBO was doped with $SrSO_4$ with five distinct concentrations (0.25, 0.50, 1, 2 and 2.5 wt%) was added to the host matrix, separately and heated at the same temperature for the same duration of time, similar to the synthesized condition of the host lattice. The mixtures were subjected by mechanical attrition by Fritsch Pulverisette mill to obtain uniformity. After the milling operation (2 minutes), the mixtures were heated into electrical furnace at 900 °C for 2 h in air atmosphere.

The first results (not given in the text) indicated that MBO could be synthesized in

a short time using just 2 minutes mill due to the uniformity and narrow particle size, comparing the literature [9,85]. In addition, on the contrary of literature, highest TL and PL sensitivity was obtained by the addition of dopant after synthesis of MBO and the highest TL intensity was recorded with 0.25 wt% Sr-doped phosphor. Therefore all TL investigations were done on it.

On the other hand, $ZnNO_3$, H_3BO_3, Urea and KCl have been used as starting materials for the synthesis of zinc borates and as an activator. After the solution combustion synthesis methods, the solid parts were calcinated in PLF125 Model Muffle furnace (220 V, 50 Hz, 12700 W) at air atmosphere. Maximum temperature achievable is 1300°C. In addition, same furnace was used for doping procedure.

4.3 Measurements and Investigation of Samples

Phase composition and crystallinity of the undoped and Sr-doped MBO were identified by X-Ray powder diffraction using Rigaku Miniflex 600 with Cu Kα (40 kV, 15 mA, λ=1.54050 Å) radiation. To support the XRD results, functional groups of the synthesized samples were defined by FTIR analysis using Perkin Elmer Spectrum One. Morphology was determined using LeO EVO 40 scanning electron microscope. The particle size was done by Malvern Mastersizer 2000 particle size analyzer.

Thermoluminescence glow curves (TL) of undoped and Sr doped MBO were obtained using a Harshaw QS 3500 Manual type TL reader, having S-11 reply photomultiplier tube (Figure 4.2). TL curves were obtained at a linear heating rate of 1 $^oC/s$ up to 400 ^oC in desired experiments. The samples were weighted as fifteen milligrams and were irradiated for 5 minutes at room temperature with a $^{90}Sr–^{90}Y$ beta source (0.9 Gy/min.)

The photoluminescence (PL) properties, including the excitation, emission spectra and decay curve of the materials, were analyzed by a spectrophotometer with xenon lamb (Photon Technology International, PTI), QuantaMaster™ 30).

KCl doped ZnB_2O_4, which was synthesized with solution combustion method. Zinc borate was doped with KCl at several different concentrations in the study. The aim to examine the effect of KCl and KCl concentrations on thermoluminescance (TL) properties of compound, ZnB_2O_4.

4.3.1 Radiation Source and Irradiation Process

In this work, beta rays ^{90}Sr- ^{90}Y was used as radiation source during experiment in Figure 4.1. The beta rays ^{90}Sr- ^{90}Y radiation source with the opened lid was placed into a special lead block. With this system, the sample is irradiated for at least 1 second. By using a computer-controlled system, irradiation can be applied for any material in any time interval.

Figure 4.1 Radiation source of beta rays a ^{90}Sr- ^{90}Y source (≈ 0.04 Gy/s).

In experiment the samples were irradiated about 25^{0}C (room temperature) with beta radiation from a calibrated ^{90}Sr- ^{90}Y radiation device (Figure 4.1). The high-energy beta particles are emitted from their daughter products (^{90}Sr β-0.546 MeV together with ^{90}Y β-2.27 MeV). In the computer part the 9010 Optical Dating System from Little More Scientific Engineering, UK [41]. The maximum influence area of Y–90 beta particles in air is approximately 9 meter. In work the synthesized samples were weighed with precision scales then the samples were irradiated for 5 minutes at room temperature with ^{90}Sr- ^{90}Y beta source (0.9 Gy/min.). In each measurement 15 mg of powder were used for irradiation process. All experiments were done in a dark room to prevent effects of the ambiance light on the glow curves.

4.3.2 TLD Reader System and Emission Process

In this experiment, QS 3500 Harshaw TLD reader systems were used in order to detect the TL emission. This system is a reader which is computer connected to hand-operated in Figure 4.2. The system consists of TLD reader and a computer program that runs the WinREMS (Windows Radiation Evaluation and Management System).

Figure 4.2 QS 3500 Harshaw TLD reader

In this system, the sample tray is designed for a single sample. There is a typical clear glass filter between the planchet and photomultiplier tube in the reader in order to prevent the produced infrared lights affecting the reader. Luminescent emission of the sample is detected by a PMT (Photomultiplier Tube) during the heating process. By increasing the emission, signals from the PMT are displayed and recorded with the help of computer programs on the Winrems.

In operation irradiated sample material is placed in the tray and heated. Then, the irradiated samples were read out with the reader and TL signal is obtained on the computer with Winrems program. The program resolves the separate peaks in the glow curve, and then the best values are obtained parameters. Glow curves were measured at a linear heating rate of 1 ^{0}C/s from room temperature up to 400 ^{0}C. The essential scheme of TL reader can be shown in figure 4.3.

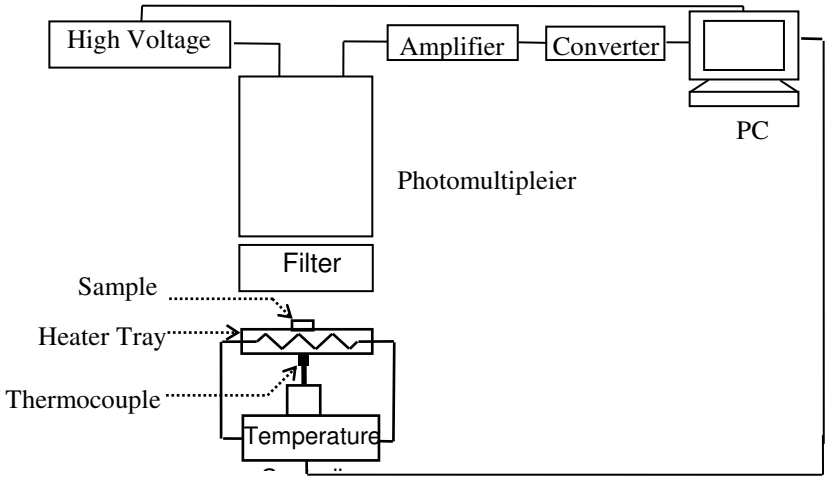

Figure 4.3 Essential scheme diagram of TL reader [41].

There is The Time Temperature Profile (TTP) in Winrems program. It consists of three segments: Preheat, Acquire, and Anneal, each with independent times (Pre-read anneal: adjustable 0 to 1000 sec, Linear ramp: adjustable from 1 ^{o}C to 50 ^{o}C per second, Post-read anneal: 0 to 1000 sec) and temperature (Pre-read anneal -room temperature to 200 ^{o}C, Post-read anneal: up to 400 ^{o}C).

The typical time temperature profile is shown in figure 4.4. In order to increase the planchet life and precision of low-exposure readings, the nitrogen is given to the planchet area. Nitrogen is also used through the photo-multiplier tube (PMT) chamber in order to remove moisture produced by condensation.

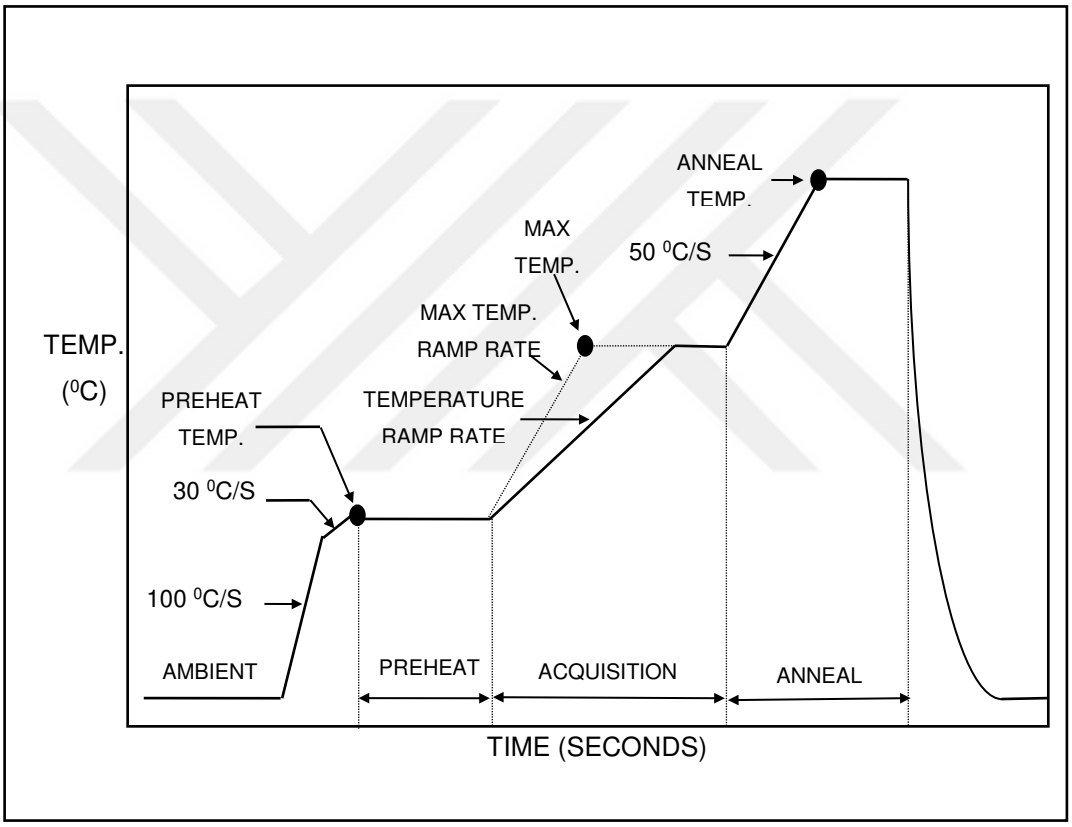

Figure 4.4 Typical time -temperature profile (TTP) [41].

4.3.3 Annealing Oven and Heat Process

Annealing is a process, which is completely discharging electrons, which are trapped inside the crystals. In this process, annealing is performed separately at different temperatures; the optimal temperature is determined, to get rid of electrons from traps. In this experiment microprocessor controlled Nuve FN 501 type electrical oven is used for different temperatures and different time intervals between 1 min to 24 hours in Figure 4.3.

Figure 4.5 Nuve FN 501 type electrical oven

In this procedure, the samples were annealed at 400±1^{0}C for 1 hour through the experiments. The temperature of the electrical oven was continuously observed during the annealing period. Furthermore, the oven is used for the method of high - temperature solid state. Synthesized material is heated at selected high temperature value with an appropriate time for the formation of material.

CHAPTER 5

EXPERIMENTAL RESULTS

The various dosimeter systems are used in order to determine the reliability of the dose at radiation measurements. Thermoluminescent dosimeters, which are useful and sensitive dosimeters, are used widely in various fields to detecting the radiation values. Such as radiation dosimeter, archaeological dating, etc. [1]

Researchers have worked to get understand and improve the properties of the material and to produce a new thermoluminescent material. Today, (TLD) is a well-known dosimetric method for measured dose in the dosimeter field such as personnel, clinical and environmental.

Generally TLD working principal is thermoluminescent material give off light while materiel are heated. The defects are generated by putting the impurities inside the energy bands in the thermoluminescence materials [80]. The studies of Thermoluminescence dosimeter with borate compounds has been applied recent 25 years and has been found important results. For example $Li_2B_4O_7$ and MgB_4O_7 are good candidate for their TL dosimeter properties due to close tissue equivalence. In recent years, studies of B_4O_7Zn material have been performed by researcher for candidate of TL dosimeter.

In this study we have examined properties of TL dosimeter for MgB_4O_7 and ZnB_2O_4 materials by using some methods such as The Heating Rate, The Peak Shape, Computer Glow Curve Deconvulation CGCD. Also, we have examined the effect of Sr^{2+} ion and Sr concentrations on photoluminesance (PL) properties of compound, MBO.

5.1 Experimental Results for MgB_4O_7

As mentioned previously, borate compound as worthy nominees for thermoluminesance (TL) study due to close tissue equivalent absorption coefficient (Z_{eff} =8.4 - 8.55 dependent on the activator) and unique properties. In several studies, magnesium tetraborate (MgB_4O_7, MBO) is one of the most selected boron compounds for TL dosimetry investigations. In these studies, to increase and improve TL properties of

MBO several dopants (activators), like dysprosium, thulium, terbium, sodium, calcium, etc. have been applied [12,14-16,84,85,86-89].

According to Prokic, [83,85] more deficiencies arise in complex crystal structure of MBO after adding dopants rather than the other alkaline halides. Because of this to improve new and appropriate dosimeter it should be used different dopants.

In this field, several researchers worked on MgB_4O_7 structure and detected huge resemblance to SrB_4O_7 [13,90-92]. In this study strontium " Sr^{2+}" was chosen as a dopant and thought that Sr^{2+} may stabilize primarily at Mg^{2+} site in the host lattice of MgB_4O_7.

According to literature, no work on this subject, which is strontium ion as a dopant for MBO. Because of this magnesium tetraborate was doped with Sr^{2+} at five different concentrations (0.25, 0.50, 1, 2 and 2.5 wt%) in the study. The aim to examine the effect of Sr^{2+} ion and Sr concentrations on photoluminesance (PL) and thermoluminescance (TL) properties of compound, MBO.

After many trials for synthesis material, the best synthesized heat conditions were detected at 900 °C for the host lattice of material. Then, experiments were performed for undoped and Sr-doped MBO which were synthesized at 900 °C for 2 h.

The X-ray diffraction (XRD) devise was used to determine that the material occurs and patterns of the undoped and the Sr-doped MBO polycrystalline powders are plotted in Figure 5.1. According to International Centre for Diffraction Data, ICDD, (PDF 2.DAT - Card number 00-031-0787), all results fitted with MgB_4O_7 card.

According to these results, MBO was obtained as a pure form and the dopant did not change the host lattice structure as expected like the literature data [82,93]. Additionally, cell parameters of Sr-doped MBO was computed by the least square procedure employing a locally modified version of the program CELLREFF [94]. Cell parameters of MBO were found as a = 8.617 (2) A°, b = 13,821 (2) A°, and c = 7.987 (3), which are close to the ICDD card of MBO.

IR spectra pattern of the undoped and 0.25 wt % Sr-doped MBO are obtained in Figure 5. 2. In the shape about six clear IR bands were noticed in the region 400-2000 cm^{-1}. Sr-doped MBO compared with undoped MBO for the band positions their wavenumbers did not change and no new IR bands occurred depending on the doping procedure, as a result strontium did not cause any difference in the host lattice. The obtained IR bands are given in Table 5.1[95].

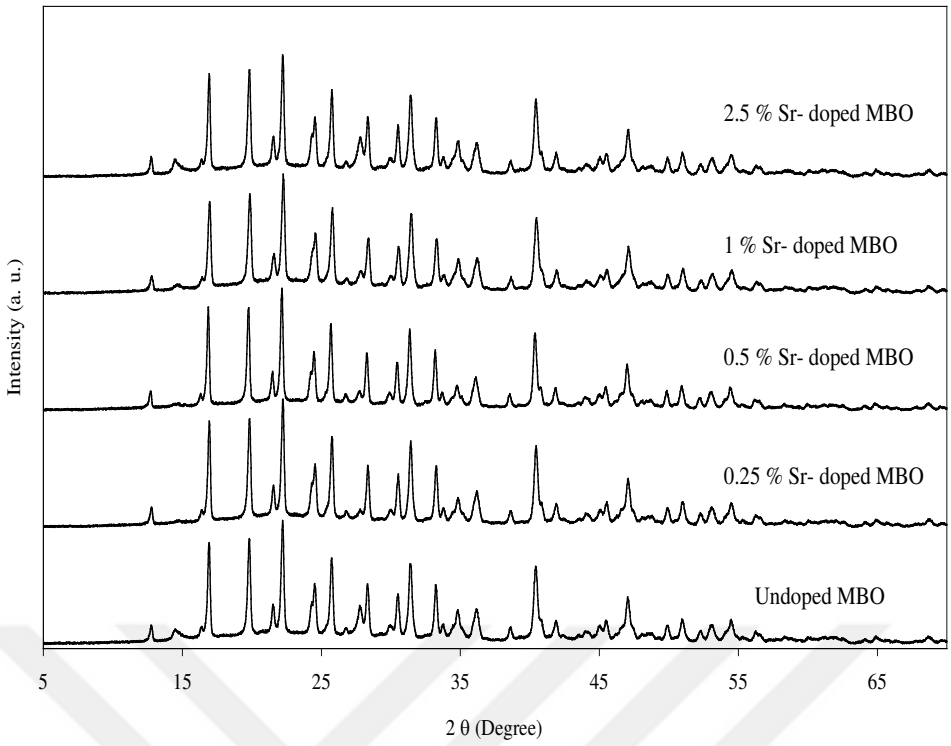

Figure. 5.1 The X-ray diffraction patterns of the undoped and the Sr-doped MBO.

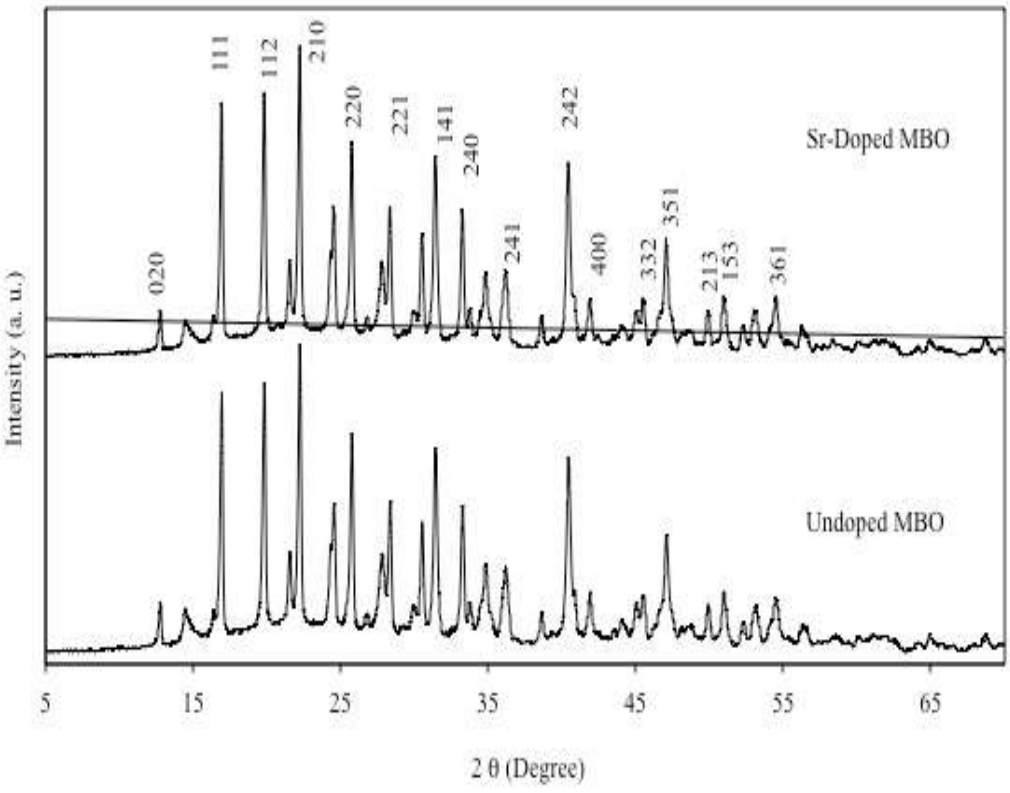

Figure. 5.2 The X-ray diffraction patterns of undoped and the 0.25 wt % Sr-doped MBO.

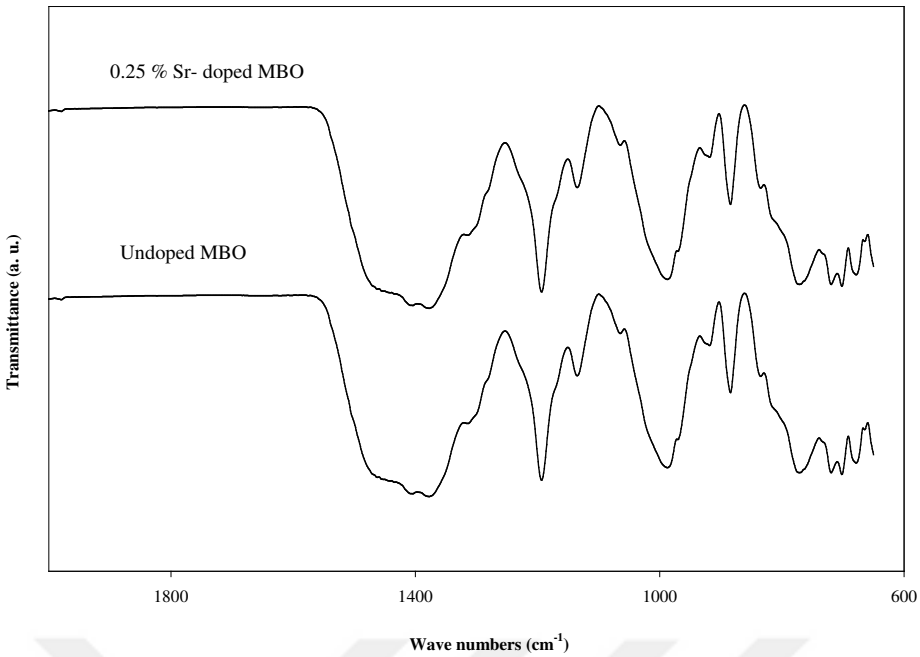

Figure 5.3 IR spectra of undoped and 0.25 wt % Sr-doped MBO.

Table 5.1 Wavenumbers of FTIR Spectra of the undoped and Sr-doped MBO

Frequency, cm^{-1}	**Assignment**
1420 - 1365	Asymmetric streching of the three-coordinate boron [$\upsilon_{as}(B_{(3)}$-O]
1200	Bending of B-O-H
991	Four-coordinate boron [$\upsilon_{as}(B_{(4)}$-O]
898	Symmetric streching of the three-coordinate boron [$\upsilon_{s}(B_{(3)}$-O]
717	Bending of $B_{(3)}$–O
671	Bending of the three-coordinate boron [$\delta(B_{(3)}$-O]

Scanning electron microscope (SEM) device by producing various signals is given information about the sample's surface shape and composition. There are some SEM images of the undoped and doped Sr-doped MBO in Figure 5.3. Due to mechanical attrition by ball mill, the particle size decreased and uniformity was increased. There is no big difference on the morphology of MBO was observed depending on both the activator and doping procedure.

According to obtained all images, MBO had clustered granule structure in this state [96]. Also the increasing of the dopant concentration produced vitreous structure, as in Fig. 5.3 c. In this study MALVERN Mastersizer 2000 particle analyzer was used for uniformity and particle size of the Sr-doped MBO. According to the particle size analyzer

one sharp peak is obtained (not given in text), showing the uniformity, and below 100 nm as an average particle size.

In this study the TL properties of Sr doped MgB_4O_7 were examined in detail. In experiment by using different amounts of Sr doped MgB_4O_7 powder samples, the glow curve obtained. Then the best of the glow curve was selected in many of the glow curves. According to selected TL glow curves the dopant concentration did not produce any change on the glow curve structure and the maximum TL intensity of Sr -doped MBO with dopant concentration of 0.25 wt % in Figure 5.4. Looking at the the figure TL intensities decreased with increasing the dopant concentration. The reason of this quenching effect of which occurs due to the competition between non-radiative transitions and traps [1, 15,97, 98]. According to figure 5.4 the TL intensity of 0.25 wt % Sr-doped MBO phosphor is much stronger than the other obtained samples. The obtained glow curve structure and peak temperature closely same as that have been reported by Kitis [82] et al.

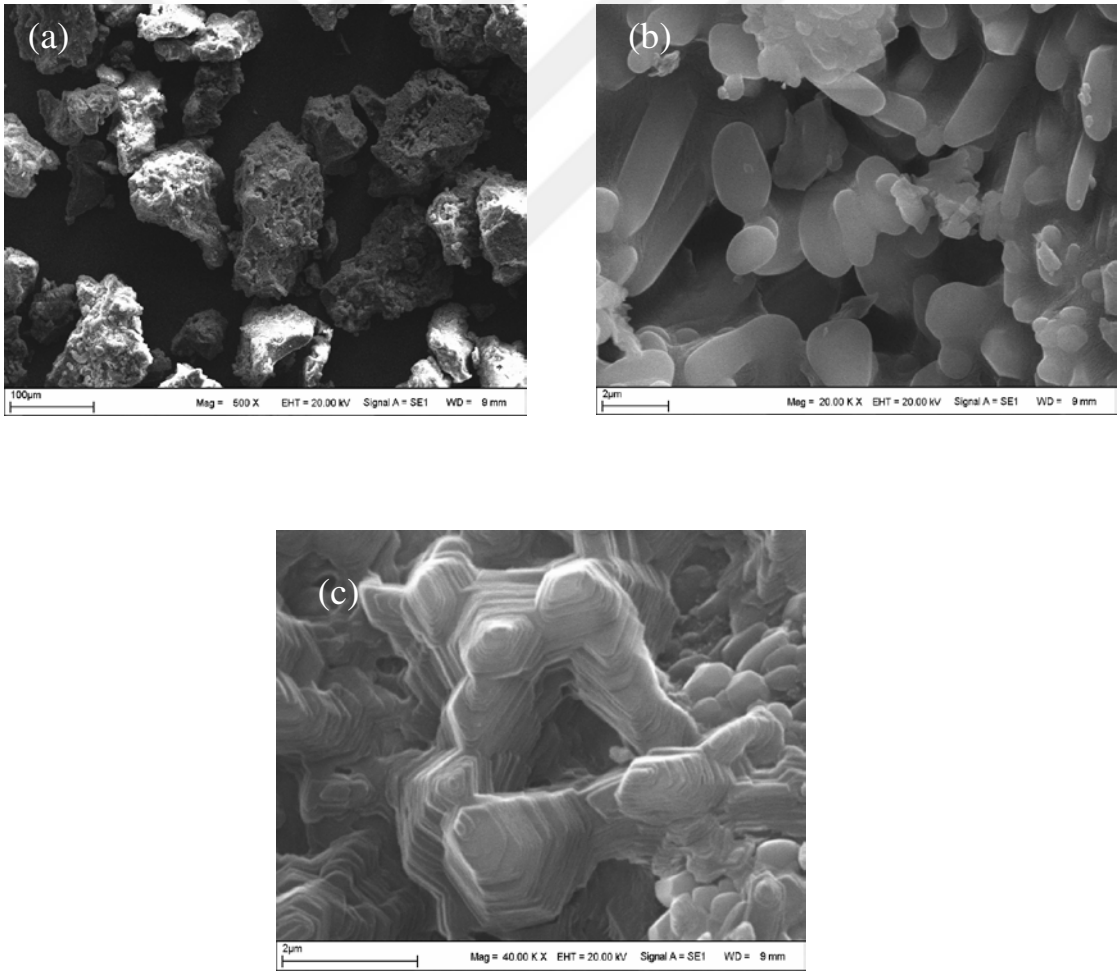

Figure 5.4 SEM images of 0.25 wt % Sr-doped MBO (a) before milling (b) after milling (c) 2.5 wt % Sr-doped MBO.

As it is known the undoped material can be also defined as a host lattice, usually exhibits weak TL efficiency, there are main some defects or some unwanted impurity in the initial chemical compounds. After addition of activators, called impurities or dopants, like metals or rare-earth impurities, as a result of event TL signals should be increased. There are two expected possibilities for glow curve structure of undoped sample.

After doping procedure, the structure either totally changes after doping procedure or its shape stay constant, just the relative intensities and peak temperature change. In contrast to adding Sr into host lattice there was no big difference observed in the glow curve structures of all the samples.

The changes were observed on the TL intensity and a soft peak temperature at 200 °C and 350 °C. It can be inferred, as there are no huge interactions between intrinsic defects and Sr ions and the event associated with the luminescence centers, nothing to do with the electron traps.

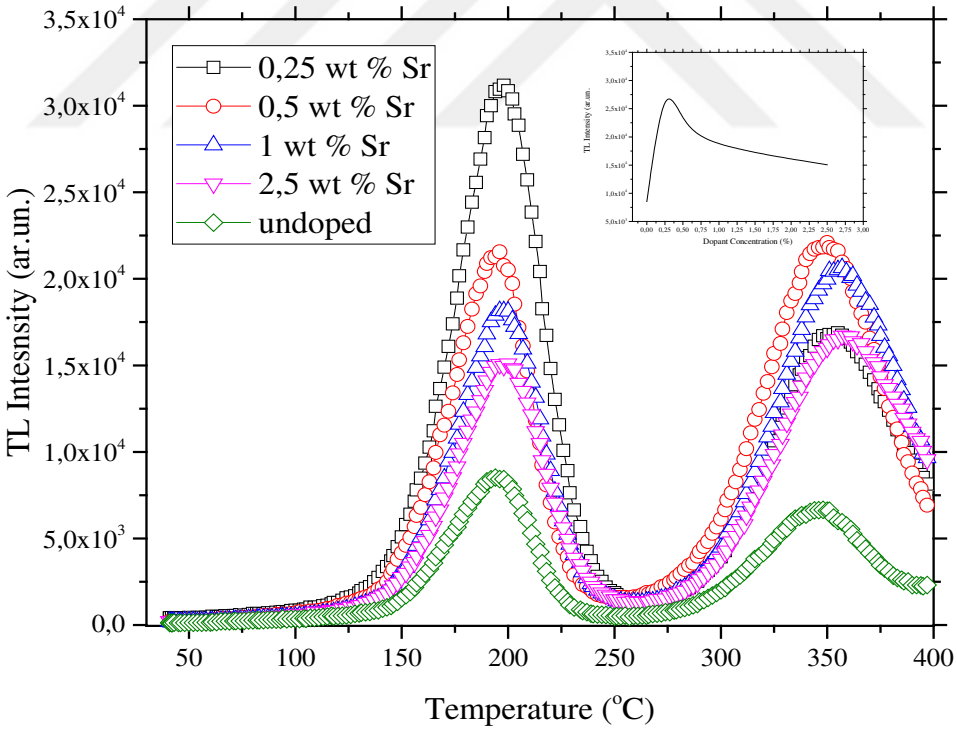

Figure 5.5 TL glow curves of Sr-doped MBO depend on the dopant concentration.

To determine TL sensitivity of the 0.25 wt % Sr-doped MBO was also compared with TLD-100 at room temperature (5 Gy) by using to TL glow curves of TLD-100.

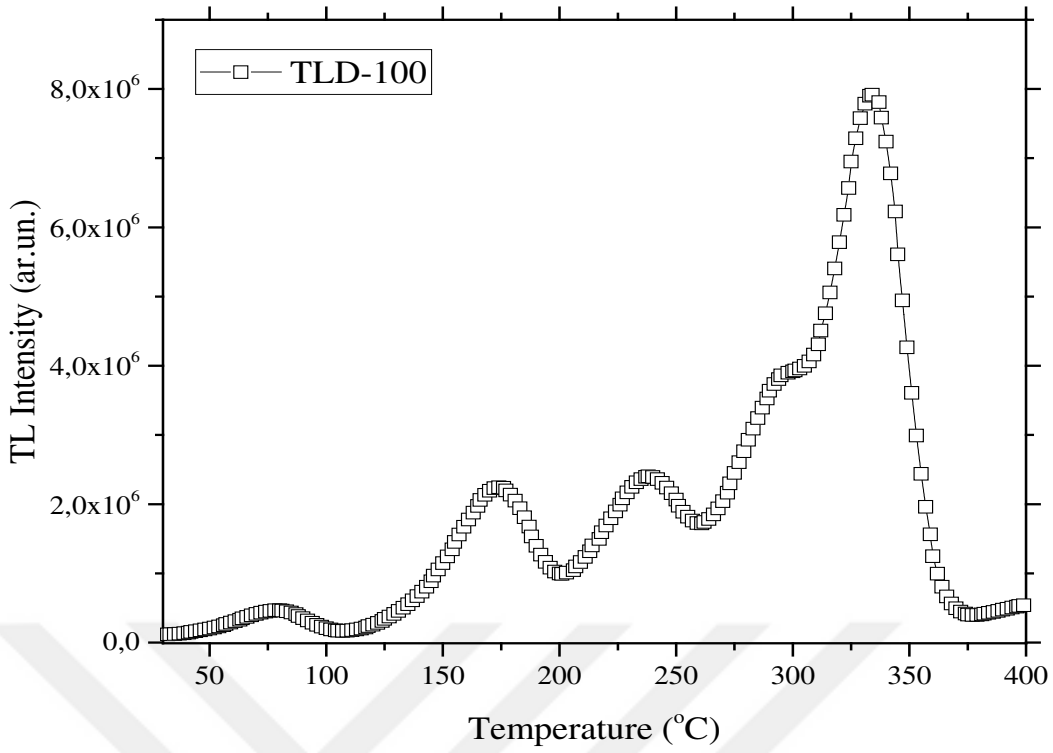

Figure 5.6 TL glow curves of TLD-100

The TL sensitivity is expressed as glow curve area per unit of mass of dosimeter and per unit of dose of beta rays, and the data are given in relation to the TL sensitivity of LiF:Mg,Ti (TLD-100). According to the result of the comparison TL sensitivity of MgB_4O_7:Sr approximately 2 times higher than that of TLD-100.

In TL dosimetry investigation, one of the most important works is the behaviour of different dose levels. Experiments were conducted for this purpose and all samples were readout immediately after irradiation. The glow curve structures of Sr-doped MBO is obtained on different dose levels in Figures 5.7-9. According to the depending on different dose levels, one strong peak at about 200 °C and a low intensity peak at around 350 °C were occurred.

Also, it can be inferred that the glow curve structures are independent dose levels and just TL intensities increased with increasing dose levels. Besides the peak temperatures at 200 °C and 350 °C were slightly shifted toward the lower temperature sides with increasing dose levels [22]. The same behavior was seen lots of other phosphors.

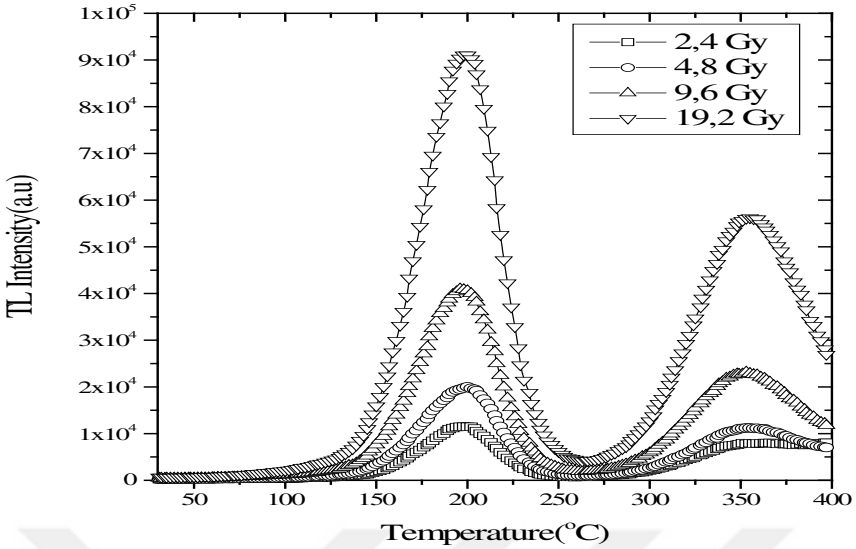

Figure 5.7 Some of the selected glow curves of 0.25 wt % Sr-doped MBO measured at 1 °C /s after different doses.

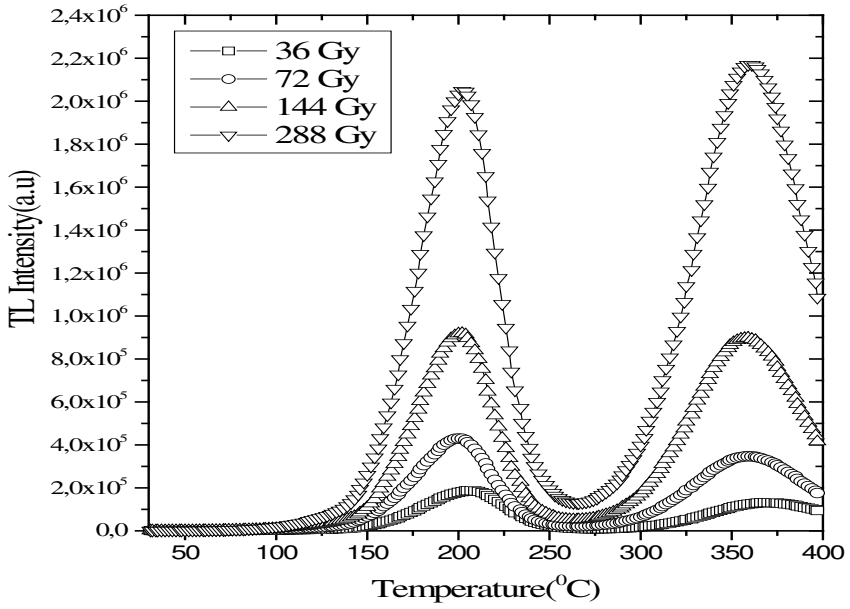

Figure 5.8 Some of the selected glow curves of 0.25 wt % Sr-doped MBO measured at 1 °C /s after different doses.

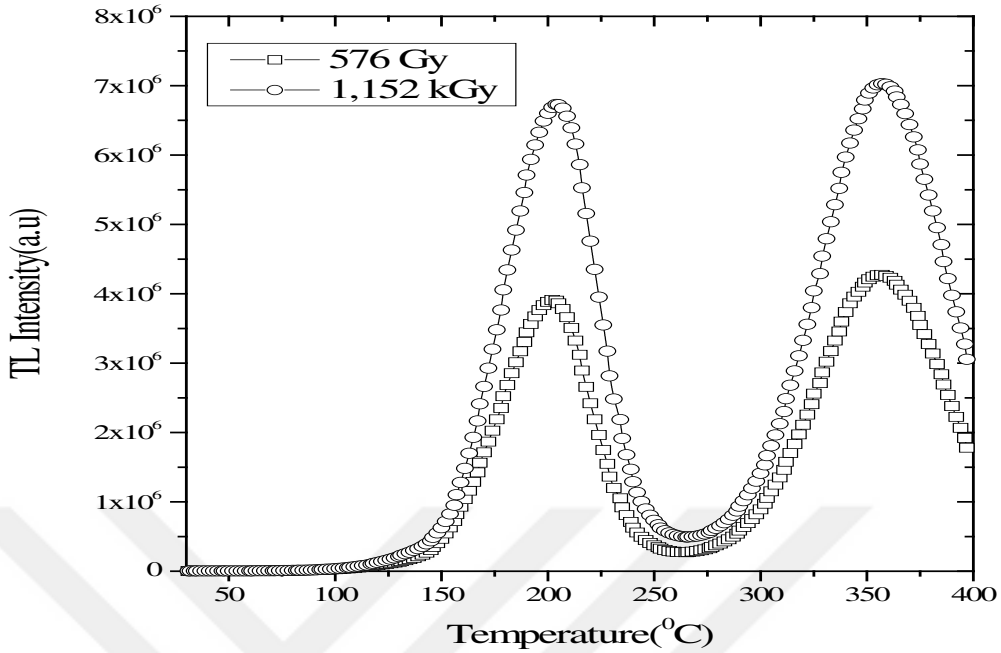

Figure 5.9 Some of the selected glow curves of 0.25 wt % Sr-doped MBO measured at 1 °C /s after different doses.

In this current study, the peak height technique was performed for the effect of heating rates between 1 °C and 10 °C on the peak temperatures and peak intensities of glow peaks of Sr doped MgB_4O_7. A series of glow curves obtained with different heating rates is shown in Figure 5.10 and 5.11.

The peak temperatures of glow peaks in the glow curves of Sr doped MgB_4O_7 was shifted to higher side as the heating rate increases and this results in accordance with theory. As you seen the rate of shifting is decreased with increasing heating rate. According to the obtained figure, the effect of heating rates on the intensities of glow peaks is nearly equal to each other and is very available with increasing heating rate. To explain the decrease in the luminescence efficiency an expression of the form have been suggested below.

$$\eta = (1 + C\exp(-W / kT))\text{-}1$$

here W and C are the quenching parameters. It is known that the increased probability of non-radiative transitions competing with radiative transitions. Essentially, the

luminescence efficiency of a phosphor is written by η=Pr/(Pr+Pnr), where Pr is the probability of luminescence transitions, temperature independent and Pn r is the probability of non-radiative transitions, which is temperature dependent.

In this here, the increase in the heating rate resulted in an increase in the temperature of the TL glow peak, this shift in temperature was held responsible for the increase in the contribution of non-radiative transitions.

According to result it was inferred that the glow peaks exist at higher temperatures may display higher thermal quenching than those exist at lower temperatures any TLD material. Furthermore, the increased probability of non-radiative transitions at higher temperatures, the dedected effects have also been appointed to the effects of heating rate on the moved of charge carriers released during the TL readout.

The raise in the moving of the charge carriers reduce the luminescence efficiency with temperature, if the lattice parameters are important to the non-radiative transitions. In fact, explanation of the variation of peak intensities with the heating rate may not be sufficient to explain the observed variations for a single model. Because, many models can play a role in the variations of TL response of this material. The effects of heating rate on the peak temperatures are investigated as shown in figure 5.10 and 5.11.

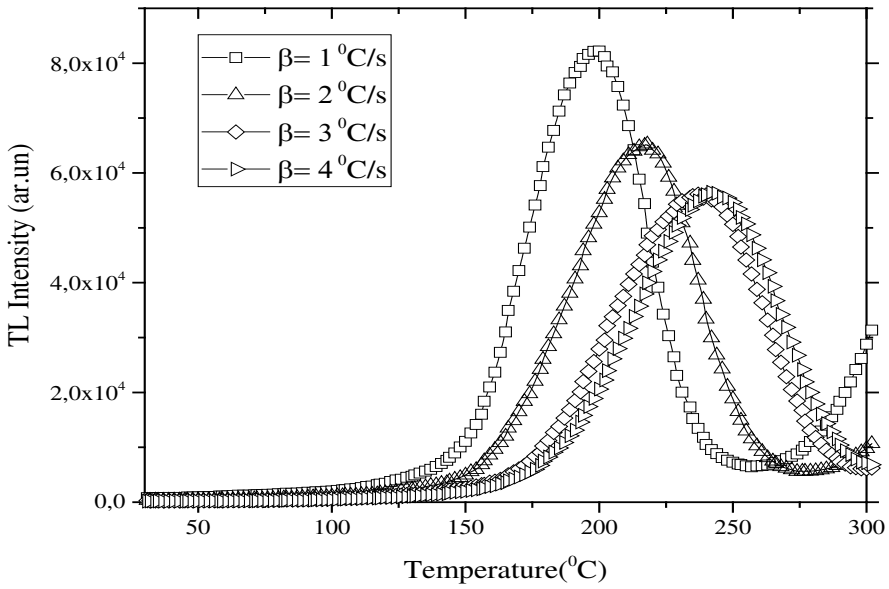

Figure 5.10 Typical glow curves of Sr-doped MBO exposed to beta rays of 12 Gy and

readout at linear heating rate between β = 1 ºC/s and β = 4 ºC/s

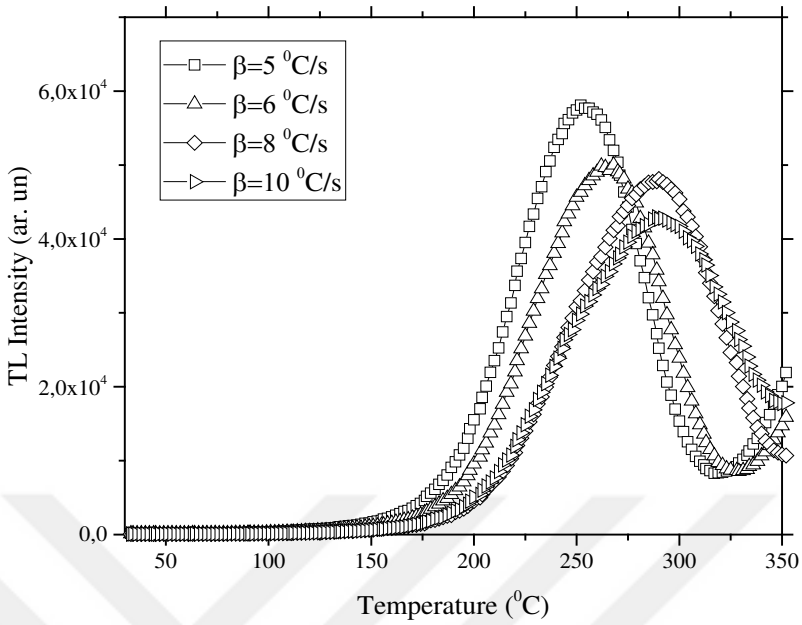

Figure 5.11 Typical glow curves of Sr-doped MBO exposed to beta rays of 12 Gy and readout at linear heating rate among β = 5 ºC/s, β = 6 ºC/s β = 8 ºC/s and β = 10 ºC/s

In a TL dosimetry, certain physical parameters are calculated for many dosimetric application such as trap depth (E) and frequency factor (s). In this study, these physical parameters were determined with well-known two different methods, which are CGCD, and variable heating rate (VHR) method.

CGCD method was used to analyze and determine the structure of the glow curve of 0.25 wt % Sr-doped MBO and to calculate its trapping parameters.

In order to obtain better and accurate kinetic parameters, the method of computerized curve fitting has been used on several occasions with apparent success [99,100].

For calculations, the program that was written at Reactor Institute at Delft, The Netherlands [101] was used. The TL glow curves were analyzed by using the following equation of the general-order kinetics of the TL;

$$I(T) = n_0 s \quad \exp(-\frac{E}{kT})\left[1+(-\frac{(b-1)s}{\beta}\frac{kT^2}{E}\exp(-\frac{E}{kT})*(0.9920-1.620\frac{kT}{E_a})\right]^{\frac{b}{b-1}}$$

as mentioned earlier, where n_0 (m^{-3}) is the concentration of trapped electrons at t=0, s (s^{-1}) is the frequency factor for first-order and the pre-exponential factor for the general-order, E (eV) the activation energy, T (K) the absolute temperature, k (eV/K) Boltzmann's constant, β (C/s) heating rate and b the kinetic order.

By using this model and computer program the glow curve analyzes was given in Figure 5.12. According to program the glow curve structure of Sr-doped MBO was determined by a linear combination of at least three glow peaks between room temperature and 400 °C. Besides, it can be inferred that best overall fit and designated high priority features of the TL results, the kinetic parameters were calculated and are given in Table 5.2.

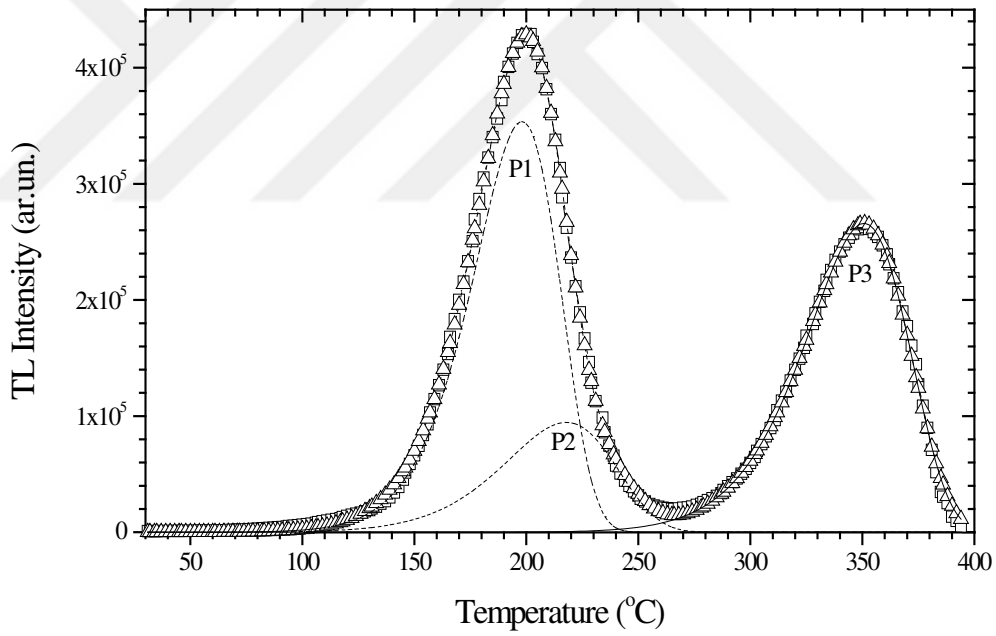

Figure 5.12 The CGCD analyzed glow curves of Sr-doped MBO (measuring after 12 Gy irradiation by beta ray at room temperature)

Another important method is the variable heating rate (VHR) method was also applied to determine the kinetic parameters. In this study the eight heating rates (1, 2, 3, 4, 5, 6, 8, and 10 °C/s) were performed with the VHR method. Also, shift position, which is occurred on the position of the temperature (T_m) at the maximum point of intensity (I_m), is

determined and to calculate the kinetic parameters, $\ln(T_m^2/\beta)$ against $1/(kT_m)$ plot is drawn in Figure 5.13.

As is clearly seen in Figure 5.11 the temperature of a TL peak shifted to higher values as the heating rate increased, effect of non-radioactive transitions and this behavior is frequently observed in the practice. Because of the thermal quenching effect the influence of the luminescence reduces in this situation [45,102]. To prevent problem temperature lag (TLA) problem the equation which is given below has been proposed as a proposal for a solution by Kitis [45].

$$T_m^j = T_m^i - C\ln\left(\frac{\beta_i}{\beta j}\right)$$

where T_m^j and T_m^i are the maximum temperatures of a glow peak with heating rates β_j and β_i, respectively, and C is a constant, which is initially evaluated by using two very low heating rates where TLA can be considered as negligible. In preference, the low heating rates should be chosen below 1 $^oC\ s^{-1}$ to calculate the constant C. The E_a and s values of the main dosimetric peak at 200 ^0C evaluated different techniques, which were used above, were summarized in Table 5.2.

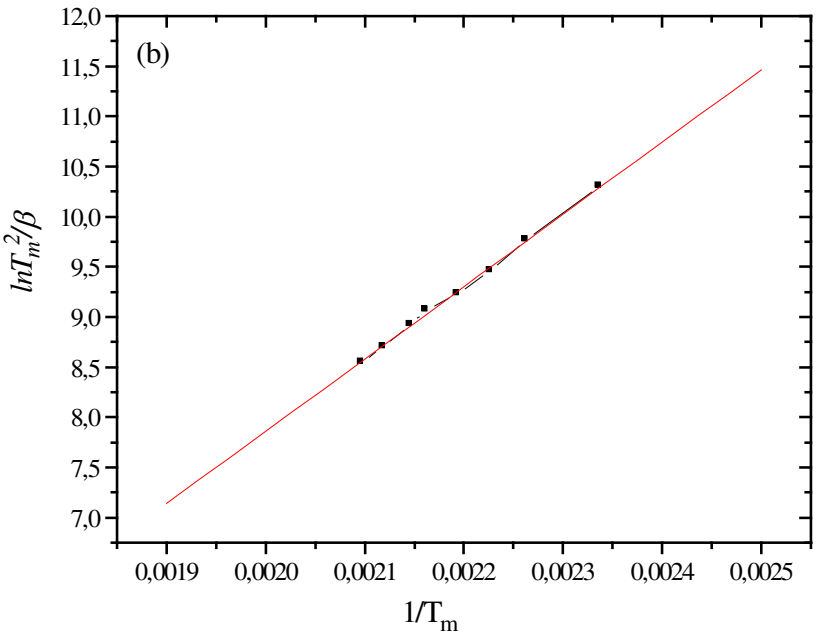

Figure 5.13 Plot of $\ln(Tm^2/\beta)$ versus $1/T_m$ for 0.25 % Sr-doped MBO at 5 Gy (different heating rates 1, 2, 3, 4, 5, 6, 8 and 10 $^oC/s$).

Table 5.2 The values of the trapping parameters of Sr-doped MBO

Mazumdar P.S				**Chen P.S**				
Sr-doped MBO	1/2 ratio	2/3 ratio	4/5 ratio	E_τ	E_δ	E_ω	**CGCD**	**VHR**
E (eV)	0,851	0,86	0,88	0,811	0,896	0,852	0,853	0,825
b	1	1	1	1	1	1	1	
lns(s^{-1})	17,8	17,8	17,8	17,8	17,8	17,8	19,11	18,15

In this thesis, the dose response of Sr-doped MBO was investigated as a function of irradiation from 1 s (≈ 0.015 Gy) to 48 h (≈2.6 kGy) in Figure 5.10. According to figure peak intensity (I_m) of main glow curve peak (P1) at about 200 °C was linearly raised up with dose increasing up to nearly 570 Gy (maximum dose in the study) and then a saturation effects started. The plot of the total peak area (A), which was obtained by CGCD glow curves program exhibited similar tendency. Because of both curves exhibited perfect linearity, which its TL response with up to 570 Gy and first peak (P1), Sr-doped MBO may be used as a dosimetric peak in medical applications. As result of this, it can be determined that the phosphor showed sublinearity beyond the defined dose.

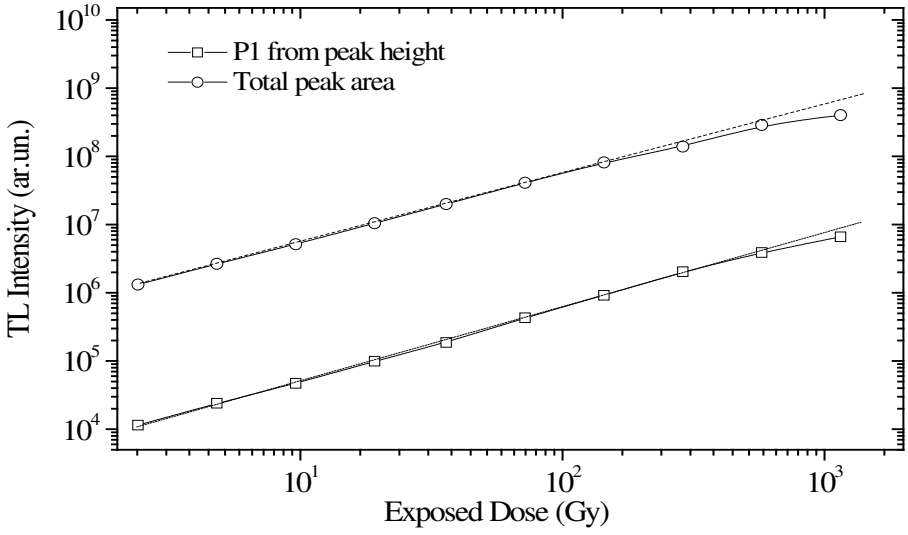

Figure 5.14 The TL dose response curve of dosimetric glow peak of Sr-doped MBO determined by the peak heights and area of glow peaks.

For a perfect TL dosimeter, a glow curve peak of material should be nearly at 200 °C and stable (non fade). According to this study, the results showed that Sr-doped MBO may be a good candidate for TL dosimeter in point of the peak temperature. In order to determine characteristic of fading, the irradiated Sr-doped MBOs were kept in dark room at the temperature nearly 25 °C and in the time period. The results of experiment were given for the time period in Figure 5.11 and 5.12. It can be inferred that the main problem of Sr-doped MBO was the high fading ratio (80 %) within one month. When it is examined in more detail after 2 days, the intensity drastically decreased. Fading and sensitive problems were also encountered earlier on Dy-doped MBO in the literature [12,97,102]

To eliminate this problem, experimenters have worked and several co-dopants are added into host lattice. [35,85] According to above mentioned characteristics of Sr-doped MBO this phosphor is a promising material for dosimetric application, so it is worth to systematic studies on it to improve TL properties and solve particularly fading problem. As a result we can say that our investigation is ongoing with addition of another activators as a co-dopant. According to fading, read out all glow curves at 1 ^{o}C / s after exposing to an irradiation of 36 Gy.

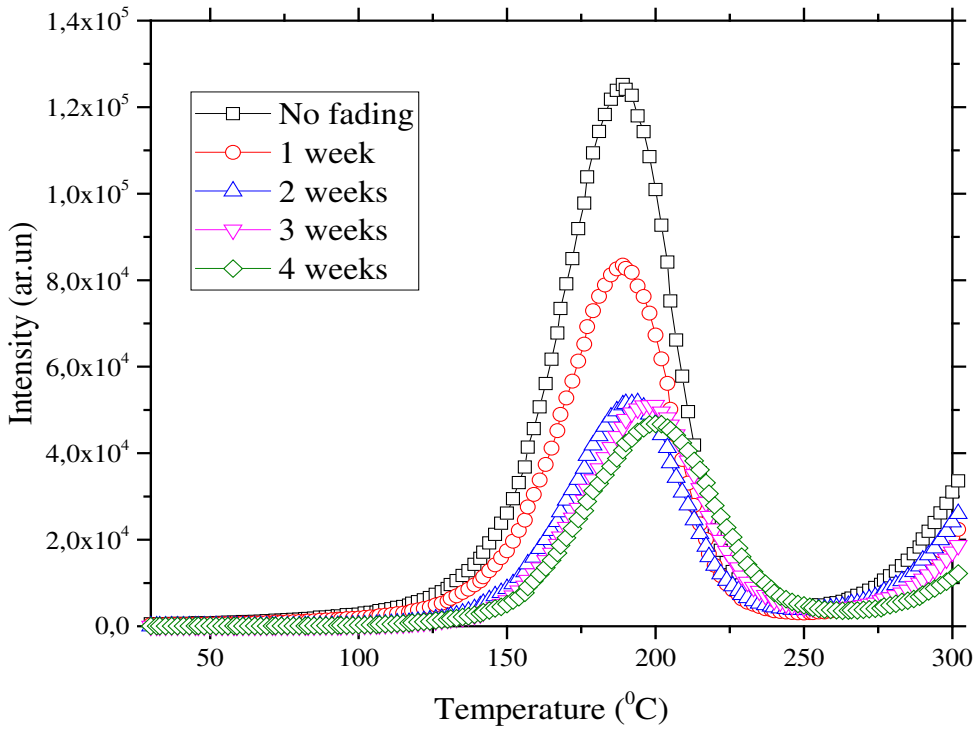

Figure 5.15 A set of TL glow curves for Sr-doped MBO measured after various storage periods at room temperature.

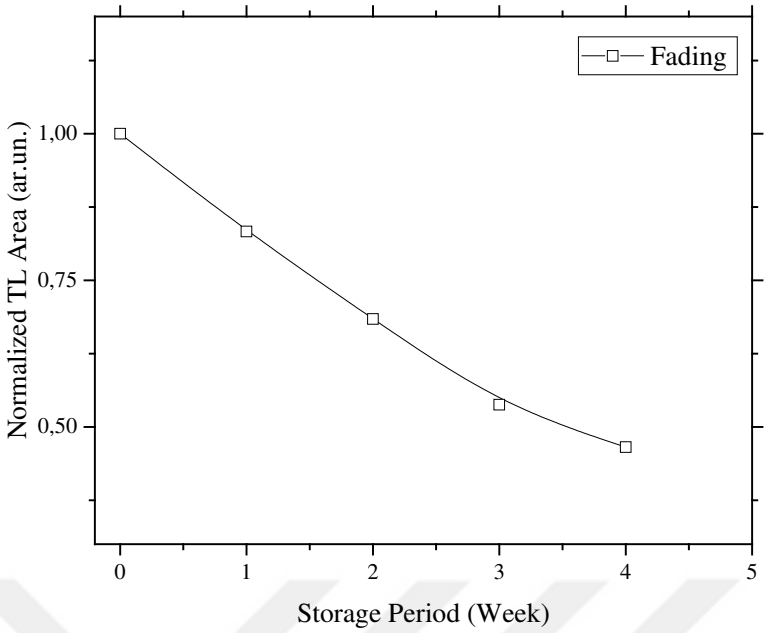

Figure 5.16 Normalized TL intensity of Sr-doped MBO after different storage times at room temperature. (β=1 ºC / s and D=36 Gy).

Another important properties for a optimum dosimeter is luminescence decay. In this study Luminescence Decay curves of sample are plotted in Figure 5.10 and decay times of Sr- doped MBO were calculated by a curve fitting method using the equation below:

$$I = A_1 exp(-t/\tau_1) + C$$

where I is phosphorescence intensity; A_1 and C are constants; t is time; and τ_1 is the lifetime for the exponential components. Decay times (τ_1) are given in Table 5.3. Fig. 5.10 and Table 5.3 obviously indicated that 0.25 % Sr- doped phosphor had longer decay time and more severe emission band than others. It means that 0.25 wt % Sr^{2+} ratio plays an important role in prolonging the afterglow.

Table 5.3 Decay curves of Sr-doped MBOs.

Sample	**0.25 wt% Sr**	**0.5 wt% Sr**	**1 wt% Sr**	**2.5 wt% Sr**
τ_1 (μs)	7.227	6.757	6.289	6.750

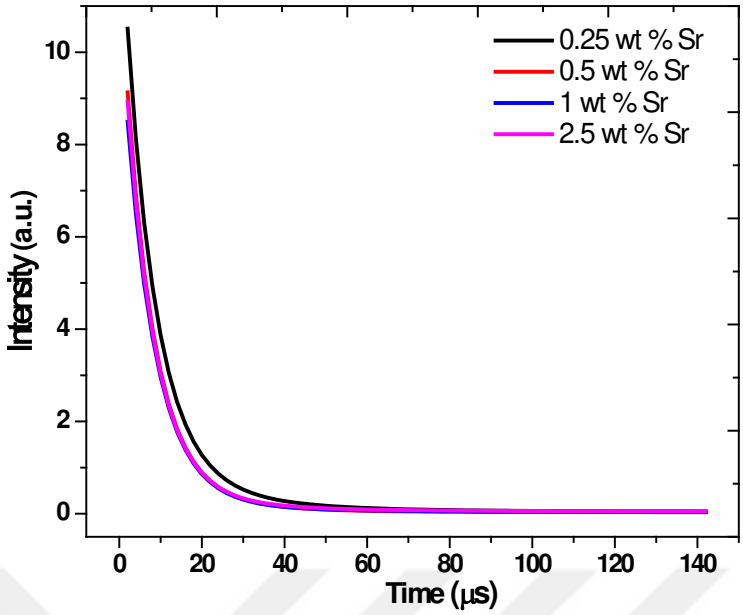

Figure 5.17 The decay curve of the Sr-doped MBOs.

The MBO framework and SrB_4O_7 (SBO)[13,88-90] similarity condition can be examined in more detail. The event can be expressed as fallows, when the Sr^{2+} ions were doped into MBO crystal structure, the Sr^{2+} ions might be shifted with Mg^{2+} ions in crystal structure, thus the dopant Sr^{2+} ions have a similar coordination site to Mg^{2+} ions coordinated with 9 oxygen ions [96,97].

According to knowledge and the theoretical calculations, the conduction band located at the upper level in this type crystal structure and largely composed of both the 4d orbitals of Sr atoms and the 2p valence orbitals of B atoms.

Hence, both the Sr–O charge transfer transition (CT) and the $(BO_4)^{5-}$ groups contribute to the host crystal absorption so, the charge transfer between Sr^{2+} ions and O^{2-} ions are expected [103,104]. The all the MBO samples having different concentrations of Sr^{2+} had the broad excitation band at 293 nm, attributing to the charge-transfer transition (CT) between the Sr^{2+} ions and the surrounding oxygen anions ligands (Fig. 5.5).

According to photoluminescence measurement, the broad emission band at 350-520 nm was obtained depending on the excitation wavelength at 293 nm. The blue-shifted band was located at about 460 nm, giving rise to the strong blue luminescence of the all samples at room temperature.

It can be inferred from Figure 5.5 that the broad wavelength band at 460 nm was due to the $^1So \rightarrow {}^1P_1$ transitions, involving several excited states of Sr^{2+}. The literature data also support this assignment. Rubinsztein-Dunlop et al., [105] mention that strontium atoms at about 460 nm wavelengths are excited because of their ground state $5s^2$ to $5s^15p^1$ state ($^1So \rightarrow {}^1P_1$).

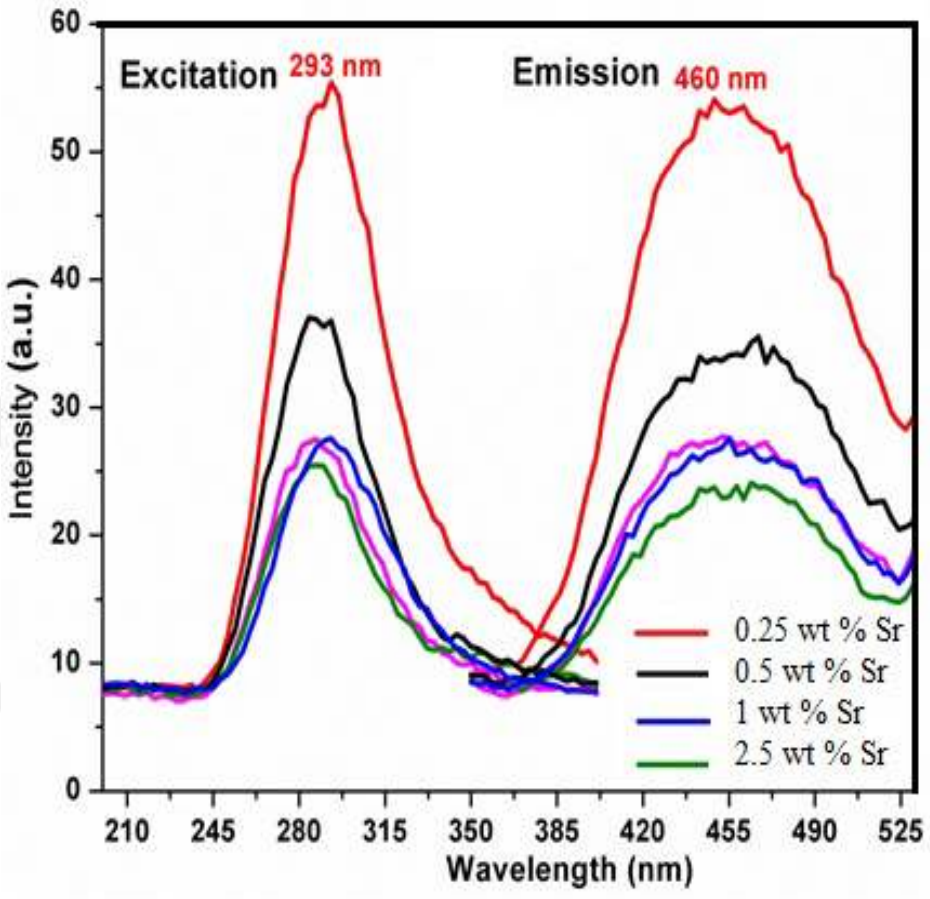

Figure 5.18 Photoluminescence excitation and emission spectra of ion beams irradiated Sr-doped MBO.

This result supports the TL emission and there is a good correlation between the TL and PL results.

5.2 Experimental Results for ZnB_2O_4

As mentioned previously, borate and its compounds are eye-catching candidates due to unique properties in TLD for radiation dose measurement. Nowadays, borate and its compounds has been widely examined because of their near tissue equivalent absorption feature [106]. In some studies, borate and its compounds has been observed several features such as good thermal stability, lower synthesis temperature, mechanical properties

and higher sensitivity during this time [107-109].

In several studies, Zinc borate (ZnB_2O_4) is a boron-based material widely used for TL dosimetry investigations. In several studies, to increase and improve TL properties of ZnB_2O_4 several dopants (activators), like lanthanum, thulium, bismuth, dysprosium etc. have been applied on photoluminescence and thermoluminescence [38-40].

According to literature, no work on this subject, which is Potassium chloride (KCl) on as a dopant for ZnB_2O_4. Because of this Zinc borate was doped with KCl at several different concentrations in the study. The aim to examine the effect of KCl and KCl concentrations on thermoluminescance (TL) properties of compound, ZnB_2O_4.

In this experiment, $ZnNO_3$, H_3BO_3, Urea and KCl have been used as starting materials for the synthesis of zinc borates and as an activator. After many trials, solution combustion synthesis methods, the solid parts were calcinated in PLF125 Model Muffle furnace (220 V, 50 Hz, 12700 W) at air atmosphere. Maximum temperature achievable is 1300°C. In addition, same furnace was used for doping procedure. Then, experiments were performed for KCl doped ZnB_2O_4, which were synthesized.

The X-ray diffraction (XRD) device was used to determine that the material occurs and patterns of the KCl doped ZnB_2O_4 polycrystalline powders are plotted in Figure 5.15. Scanning was recorded between $5°<2\theta<70°$ and the measurements were made with 0.01 and 0.05 degree steps and 2 degree / minute rate.

The divergence slit was variable and scattering and receiving slit were 4.2 degree and 0.3 mm, respectively. The peak positions belonging to undoped and K-doped zinc borates were compared with that of the ICDD (PDF2.DAT) cards to identify the crystalline phases of the synthesized compounds.

According to International Centre for Diffraction Data, ICDD, (PDF 2.DAT - Card number 00-031-0787), all results fitted with ZnB_2O_4 card. The powder XRD data proved that all intense reflections matched with the powder diffraction data reported in ICDD (PDF2.DAT), Card No: 00-039-1126.

The cell parameters were found as a = b = c 7.4777 A. with the space group 229:Im-3m. In XRD pattern of K-doped ZnB_2O_4, there was no difference were observed depending on the dopant and doping procedure. No diffractions were associated with these activators. According to these results, ZnB_2O_4 was obtained as a pure form and the dopant did not change the host lattice structure.

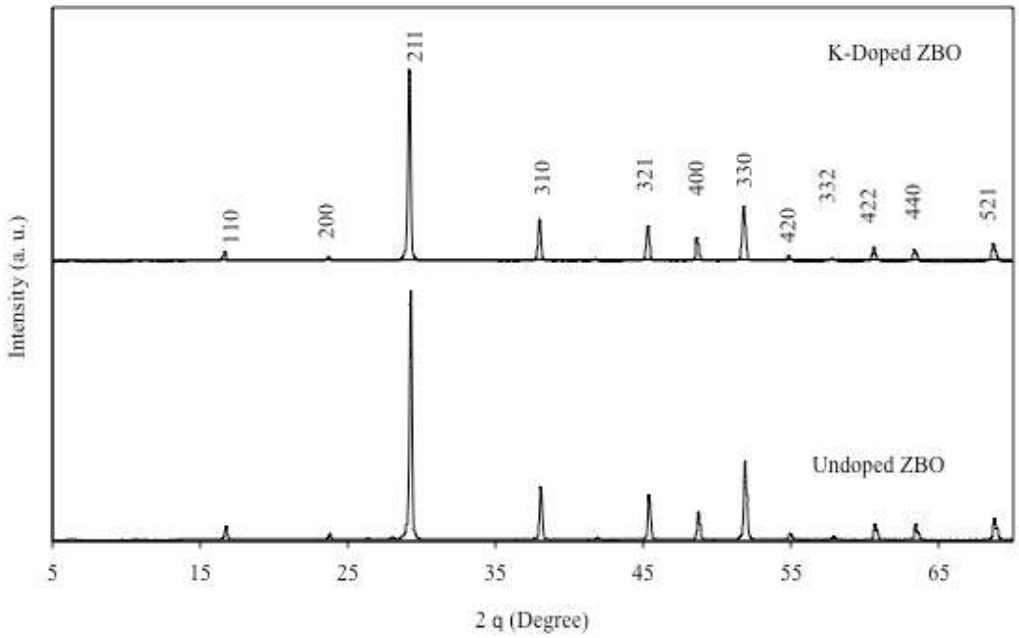

Figure 5.19 The Powder X-ray diffraction patterns of undoped and K-doped ZnB_2O_4

The vibrational modes of functional groups of the undoped and K-doped zinc borate were investigated by FTIR analysis. Infrared (IR) spectroscopy is a chemical analytical technique, which measures the infrared intensity versus wave number of light.

The IR spectra of synthesized compounds were measured in the range of 400 to 2000 cm^{-1} by the KBr pellet method and using PerkinElmer Precisely Spectrum One FTIR Spectrometer. IR pellets were prepared using spectroscopic grade KBr with a KBr: Sample ratio of 100 mg: 3 mg. KBr was dried for several hours before the preparation of pellets. The IR spectrum of undoped and K-doped ZnB_2O_4 were given in Figure 5.16. It can be seen that the IR spectra of obtained materials are similar.

The vibrations did not change and no IR bands were observed associated with KCl dopant in the spectra, meaning that no new compounds were occurred depending on the dopant and doping procedure.

All IR bands confirm the zinc borate structure that has the specific wavenumbers between the 800 cm^{-1} and 1080 cm^{-1}, describing the co-ordinated tetrahedrally boron and at 1080 cm^{-1} [110], attributing to the asymmetric stretching vibration of tetrahedrally co-ordinated boron and at 1394 cm^{-1}, corresponding to the asymmetric stretching vibration of B-O bond in BO_3 units [111-114].

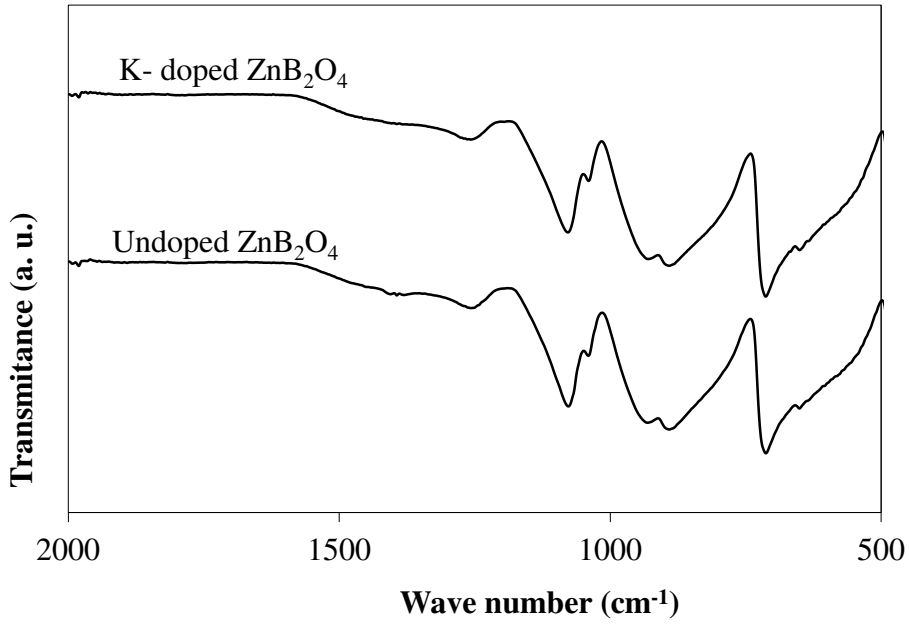

Figure 5.20 IR spectra of undoped and KCl-doped ZnB_2O_4.

Scanning electron microscope (SEM) device by producing various signals is given information about the sample's surface shape and composition. There are some SEM images of the KCl doped ZnB_2O_4 in Figure 5.17. It can be seen that the regularly shaped particles and narrow size distribution was observed and the particle sizes were between 60 and 90 nm, agglomeration was seen due to the low resolution. There is no big difference on the morphology of ZnB_2O_4 was observed depending on both the activator and doping procedure.

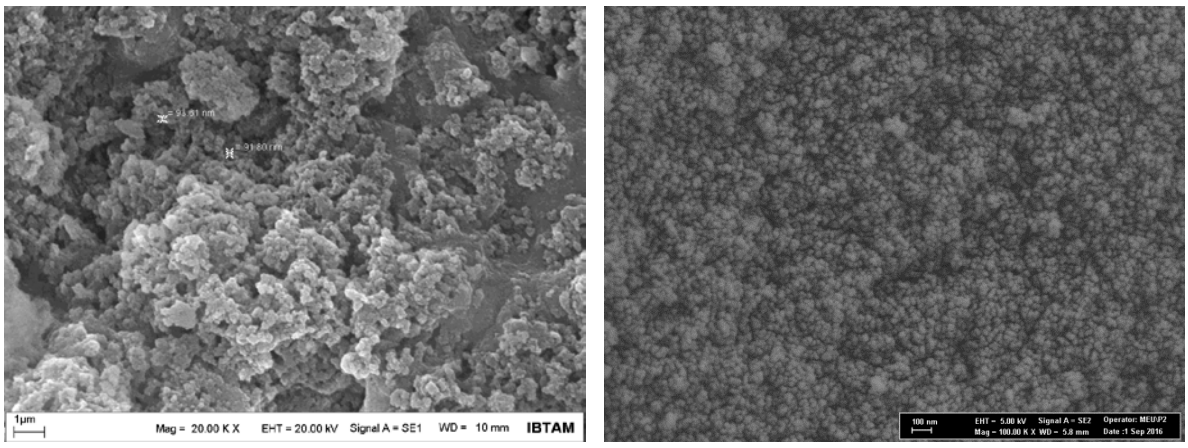

Figure 5.21 SEM images of undoped ZnB_2O_4 (left) and K-doped ZnB_2O_4 (right)

In this study the TL properties of KCl doped ZnB_2O_4 were examined in detail. In experiment by using different amounts of KCl doped ZnB_2O_4 powder samples, the glow curve obtained. Then the best of the glow curve was selected in many of the glow curves.

According to results, 0.5 wt % KCl doped ZnB_2O_4 phosphor is much stronger than the other obtained samples. The obtained glow curve structure and peak temperature closely same as that have been reported by Kitis [79] et al.,

As it is known the undoped material can be also defined as a host lattice, usually exhibits weak TL efficiency, there are main some defects or some unwanted impurity in the initial chemical compounds. After addition of activators, called impurities or dopants, like metals or rare-earth impurities, as a result of event TL signals should be increased. There are two expected possibilities for glow curve structure of doped sample.

The structure either totally changes after doping procedure or its shape stay constant, just the relative intensities and peak temperature change. In contrast to adding KCl into host lattice there was no big difference observed in the glow curve structures of all the samples. The changes were observed on the TL intensity and a soft peak temperature at 100 °C and 183 °C. It can be inferred, as there are no huge interactions between intrinsic defects and KCl ions and the event associated with the luminescence centers, nothing to do with the electron traps.

To determine TL sensitivity of the 0.5 wt % KCl doped ZnB_2O_4 was also compared with TLD-100. The TL sensitivity is expressed as glow curve area per unit of mass of dosimeter and per unit of dose of beta rays, and the data are given in relation to the TL sensitivity of LiF:Mg, Ti (TLD-100). According to the result of the comparison TL sensitivity of KCl doped ZnB_2O_4 approximately 2,3 times higher than that of TLD-100 (Figure 5.6 TL glow curves of TLD-100)

In TL dosimeter investigation, one of the most important works is the behavior of different dose levels. Experiments were conducted for this purpose and all samples were readout immediately after irradiation. The glow curve structures of KCl doped ZnB_2O_4 is obtained on different dose levels in Figure 5.23. According to the depending on different dose levels, one strong peak at about 100 °C and a low intensity peak at around 183 °C were occurred.

Also, it can be inferred that the glow curve structures are independent dose levels and just TL intensities increased with increasing dose levels. Besides the peak temperatures at 100 °C and 183 °C were slightly shifted toward the lower temperature sides with increasing dose levels. Same behavior was seen lots of other phosphors.

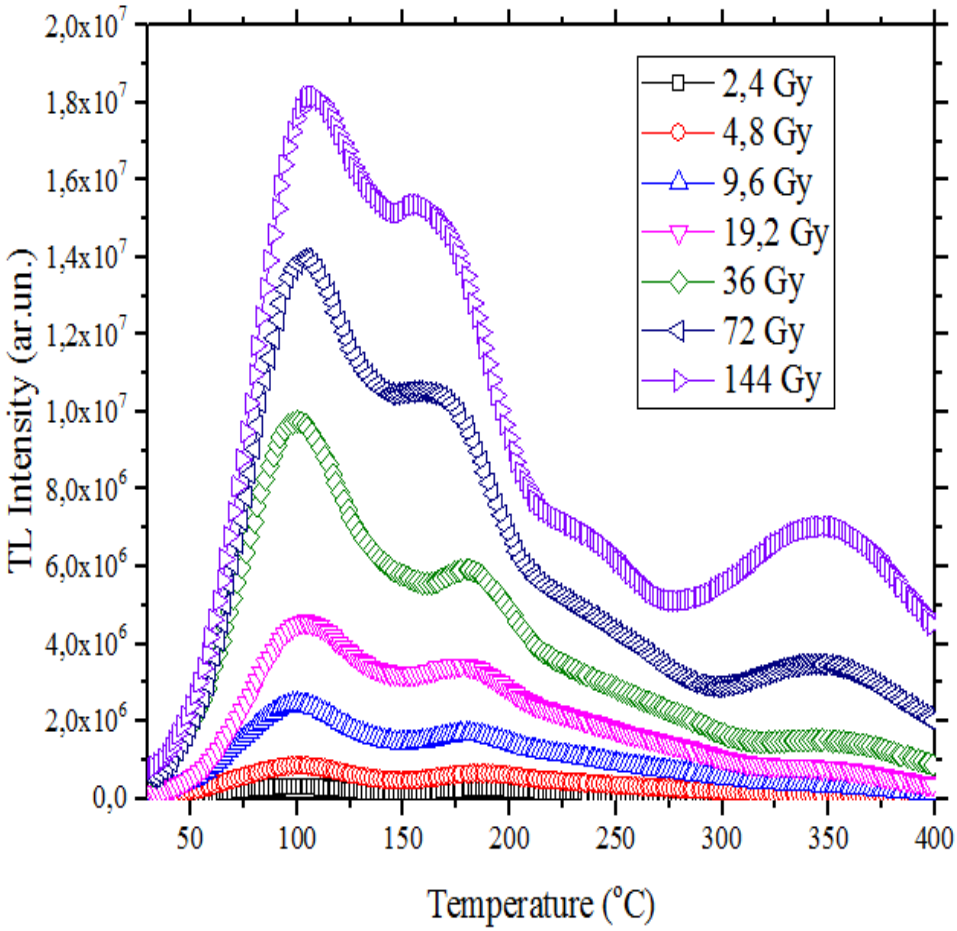

Figure 5.22 Some of the selected glow curves of 0.5 wt % KCl doped ZnB_2O_4 measured at 1 °C /s after different doses.

In a TL dosimeter, certain physical parameters are calculated for many dosimetric application such as trap depth (E) and frequency factor (s). In this study, these physical parameters were determined with CGCD method.

CGCD method was used to analyze and determine the structure of the glow curve of 0.5 wt % KCl doped ZnB_2O_4 and to calculate its trapping parameters.

In order to obtain better and accurate kinetic parameters, the method of computerized curve fitting has been used on several occasions with apparent success [101,102]. For calculations, the program which was written at Reactor Institute at Delft, The Netherlands [101] was used.

The TL glow curves were analyzed by using the following equation of the general-order kinetics of the TL;

$$I(T) = n_0 s \quad \exp(-\frac{E}{kT})\left[1+(-\frac{(b-1)s}{\beta}\frac{kT^2}{E}\exp(-\frac{E}{kT})*(0.9920-1.620\frac{kT}{E_a})\right]^{\frac{b}{b-1}}$$

as mentioned earlier, where n_0 (m^{-3}) is the concentration of trapped electrons at t=0, s (s^{-1}) is the frequency factor for first-order and the pre-exponential factor for the general-order, E (eV) the activation energy, T (K) the absolute temperature, k (eV/K) Boltzmann's constant, β (C/s) heating rate and b the kinetic order.

To obtain the kinetic parameters from the glow curves of TL materials one of the best methods is the computerized glow curve deconvolution (CGCD) method. The kinetic parameters such as, activation energies (E_a) and kinetic order (b) for obtained the dosimetric peaks.

By using this model and computer program the glow curve analyzes was given in Figure 5.16. According to program the glow curve structure of KCl doped ZnB_2O_4 was determined by a linear combination of at least nine glow peaks between room temperature and 400 ^oC. Besides, it can be inferred that best overall fit and designated high priority features of the TL results, the kinetic parameters were calculated and are given in Table 5.4.

Table 5.4 summarizes the E_a and b values of the deconvulated peak. In this study, the following general order kinetic analytical equation was used by the approximation for b≈1.1

$$I(T) = I_m \cdot b^{b/b-1} \cdot \exp\left(\frac{E}{kT}\cdot\frac{T-T_m}{T_m}\right) \cdot [(b-1)\cdot(1-\Delta)\cdot\frac{T^2}{T_m^2}\cdot\exp\left(\frac{E}{kT}\cdot\frac{T-T_m}{T_m}\right)+Z_m]^{-b/b-1}$$

where;

$$\Delta = \frac{2kT}{E} \ , \ \Delta_m = \frac{2kT_m}{E} \ , \ Z_m = 1+(b-1)\cdot\Delta_m$$

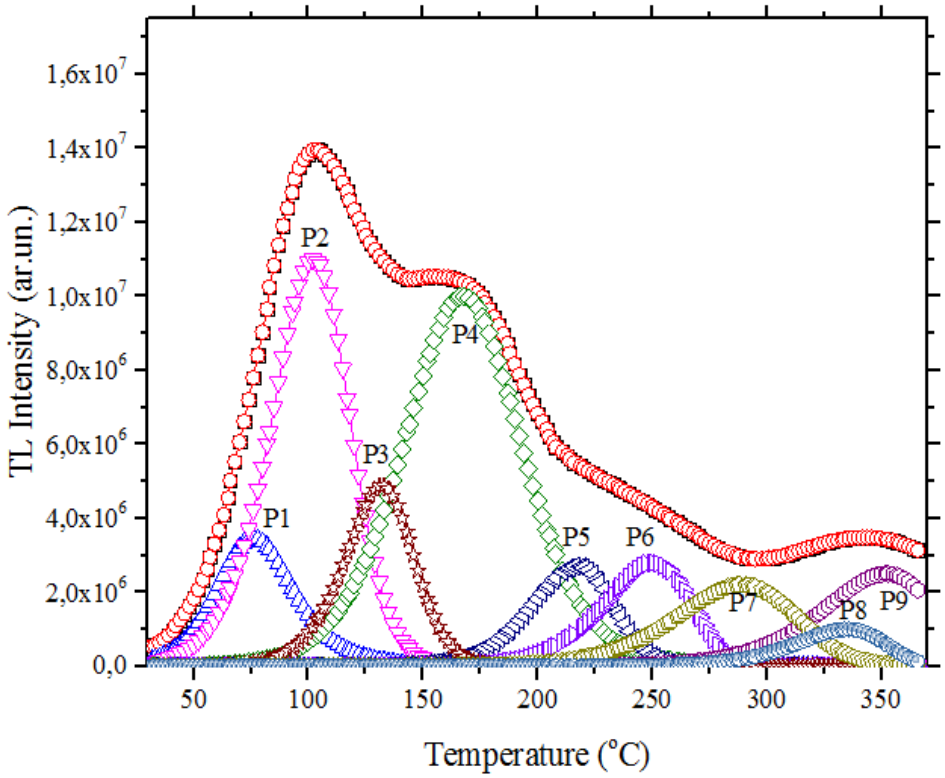

Figure 5.23 The CGCD analyzed glow curves of KCl doped ZnB_2O_4 (measuring after 12 Gy irradiation by beta ray at room temperature) (FOM: 1.49 %)

Table 5.4 The values of the trapping parameters of KCl doped ZnB_2O_4 (CGCD methods)

Values	**Peak#1**	**Peak#2**	**Peak#3**	**Peak#4**	**Peak#5**
b	1,99	1,35	1,6	1,2	1,12
E_a(eV)	0,88	0,8	0,8	1,25	1,3
Values	**Peak#6**	**Peak#7**	**Peak#8**	**Peak#9**	
b	1,01	1,4	1,2	1,01	
E_a(eV)	1,35	1,1	1,1	1,6	

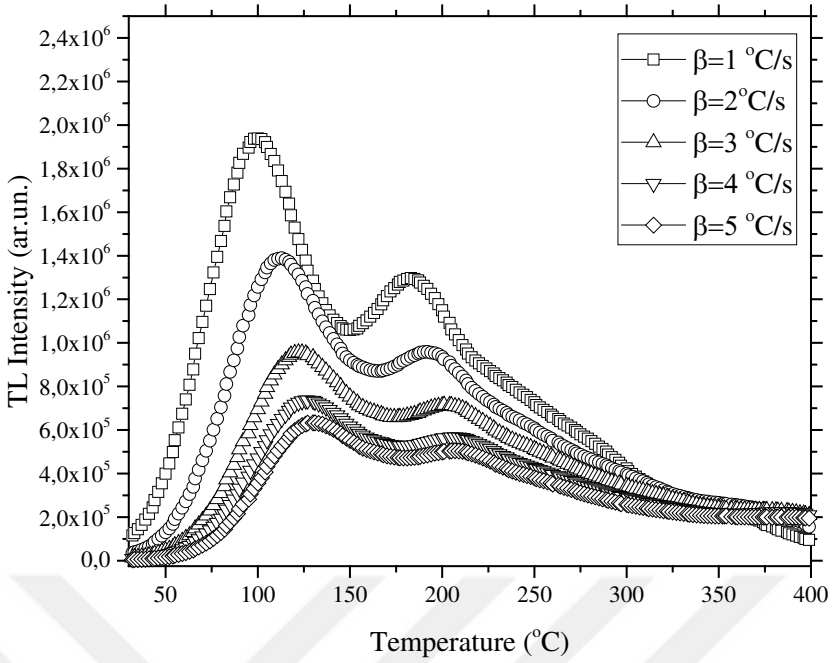

Figure 5.24 Typical glow curves of KCl doped ZnB_2O_4 exposed to beta rays of 12 Gy and readout at linear heating rate between β = 1 °C/s and β = 5 °C/s

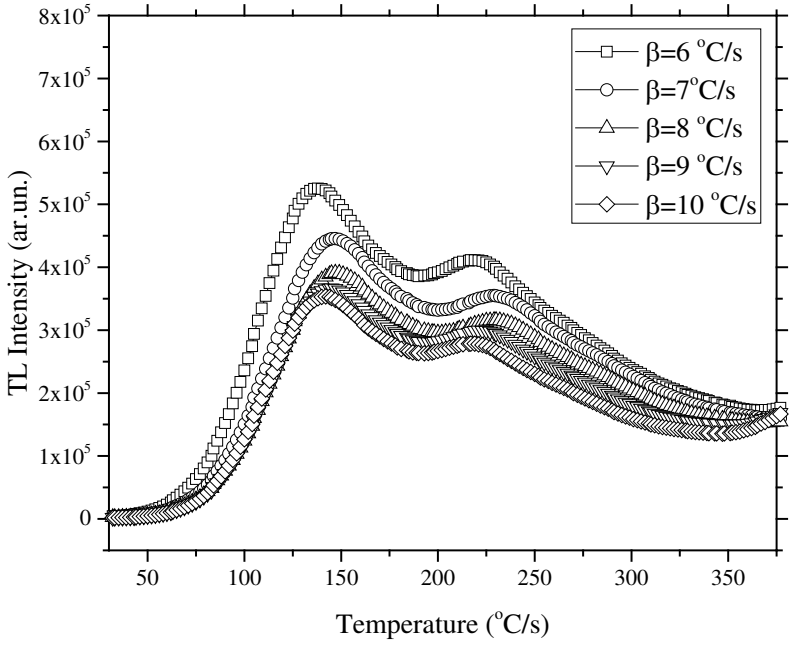

Figure 5.25 Typical glow curves of KCl doped ZnB_2O_4 exposed to beta rays of 12 Gy and readout at linear heating rate between β = 6 °C/s and β = 10 °C/s

In this study the ten heating rates (1-10 ºC/s) were performed with the VHR method. Also, shift position, which is occurred on the position of the temperature (T_m) at the maximum point of intensity (I_m), is determined. Besides, the effect of heating rate on the peak temperatures and normalized TL area was also investigated. As shown from figures 5.22 to 5.23 the peak temperatures of P1 and P2 increases also the area under the glow curve increase as the heating rate increases.

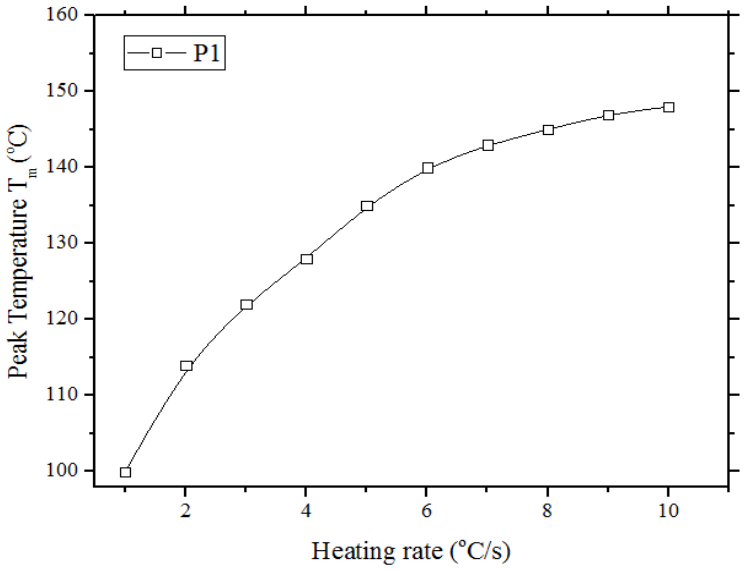

Figure 5.26 The effect of heating rate on the peak temperature of P1

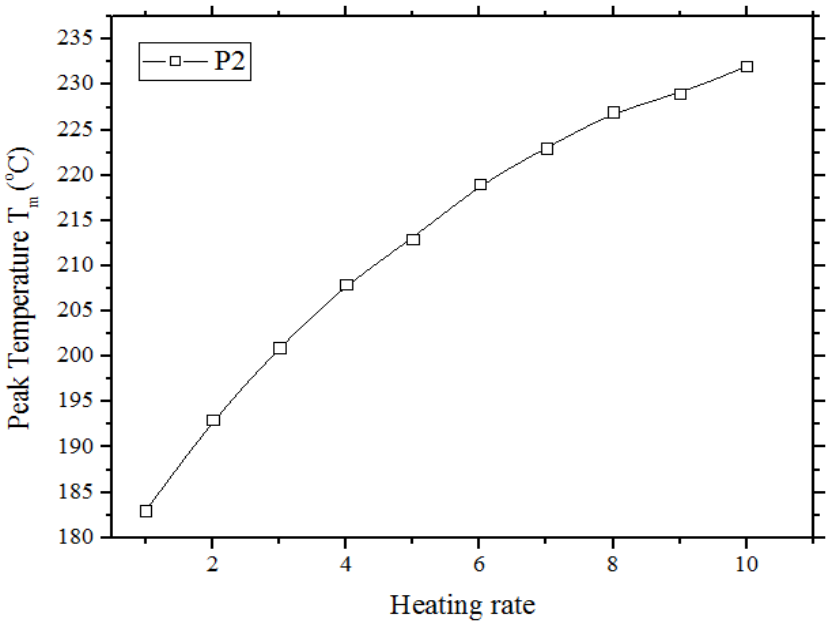

Figure 5.27 The effect of heating rate on the peak temperature of P2.

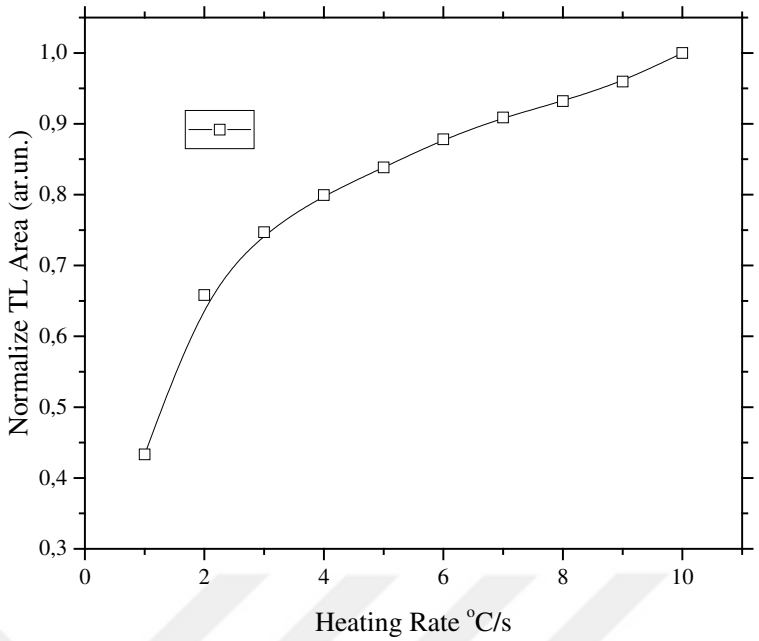

Figure 5.28 The effect of heating rate on the normalized TL area of KCl doped ZnB_2O_4

According to this study, the results showed that KCl doped ZnB_2O_4 may be a good candidate for TL dosimeter in point of the peak temperature. In order to determine characteristic of fading, the irradiated KCl doped ZnB_2O_4 were kept in dark room at the temperature nearly 25 °C and in the time period.

The results of experiment were given for the time period in Figure 5.25. It can be inferred that the main problem of KCl doped ZnB_2O_4 was the high fading ratio (70 %) within one month. When it is examined in more detail after 2 days, the intensity drastically decreased. Fading and sensitive problems were also encountered earlier on Dy-doped ZnB_2O_4 in the literature [12,95,104]

To eliminate this problem, experimenters have worked and several co-dopants are added into host lattice. [35,79] According to abovementioned characteristics of KCl doped ZnB_2O_4 this phosphor is a promising material for dosimetric application, so it is worth to systematic studies on it to improve TL properties and solve particularly fading problem. As a result we can say that our investigation is ongoing with addition of another activators as a co-dopant.

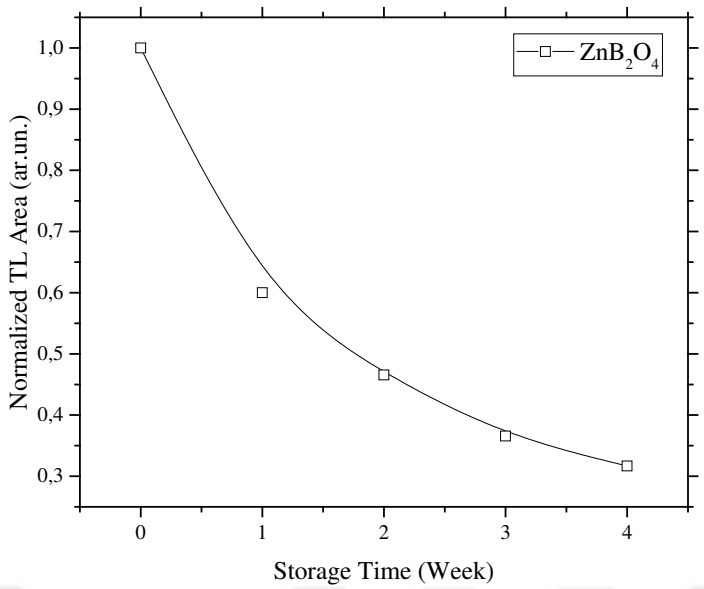

Figure 5.29 Normalized TL intensity of KCl-doped ZnB_2O_4 after different storage times at room temperature. (β=1 ºC / s and D=36 Gy).

CHAPTER 6

CONCLUSION

This thesis describes preliminary investigations on suitability of strontium ion as an activator for magnesium tetraborate to use it at dosimetric application. In terms of the experimental results, the following conclusions were obtained for Sr doped MgB_4O_7:

1. Magnesium tetraborate as a polycrystalline form was synthesized by high temperature solid state method at 900 °C for 2 h with ball milling assisted as much as pure form without any impurities.
2. Contrary to the literature data, which is presented for the synthesis of magnesium tetraborate phosphor, first MBO was synthesized as the host compound and then the activator was added into it. As expected, the characterization studies showed that the doping procedure and the activator did not cause any difference in the MBO structure.
3. Dosimetric materials should have simple glow curve structure and the mean peak should be at around 200°C. Sr –doped MBO compounds gave the main peak with the highest intensity at 200 °C like ideal case. The maximum TL intensity of Sr - doped MBO was obtained at the dopant concentration of 0.25 wt %. TL intensities decreased with increasing the dopant concentration, attributing to the quenching effect. In addition, the glow curve structure of the host compound showed Sr^{2+} concentration independent character, indicating that Sr^{2+} ions are related with the luminescence centers not with the electron traps.
4. PL results indicated that 0.25 % Sr- doped phosphor had longer decay time and more severe emission, meaning that 0.25 wt % Sr ratio plays an important role in prolonging the afterglow. This result supports the TL emission and there is a good correlation between the TL and PL results.

Consequently, it can be said that Sr^{2+} is a promising activator for MBO and Sr-doped compound seemed to be suitable for dosimetric applications, and it would be worth more investigation into it.

In terms of the experimental results, the following conclusions were obtained for

KCl doped ZnB_2O_4: In this study we have also synthesized and investigated the thermoluminescence properties of KCl doped zinc borate (ZnB_2O_4) nano phosphors using solution combustion method.

In TL dosimeter investigation, one of the most important works is the behavior of different dose levels. Experiments were conducted for this purpose and all samples were readout immediately after irradiation. The glow curve structures of KCl doped ZnB_2O_4 is obtained on different dose levels. According to the depending on different dose levels, one strong peak at about 100 °C and a low intensity peak at around 183 °C were occurred. In this study the TL properties of KCl doped ZnB_2O_4 were examined in detail.

In experiment by using different amounts of KCl doped ZnB_2O_4 powder samples, the glow curve obtained. Then the best of the glow curve was selected in many of the glow curves. According to results, 0.5 wt % KCl doped ZnB_2O_4 phosphor is much stronger than the other obtained samples. In a TL dosimeter, certain physical parameters are calculated for many dosimetric application such as trap depth (E) and frequency factor (s). In this study, these physical parameters were determined CGCD method.

The experimental results for KCl doped ZnB_2O_4 nano phosphor has shown that it has a broad glow curve structure which consists of nine general order glow peaks. At the end of the planned storage times the normalized TL area, of the sample reduced 70 % of its original value. The results of the experiments have proved that KCl doped ZnB_2O_4 is a good candidate for TL dosimeter, just need to solve the fading problem with addition of another activators as a co-dopant.

REFERENCES

[1] McKeever, S.W.S. (1985). Thermoluminescence of Solids, Cambridge Solid State Science Series, Cambridge University Press, New York

[2] Randall, J.T. & Wilkins, M.H. F. (1945). Phosphorescence and electron traps: I. The study of trap distribution. *Proceedings of the Royal Society A*, 184, 366-389.

[3] Furetta, C., Kuo, C.H. & Weng, P.S. (1999). Fading prediction in thermoluminescent materials using computerised glow curve deconvolution (CGCD). *Nuclear Instruments &Methods In Physics Research,* ***423***, 183-189.

[4] Furetta, C.(1989). *Review Models in Thermoluminescence.* Kluwer Academic Publiher; ISBN 0022-2461.

[5] Bos, A.J.J. & Dielhof, J.B. (1991). The analysis of thermoluminescent glow curves in CaF_2:Tm (TLD-300). *Radiation Protection Dosimetry*, **36**, 231-239.

[6] Chen, R., Yang, X.H. & McKeever, S.W.S, (1988) Strongly Superlinear Dose Dependence of Thermoluminescence in Synthetic Quartz, *J. Phys. D: Appl. Phys*., 21, 1312.

[7] Park S. & Vogt, T. (2009). Luminescent phosphors, based on rare earth substituted oxyfluorides in the $A(1)_{3-x}$ $A(2)_xMO_4F$ family with A(1)/A(2)=Sr, Ca, Ba and M=Al, Ga, *Journal of Luminescence* 129, 952- 957.

[8] Anishia, S.R., Jose, M.T., Annalakshmi O. & Ramasamy, V. (2011). Thermoluminescence properties of rare earth doped lithium magnesium borate phosphors. *Journal of Luminescence*, 131 (12), 2492–2498.

[9] Annalakshmi, O., Jose, M.T., Madhusoodanan, U., Venkatraman, B. & Amarendra, G. (2013). Synthesis and thermoluminescence characterization of MgB4O7:Gd,Li. *Radiation Measurements*, 59, 15–22.

[10] Doull, B. A., Oliveira, L. C., Wang, D. Y., Milliken, E. D. & Yukihara, E. G. (2014). Thermoluminescent properties of lithium borate, magnesium borate and

calcium sulfate developed for temperature sensing. *Journal of Luminescence*, *146*, 408–417.

[11] Furetta, C., Kitis, G., Weng, P. S. & Chu, T. C. (1999). Thermoluminescence characteristics of MgB4O7 : Dy,Na. *Nuclear Instruments and Methods in Physics Research, Section A: Accelerators, Spectrometers, Detectors and Associated Equipment*, *420*(3), 441–445.

[12] Furetta, C., Prokic, M., Salamon, R. & Kitis, G. (2000). Dosimetric characterisation of a new production of MgB4O7:Dy,Na thermoluminescent material. *Applied Radiation and Isotopes*, *52*(2), 243–250.

[13] Porwal, N. K., Kadam, R. M., Seshagiri, T. K., Natarajan, V., Dhobale, A. R. & Page, A. G. (2005). EPR and TSL studies on MgB4O7 doped with Tm: role of BO32− in TSL glow peak at 470K. *Radiation Measurements*, *40*(1), 69–75.

[14] Sahare, P. D., Singh, M., & Kumar, P. (2015). Synthesis and TL characteristics of MgB4O7:Mn,Tb phosphor. *Journal of Luminescence*, *160*, 158–164.

[15] Souza, L.F., Vidal, R.M., Souza, S.O., & Souza, D.N. (2014). Thermoluminescent dosimetric comparison for two different MgB4O7:Dy production routes. *Radiation Physics and Chemistry*, *104*, 100–103.

[16] Souza, L. F., Antonio, P. L., Caldas, L. V. E., & Souza, D. N. (2015). Nuclear Instruments and Methods in Physics Research A Neodymium as a magnesium tetraborate matrix dopant and its applicability in dosimetry and as a temperature sensor. *Nuclear Inst. and Methods in Physics Research, A*, *784*, 9–13.

[17] Yukihara, E.G., Milliken, E.D., & Doull, B.A. (2014). Thermally stimulated and recombination processes in MgB4O7 investigated by systematic lanthanide doping. *Journal of Luminescence*, *154*, 251–259.

[18] Pinto, R., Ferreira, M.G.S., Carmezim, M.J., & Montemor, M. F. (2011). The corrosion behaviour of rare-earth containing magnesium alloys in borate buffer solution. *Electrochimica Acta*, *56*(3), 1535–1545.

[19] Haberer, A., Heymann, G., & Huppertz, H. (2007). Pr4B10O21: A new composition of rare-earth borates by high-pressure/high-temperature synthesis. *Journal of Solid State Chemistry*, *180*(5), 1595–1600.

[20] Kipcak, A.S., Senberber, F.T., Yuksel, A.S., Derun, E.M., & Piskin, S. (2015). Synthesis, characterisation, electrical and optical properties of copper borate compounds. *Materials Research Bulletin*, *70*, 442–448.

[21] Rejisha, S. R., Anjana, P. S., Gopakumar, N., & Santha, N. (2014). Synthesis and characterization of strontium and barium bismuth borate glass-ceramics. *Journal of Non-Crystalline Solids*, *388*, 68–74.

[22] Santiago, M., Marcazzó, J., Grasselli, C., Lavat, A., Molina, P., Spano, F., & Caselli, E. (2011). Thermo and radioluminescence of undoped and Dy-doped strontium borates prepared by sol-gel method. *Radiation Measurements*, *46*(12), 1488–1491.

[23] Menon, S.N., Kadam, S., Watanabe, S., Gundu Rao, T.K., Kulkarni, M.S., & Babu, D.R. (2015). Thermoluminescence and defect centres in Tb doped lithium magnesium borate phosphor. *Journal of Luminescence*, *167*, 140–145.

[24] Furetta, C., Prokic, M., Salamon, R., Prokic, V., & Kitis, G. (2001). Dosimetric characteristics of tissue equivalent thermoluminescent solid TL detectors based on lithium borate. *Nuclear Instruments and Methods in Physics Research, Section A: Accelerators, Spectrometers, Detectors and Associated Equipment*, *456*(3), 411–417.

[25] Azorin, J. (2014). Preparation methods of thermoluminescent materials for dosimetric applications: An overview. *Applied Radiation and Isotopes*, *83*, 187–191. 1.

[26] Kayhan, M. & Yilmaz, A. (2011). Effects of synthesis, doping methods and metal content on thermoluminescence glow curves of lithium tetraborate. *Journal of Alloys and Compounds*, *509*(30), 7819–7825.

[27] Depçi, T. (2009) Synthesis and Characterization of Lithium Triborate by Different Synthesis Methods and Their Thermoluminescent Proporties *PhD Thesis*, Middle East Technical University/School of Natural and Applied Sciences

[28] Driscoll, C.M.H. & McKinlay, A.F. (1981). Particle size effects in thermoluminescent lithium fluoride. *Phys. Med. Biol.*, Vol. 26, No. 2, 321-327.

[29] Dhoble, S.J., Sahare, P.D. & Moharil, S.V. (1991). Thermoluminescence and

colour centres in KI: particle size effect. *J. Phys.*: Condens. Matter 3, 1189- 1195.

[30] Gong, X. , Wu, P., Chan, W.K. & Chen, W.(2000). Effect of γ-ray irradiation on structures and luminescent properties of nanocrystalline $MSO_4:xEu^{3+}$ (M Ca; Sr; Ba; x = 0.001–0.005)J. *Phys. Chem. Solids* 61, 115-121.

[31] Salah, N., Sahare, P.D., Lochab, S.P. & Kumar, P. (2006). TL and PL studies on $CaSO_4$: Dy nanoparticles. *Radiation Measurements*, *41*(1), 40–47.

[32] Salah, N., Habib, S.S., Khan, Z.H., Al-Hamedi, S. & Lochab, S. P. (2009). Nanoparticles of $BaSO_4$:Eu for heavy-dose measurements. *Journal of Luminescence*, *129*, 192–196.

[33] Yazici, A.N., Öztaş, M., Bedir, M. (2007). The thermoluminescence properties of copper doped ZnS nanophosphor. *Optical Materials*, *29*, 1091–1096.

[34] Shinsho, K., Harada, K., Yamamoto, Y. & Urushiyama, A. (2008). Differences in glow curves structure of nano and microcrystals of $CaSO_4$:Dy measured at a low heating rate. *Radiation Measurements*, *43*(2-6), 236–240.

[35] Prokic, M., (1993). MgB_4O_7:Mn as a new TL dosemeter. Radiation Protection Dosimetry, 47(1-4), 191-193.

[36] Bahl, S., Pandey, A., Lochab, S.P., Aleynikov, V.E., Molokanov, G. & Kumar, P. (2013). Synthesis and thermoluminescence characteristics of gamma and proton irradiated nanocrystalline MgB_4O_7: Dy, Na. *Journal of Luminescence*, 134, 691–698.

[37] Salah, N., Habib, S., Babkair, S.S., Lochab, S.P. & Chopra, V. (2013). TL response of nanocrystalline MgB_4O_7:Dy irradiated by 3 MeV proton beam, 50 MeV Li^{3+} and 120 MeV Ag^{9+} ion beams. *Radiation Physics and Chemistry*, *86*, 52–58.

[38] Kucuk, N., Kucuk, I., Cakir, M., & Keles, S. K. (2013). Synthesis, thermoluminescence and dosimetric properties of La-doped zinc borates. *Journal of Luminescence*, *139*, 84-90.

[39] Annalakshmi, O., Jose, M. T., Madhusoodanan, U., Subramanian, J., Venkatraman, B., Amarendra, G. & Mandal, A. B. (2014). Thermoluminescence dosimetric characteristics of thulium doped ZnB_2O_4 phosphor. *Journal of Luminescence*, *146*,

295-301.

[40] Mu, Z., Hu, Y., Chen, L., Wang, X., Chen, R., Wang, T. & Xu, J. (2014). Synthesis of Bi^{3+} and Gd^{3+} doped ZnB_2O_4 for evaluation as potential materials in luminescent display applications. *Displays*, *35*(3), 147-151.

[41] McKeever, S.W.S., Moscovitch, M. & Townsend, P.D. (1995). *Thermoluminescence Dosimetry Materials: Propeties and Uses*, Nuclear Technology Publishing, Ashford, Kent TN23 1YW England.

[42] Mahesh K., Weng P.S. & Furetta C. (1989) Thermoluminescence in Solids and Applications, Nuclear Technoloy Publishing; Ashford, Kent TN25 4NW England ISBN 1870965000

[43] Chen,R. & McKeever, S.W.S. (1997). *Theory of Thermoluminescence and Related Phenomena*, World Scientific, Singapore, 576.

[44] Chen, R., & Horowitz, Y.S. (1984). Thermoluminescent and Thermoluminescent Dosimetry, Vol. 1, CRC Press, Boca Raton, FL.

[45] Kitis, G., Gomez-Ros J.M. & Tuyn, J.W.N. (1998). Thermoluminescence glow curve deconvolution functions for first, second and general orders of kinetics. *Journal of Physics D:Applied Physics*, 31**,** 2636-2641.

[46] Garlick, G.F.J & Gibson, A.F. (1948). The electron trap mechanism of luminescence in sulphide and silicate phosphors. *Proceedings of the Physics Society*,60, 574-589.

[47] May, C.E. & Partridge, J.A.(1964). Thermoluminescence kinetics of alpha irradiated alkali halides. *Journal of Chemical Physics*, 40, 1401-1415.

[48] Chen, R. and Winer, A.A. (1970). Effects of various heating rates on glow curves. *Journal of Applied Physics*, 41, 5227-5232.

[49] Piters, T.M. & Bos, A.J.J. (1993). Thermoluminescence Emission Spectra of LiF (TLD-100) after different Thermal Treatments. *Journal of Physics D:Applied Physics*, 47, 91-94.

[50] McKeever, S.W.S., (1983). *Thermoluminescence of solids*. Oklahoma State University Press.

[51] Randall, J.T. & Wilkins, M.H. F. (1945). Phosphorescence and electron traps: II. The interpretation of long-period phosphorescence. Proceedings of the Royal Society A, 184, 390-407.

[52] Chen, R. (1969). On the Calculation of Activation Energies and Frequency Factors from Glow Curves. *Journal of Applied Physics,* 40, 570-575.

[53] Azerin, J. (1986). Nuclear Tracks, 11, 159.

[54] Kitis, G. & Tuyn, J.W.N. (1998). A simple method to correct for the temperature lag in TL glow-curve measurements. *Journal of Physics D:Applied Physics*, 31, 2065-2073..

[55] Grossweiner, L.I. (1953). A note on the Analysis of First-Order Glow curves. *Journal of Applied Physics*, 24, 1306-1308.

[56] Chen, R., McKeever, S.W.S. (1994). Characterization of nonlinearities in the dose dependence of thermoluminescence. Radiation Measurements, 23, 667- 673.

[57] Halperin, A. and Braner. A. (1960). Evaluation of thermal activation energies from glow curves. Physical Review Letters, 117, 408-415..

[58] Gartia, R.K., Singh S.J. & Mazumdar, P.S. (1989). Physica Status Solidi (a), 11, 407..

[59] Bos, A. J. J., Piters, J.M., Gomez Ros, J. M. and Delgado, A. (1993). (GLACANIN, and Intercomparision of Glow Curve Analysis Computer Programs) IRI-CIEMAT Report 131-93-005 IRI Delft.

[60] Hsu, P.C. & Wang, T.K. (1986). On the annealing procedure of CaF_2:Dy. Radiation Protection Dosimetry, 16, 253-256.

[61] Kathuria ,S. P. and Sunta, C. M. (1979). Kinetics and trapping parameters of thermoluminescence in LiF TLD-100-dependence on dose**.** *Journal of Physics D:Applied Physics*, 12, 1573-1587.

[62] Rasheedy, M.S.(2005). A new evaluation technique for analyzing the thermoluminescence glow curve and calculating the trap parameters. *Thermochimica Acta*, 429, 143-147.

[63] Ramsden, J. J. (2009). Applied Nanotechnogy: The Conversation of Research Results to Products. Burlington : Elsevier Press.

[64] Wolf L. E. (2004), Nanophysics and Nanotechnology : An Introduction to Modern Concepts in Nanoscience, John Wiley, Weinheim, 3527404074

[65] Kodama R.H. (1999). Magnetic Nanoparticles. J. Magn. Magn. Mater, 200, 359-372.

[66] Vladimir V., Mitin, D.L., Sementsov and Vagidov N.Z. (2010), Quantum Mechanics for nanostructures, Cambiridge University Press

[67] Buzea C., Pacheco I.I. and Robbie K. (2007), Nanomaterials and nanoparticles: Sources and toxicity, Biointerphases, 2, (4). 17-71.

[68] Schmid G. (2004), Nanoparticles: From theory to application, Wiley, ISBN: 978-3-527-32589-4

[69] Roco M.C. (1998).Reviews of notional research programs in nanoparticle and nanotechnology research in the U.S.A. *Journal of Aerosol Science*, 29, 749-751.

[70] Wu X., Liu H., Liu J., Haley K.N., Treadway J.A., Larson J.P., Ge N., Peale F. and Bruchez M.P., (2003), Immunofluorescent labeling of cancer marker her and other cellular targets with semiconductor quantum dots, Nat. Biotechnol., 21, 41-46

[71] Vashist S.K., Tewari R., Bajpai R.P., Bharadwaj L.M., and Raiteri R., (2006). Review of quantum dot technologies for cancer detection and treatment, Journal of nanotechnology online, DOI: 10.2240/azojono 0113.

[72] Wang T.F., Letant S.E., Nikolic R.J. and Chueng C.L., (2006). Nanomaterials for Radiation Detection, FY05 LDRD Final Report, ucrl-tr-218736.

[73] Veiseh O., Sun C., Gunn J., Kohler N., Gabikian P., Lee D., Bhattarai N., Ellenbogen R., Sze R., Hallahan A., Olson J., Zhang M.Q., Veiseh O., Sun C., Gunn J., Kohler N., Gabikian P., Lee D., Bhattarai N., Ellenbogen R., Sze R., Hallahan A., Olson J. and Zhang M.Q., (2005), Optical and MRI multifunctional nanoprobe for targeting gliomas, Nano Lett., 5, 1003-1008.

[74] Larson D., (2003), Water-soluble quantum dots for multiphoton fluorescence imaging in vivo, Science; 300-1434.

[75] Chen K., Li Z.B., Wang H. and Cai W., (2008). Chen X. Dual-Modality Optical and Positron Emission Tomography Imaging of Vascular Endothelial Growth Factor Receptor on Tumor Vasculature using Quantum Dots, Eur J Nucl Med Mol Imaging, 35, 2235–2244.

[76] Mulder W.J.M., Koole R., Brandwijk R.J., Storm G., Chin P.T.K., Strijkers G.J., Donega C.M., Nicolay K. and Griffioen A.W., (2006), Quantum dots with a paramagnetic coating as a bimodal molecular imaging probe, Nano Lett., 6, (1).

[77] Wang S., Jarrett B.R., Kauzlarich S.M., and Louie A.Y., (2007), Core/Shell quantum dots with high relaxivity and photoluminescence for multimodality ıimaging, American Chemical Society, 129, 3848-385.

[78] Marczewska, B., Bilski, P., Budzanowski, M., Olko, P., Chernov, V. (2001). Dosimetry properties of Tm-doped single CaF_2 crystals, *Radiation Measurements,* **33**, 571–576.

[79] Chan W.C.W., Maxwell D.J, Gao X., Bailey R.E., Han M. and Nie S., (2002), Luminescent Quantum Dots for Multiplexed Biological Detection and İmaging, *Elsevier Science, Biotechnology*, 13, 40–46.

[80] Babu P., Sinha S. and Surolia A., (2007), Sugar-quantum dot conjugates for a selective and sensitive detection of lectins‘‘, Bioconjugate Chem, 18, 146- 151.

[81] Wen, W., & Wu, J. M. (2014). Nanomaterials via solution combustion synthesis: a step nearer to controllability. *RSC Advances*, *4*(101), 58090-58100.

[82] Barrere, M., Jaunmotte, A., DeVeubeke, B. F., and Vandenkerekhove, J., Rocket Propulsion Elsevier, Amsterdam, 1960, pp. 132 – 134..

[83] Jain, S. R., Adiga, K. C., & Verneker, V. P. (1981). A new approach to thermochemical calculations of condensed fuel-oxidizer mixtures. *Combustion and flame*, *40*, 71-79.

[84] Kawashima,Y. S., Gugliotti, C.F., Yee, M., Tatumi, S.H. & Mittani, J.C.R., (2014). Thermoluminescence features of MgB_4O_7:Tb phosphor, *Radiation Physics and Chemistry* 95 91–93.

[85] Kitis, G., Polymeris, G.S., Sfampa, I.K., Proki, M., Meriç, N. & V. Pagonis, V., (2016). Prompt isothermal decay of thermoluminescence in MgB_4O_7:Dy, Na and LiB4O7:Cu, In dosimeters, *Radiation Measurements* 84 15-25.

[86] McKeever S.W.S, (1984). Optical absorption and luminescence in lithium fluoride TLD-100, *Journal of Applied Physics*, 56, 2883-2889.

[87] Prokic, M. (1986) Radiat. Prot. Dosim. 17, 393–396.

[88] Prokic, M. (1993). MgB_4O_7:Mn as a New TL Dosemeter**.** *Radiation Protection Dosimetry,* **47**, 191-193.

[89] Yukihara, E.G., Milliken, E.D., Oliveira, L.C., Orante-Barro, V.R., Jacobsohn, L.G. and Blair, M.V., (2013) Systematic development of new thermoluminescence and optically stimulated luminescence materials, *J. Lumin.*133 203–210.

[90] Annalakshmi, O., Jose, M. T., Madhusoodanan, U., Venkatraman, B., & Amarendra, G. (2013). Kinetic parameters of lithium tetraborate based TL materials. *Journal of Luminescence*, *141*, 60–66

[91] Pei, Z., Su, Q. & Zhang, J., (1993). The valence change from RE^{3+} to RE^{2+} (RE, Eu, Sm, Yb) in SrB_4O_7: RE prepared in air and the spectral properties for RE^{2+}, *J. Alloys and Compounds* 198 51–53.

[92] Tanner, P.A, Wu, P.Z., Jun, L. Yulong, L. & Qiang, S., (1997). Luminescence of Uranium-Doped Strontium Tetraborate, *J. Phys. Chem. Solids*, 58, 1143–1146.

[93] Kadam, R.M., Rajeswarin, B., Mohapatra, M., Porwal, N.K., Hon, N.S, Seshagiri, T.K. & Natarajan, V., (2015). Radiation induced centers in irradiated SrB_4O_7 doped europium and their role in thermally stimulated reactions: Thermally stimulated luminescence, fluorescence and electron paramagnetic resonance studies, *Journal of Luminescence* 158 475–483

[94] Depci, T., Özbayoğlu, G., Yılmaz, A. and Yazıcı, A.N. (2008). The thermoluminescence Properties of Lithium Triborate (LiB_3O_5) Activated by

Aluminium. *Nuclear Instruments and Methods B*, **266**, 755-762.

[95] Altermatt, U. D., & Brown, D. (1987). CelRef version 3. *Acta Cryst A*, *34*, 125-130.

[96] Kipcak, A.S., Gurses P., Derun, E.M., Tugrul, N. & Piskin, S. (2013).Characterization of boron carbide particles and its shielding behavior against neutron radiation, Energy Convers. and Management 72 39-44.

[97] Ekdal, E., Garcia Guinea, J., Karabulut, Y., Canimoglu, A., Harmansah, C., Jorge, A., Can, N. (2015). Characterisation and luminescence studies of Tm and Na doped magnesium borate phosphors. *Applied Radiation and Isotopes*, *103*, 93–99.

[98] Lochab, S.P., Salah, N., Sahare, P.D, Chauhan, R.S, & Ranjan, R. (2007). Thermoluminescence of $Ba_{0.97}Ca_{0.03}SO_4$:Eu irradiated with 48 MeV ^{7}Li ion beam *Nucl. Instrum. and Methods* 254 231-235.

[99] Depci,T. ,Ozbayoglu, G. & Yılmaz, A., (2011). Synthesis and thermoluminescence properties of rare earth oxides (Y, Ce-Lu) doped lithium triborate, *Journal of Rare Earths*, 29, 618-622.

[100] Islam, M. M., Maslyuk, V. V., Bredow, T., & Minot, C. (2005). Structural and electronic properties of $Li_2B_4O_7$. *The Journal of Physical Chemistry B*, *109*(28), 13597-13604.

[101] Ratasa, A., Danilkina, M., Kerikmäea, M., Lusta, A., Mändarb, H., Seemanb, V., & Slavinc, G. (2012). $Li_2B_4O_7$: Mn for dosimetry applications: traps and mechanisms. *Proceedings of the Estonian Academy of Sciences*, *61*(4), 279-295.

[102] Gartia, R. K., Singh, S. J., & Mazumdar, P. S. (1989). Determination of the Activation Energy of Thermally Stimulated Lumincscence Peaks Obeying General-Order Kinetics. *physica status solidi (a)*, *114*(1), 407-411.

[103] Szabo, P. P., Pradhan, A. S., & Chandra, B. (1984). Some dosimetric parameters of MgB_4O_7: Dy sintered pellets and $CaSO_4$: Dy Teflon discs—A comparative study. *The International journal of applied radiation and isotopes*,*35*(5), 415-417.

[104] Wang, L., Wang, Y., Wang, D., & Zhang, J. (2008). Electronic structure calculations of SrB_4O_7 and SrB_4O_7:Eu crystals. *Solid State Communications*, *148*(7), 331-335.

[105] Pan, F., Shen, G., Wang, R., Wang, X., & Shen, D. (2002). Growth, characterization and nonlinear optical properties of SrB_4O_7 crystals. *Journal of Crystal Growth*, *241*(1), 108-114.

[106] Rubinsztein-Dunlop, H., Littleton, B., Barker, P., Ljungberg, P., & Malmsten, Y. (2001). Ionic strontium fluorescence as a method for flow tagging velocimetry. *Experiments in fluids*, *30*(1), 36-42.

[107] Li, J., Zhang, C. X., Tang, Q., Zhang, Y. L., Hao, J. Q., Su, Q., & Wang, S. B. (2007). Synthesis, photoluminescence, thermoluminescence and dosimetry properties of novel phosphor Zn (BO 2) 2: Tb. *Journal of Physics and Chemistry of Solids*, *68*(2), 143-147.

[108] Meijerink, A., Blasse, G., & Glasbeek, M. (1990). Photoluminescence, thermoluminescence and EPR studies on $Zn_4B_6O_{13}$. *Journal of Physics: Condensed Matter*, *2*(29), 6303.

[109] Santiago, M., Grasseli, C., Caselli, E., Lester, M., Lavat, A., & Spano, F. (2001). Thermoluminescence of SrB4O7: Dy. *physica status solidi (a)*, *185*(2), 285-289.

[110] Zeng, Q. H., Pei, Z. W., Su, Q., & Huang, S. H. (1999). Luminescence and its temperature effects on Sm^{2+} in alkaline earth borates.

[111] Pei, Z., Su, Q., & Zhang, J. (1993). The valence change from RE^{3+} to RE^{2+} (RE Eu, Sm, Yb) in SrB_4O_7: RE prepared in air and the spectral properties of RE^{2+}. *Journal of alloys and compounds*, *198*(1-2), 51-53

[112] Gautam, C., Yadav, A. K., & Singh, A. K. (2012). A review on infrared spectroscopy of borate glasses with effects of different additives. *ISRN ceramics*, *2012*.

[113] Murray, A. F., & Lockwood, D. J. (1976). Raman spectrum of Zn4O (BO2) 6. *Journal of Physics C: Solid State Physics*, *9*(19), 3691.

[114] Annalakshmi, O., Jose, M. T., Madhusoodanan, U., Subramanian, J., Venkatraman, B., Amarendra, G., & Mandal, A. B. (2014). Thermoluminescence dosimetric characteristics of thulium doped ZnB_2O_4 phosphor. *Journal of Luminescence*, *146*, 295-301.

VITA

Personal Information:

Name and Surname: Dündar Evis
Natioality: Turkish
Birth place and date: Gaziantep 21.06.1976
Marial status: Married
Phone number: +905055753689
Email: dundarevis@gmail.com

Education:

- Ph.D. Physics Engineering, University of G.antep (Turkey): 2010-2017
  Thesis Title: Synthesis and Thermoluminescence Characteristics of Rare Earth Doped Nanophosphors

  M.S. Physics Education, Kahramanmaraş Sütçü İmam University (Turkey): 2010.
- B.S. Physics Education, Çukurova University (Turkey): 1998.
- Gaziantep 19 Mayıs High School: 1993

Experiences:

- Physics Teacher

Research Interests:

Nanoscience and Nanotechnology, Thormoluminescence,

Publications :

D. Evis, A.Yucel, N.Kizilkaya, T.Depci, V.E.Kafadar, E.Öztürk, R.G.Yildirim (2016). A new activator strontium for magnesium tetraborate: PL and TL studies Applied Radiation and Isotopes, 116, 138–142.

Project :

Gaziantep University Scientific Research Project, Synthesis and Investigation of Thermoluminescence Properties of Strontium (Sr) doped MgB_4O_7 nanophosphorus Project No: MF. DT.16.04, Researcher, 2016.

Languages:

English (Fluent)

ÜDS: 67,5

Interests:

Martial Arts, Football, Swimming, Travelling and Reading